

RESEARCH REPORT no. 3

NUMERICAL TESTS FOR WIND EROSION REDUCTION SOLUTIONS UNDER THE ACTION OF THE WIND

PhD Student:	PhD Supervisors:
--------------	------------------

drd.ing. Bogdan-Iulian DOROFTEI

prof.univ.dr.ing. Mircea DEGERATU

prof.univ.dr. Georgeta BANDOC



TABLE OF CONTENTS

	UMERICAL MODELING OF AIR MOVEMENT OVER SANDY SOIL PROVIDED WITH ECTIVE SCREENS4
1.1	General elements regarding numerical modeling4
1.2	COMSOL Multiphysics finite element modeling software5
1.3	Boundary conditions6
1.4	Discretization of the computational domain
2. N	umerical TESTING, ORDENING, AND CODING OF TESTS11
2.1	Numerical tests ordening
2.2	Coding of numerical tests
3. R	ESULTS OF NUMERICAL SIMULATIONS
3.1	Numerical testing for test category CT1 (<i>U</i> (10)=8m/s)13
3.1.1 (<i>U</i> (10)	Numerical testing for the test group GT1,1 (<i>n</i> =1 screen) from the tests category CT1 (<i>n</i> =8m/s)
3.1.2 (<i>U</i> (10)	Numerical testing for the test group GT1,2 (<i>n</i> =2 screens) from the tests category CT1 (1=8m/s))
3.1.3 m/s)	Numerical testing for the test group GT1,3 (n =3 screens) from the tests category CT1 (U (10)=8 26
3.1.4 m/s)	Numerical testing for the test group GT1,4 (n =4 screens) from the tests category CT1 (U (10)=8 32
3.2	Numerical testing for test category CT2 (<i>U</i> (10)=12 m/s)
3.2.1 (<i>U</i> (10)	Numerical testing for the test group GT2,1 (<i>n</i> =1 screen) from the tests category CT2 (<i>n</i> =12 m/s)
	Numerical testing for the test group GT2,2 (<i>n</i> =2 screens) from the tests category CT2 (n=12 m/s)
3.2.3 (<i>U</i> (10)	Numerical testing for the test group GT2,3 (<i>n</i> =3 screens) from the tests category CT2 b=12 m/s)
3.2.4 (<i>U</i> (10)	Numerical testing for the test group GT2,4 (<i>n</i> =4 screens) from the tests category CT2 b=12 m/s)
3.3	Numerical testing for test category CT3 (<i>U</i> (10)=16 m/s)
3.3.1 m/s)	Numerical testing for the test group GT3,1 (n =1 ecran) from the tests category CT3 (U (10)=16 62

3.3.2	Numerical	testing	for	the	test	group	GT3,2	(n=2)	ecrane)	from	the	tests	category	CT3
(U(1)	0)=16 m/s)						•••••			• • • • • • • • • • • • • • • • • • • •		•••••		68
	Numerical 0)=16 m/s)	_				-								
3.3.4	Numerical 0)=16 m/s)	testing	for	the	test	group	GT3,4	(n=4	screens)	from	the	tests	category	СТЗ
4. (CONCLUSION	IS REGA	ARD	ING	NUI	MERIC	AL TES	STS						86
5 1	RIBLIOGRAPI	ΗY												89



1. NUMERICAL MODELING OF AIR MOVEMENT OVER SANDY SOIL PROVIDED WITH PROTECTIVE SCREENS

In the research carried out in the previous research report, ANSYS Fluent - LES (Large Eddie Simulation) numerical simulations were performed and numerical simulations k - ϵ in the finite element modeling program COMSOL Multiphysics, on the movement in the working vein of an aerodynamic tunnel. Numerical simulations have led to very close results in terms of velocity profiles similar to those in the experimental vein.

Also, in the research conducted in the previous research report, the numerical simulations k - ϵ in the finite element modeling program COMSOL Multiphysics were compared with the results of experimental tests performed in the same wind tunnel with expansion stage. In this case, too, the COMSOL numerical simulations led to very close results, in terms of speed profiles, with the experimental tests, thus considering the numerical model as being experimentally validated.

Due to this fact, it was considered that the numerical treatment of the studied problems and therefore the afferent numerical tests, can be solved, with a very good approximation, by using the finite element modeling method COMSOL Multiphysics.

1.1 General elements regarding numerical modeling

Numerical tests performed in this research report refer to the movement of air in the area of the atmospheric boundary layer above a sandy terrain with a number of permeable protective screens in order to reduce wind speed to significantly reduce the amount of soil transport caused by wind, or to reduce the effect of wind erosion.

In this third research report, a series of numerical tests were performed on the possibility of reducing wind speed at ground level for sandy soils in order to reduce sand entrainment by wind and thus reduce erosion and sand deposition in the area of sandy soils.

Numerical aerodynamic tests were performed for different categories of reference wind speeds (U(10) = 8 m/s, 12 m/s, 16 m/s) and for different protection groups characterized by the number of protection screens (n = 1,2,3,4 screens).

The numerical tests performed followed the way in which these permeable protection screens achieve the reduction of the wind speed downstream of the last row of the set of screens, compared to the incident wind speed upstream of the first row of the set of protection screens..

The numerical models were developed for 3 reference wind speeds upstream of the protection screens, i.e. for the speeds measured at a height of 10 m from the ground, as the speed is measured at the weather stations near the study area. These speeds are U(10) = 8 m/s, U(10) = 12 m/s, U(10) = 16 m/s. The 3 reference speeds (8 m/s, 12 m/s and 16 m/s) used in the numerical calculations were chosen taking into account the specific intensity classes for wind erosion, namely the moderate class (U(10) = 8 m/s) and strong class (U(10) > 11 m/s).



Numerical tests were also performed for 3 wind speed profiles of the incident wind in the section located 20 m upstream of the group of protection screens, all speed profiles being of the power law type with Davenport's exponent corresponding to a sandy terrain, i.e. $\alpha = 0.16$.

At the same time, the numerical tests were performed for 4 situations regarding the number of protection screens, i.e. with 1 protection screen, with 2 protection screens, with 3 protection screens and 4 protection screens. The protection screens have a height of H = 10 m and have a permeability characteristic of 40%. The distance between the rows of screens is 4 m.

The representation of the speed profiles downstream of the set of protection screens were made for the distances $d_{av} = 2H$, 4H, 6H and 8H from the last row of screens.

The calculation range, as part of the range of air movement in the atmospheric boundary layer, has a length between 100 m and 112 m for the case with 1 protection screen and respectively for the case with 4 protection screens.

The air velocities were observed, both upstream and downstream of the set of protection screens, at heights important for the studied phenomenon, i.e. at $z_1 = 0.20$ m, $z_2 = 1$ m and at $z_3 = 2$ m. The first two heights refers to the phenomenon of triggering the process of wind erosion and the process of wind transport, respectively. The third height was taken into account due to the fact that, above this height, the influence of the land on wind transport becomes practically negligible.

The numerical model adopted is a flat, two-dimensional model.

1.2 COMSOL Multiphysics finite element modeling software

COMSOL Multiphysics® is a simulation platform that encompasses all steps in the modeling workflow - from defining geometries, material properties and physics that describe specific phenomena to solving and post-processing models to produce accurate and reliable results.

COMSOL Multiphysics is a software for finite element analysis, solving and multiple numerical simulations. It contains a conventional user interface based on physics and coupled systems of partial differential equations (PDE). COMSOL offers a unified workflow for electrical, mechanical, fluid, acoustic and chemical applications.

To create models for use in specialized application or engineering fields, COMSOL Multiphysics® can be used with any combination of additional modules in the product suite. The interface products also make it possible to integrate the simulation with other engineering and mathematics programs used in product and process design. When a model has been developed, it can even be converted into a simulation application with a dedicated user interface, which can be designed for very specific use by people outside the research and development department.

To solve the continuous or variable flow in terms of time, the program uses the incompressible Navier-Stokes module.

The generalized equations of transport properties and velocity gradients are presented below:

$$\rho \frac{\partial \vec{u}}{\partial t} - \nabla \cdot \left[\nu (\nabla \vec{u} + (\nabla \vec{u})^T) \right] + \rho (\vec{u} \cdot \nabla) \vec{u} + \nabla p = \vec{F}$$
 (1)

$$\nabla \cdot \vec{u} = 0 \tag{2}$$

The first equation (1) is the transport equation and the second (2) is the continuity equation for incompressible fluids, where:

- ν dynamic viscosity
- p density
- \vec{u} speed field
- p pressure
- \vec{F} the field of volume forces, such as gravity

These application modules are general enough for all types of incompressible flows. In practice, however, successful turbulent flow analyzes require the simplification of the transport description.

For turbulent flow, k- ε of incompressible fluids, the Navier-Stokes equations are used to preserve momentum and the continuity equations to conserve mass..

1.3 Boundary conditions

Regarding the uniqueness conditions, the motion in the computational range being permanent, the initial conditions are superfluous, and the boundary conditions for the present application on air flow in the incompressible range described with the Navier-Stokes equations are grouped in the following types of conditions.:

- The condition at the limit of the upper wall;
- The condition at the limit of the lower wall;
- The condition for the inlet of the calculation field;
- The condition for the outlet of the calculation field;
- Boundary condition for protection screens.

a. The condition at the upper wall boundary

Boundary condition applied to the upper side of the calculation range, wall type with the Slip option prescribing a non-penetrating condition, $\vec{u} \times \vec{n} = 0$. Therefore, it implicitly assumes that there are no viscous effects on the wall and therefore no boundary layer develops. From a modeling point of view, this was considered a reasonable approximation because the main effect of the wall is to prevent fluid from escaping.

b. The condition at the lower wall boundary

For the lower side of the calculation range a boundary condition of such wall type was applied but to which a roughness was applied, respectively the specific roughness of a sandy soil, having the absolute roughness $k = 3.2 \mu m$.

c. Condition for entry into the calculation field

The limit condition for entering the calculation range was set to Inlet type with speed, introducing into the program the speed profile of the incident wind for all 3 simulations.

Thus, for the realization of real-scale numerical simulations, uniqueness conditions were proposed, at the input limit, consisting of a series of 3 power law type profiles (Davenport-Velozzi, see table 1.1) for the incident wind speed in section input of the computational domain. The 3 incident speed profiles correspond to the 3 speeds at the reference height z = 10 m (U(10)).

In the calculation of these speed profiles the relation expressing the law of power was used (Davenport-Velozzi):

$$U(z) = U(z_1) \cdot \left(\frac{z}{z_1}\right)^{\alpha} \tag{3}$$

where:

U(z) - wind speed at a current height [m/s];

 $U(z_1)$ - wind speed at a reference height [m/s];

z - current height [m];

*z*₁ - reference height [m];

α - Davenport-Velozzi exponent [-];

 δ - the thickness of the atmospheric boundary layer [m].

Tabel 1.1 – Values for the Davenport exponent

	DAVENPORT										
	Surface of the sea	Open field	Suburban field, forest	Center of big cities							
α [-]	0,12	0,16	0,28	0,36							
δ [m]	220	275	400	520							

The simulation refers to the action of the soil on wind speeds on a sandy open ground, so that the value of Davenport's exponent was chosen $\alpha = 0.16$.

It turns out that the relationship regarding the law of power, above, becomes:

$$U(z) = U(10) \cdot \left(\frac{z}{10}\right)^{0.16} \tag{4}$$

Numerical simulations were performed for 3 distinct incident speed profiles to follow the influence of permeable protection screens on the speed fields in the calculation domains.

In the numerical simulations the inlet boundaries were entered as incident speed profiles, the results of previous calculations, with the power law, for the speeds at the reference height U(10) = 8 m/s, U(10) = 12 m/s and U(10) = 16 m/s. These 3 incident wind speed profiles are shown graphically in the following figures.

Figure 1-1 shows the speed profile of the incident wind upstream of the protection screens for the exponent $\alpha = 0.16$ and the reference speed U(10) = 8 m/s.

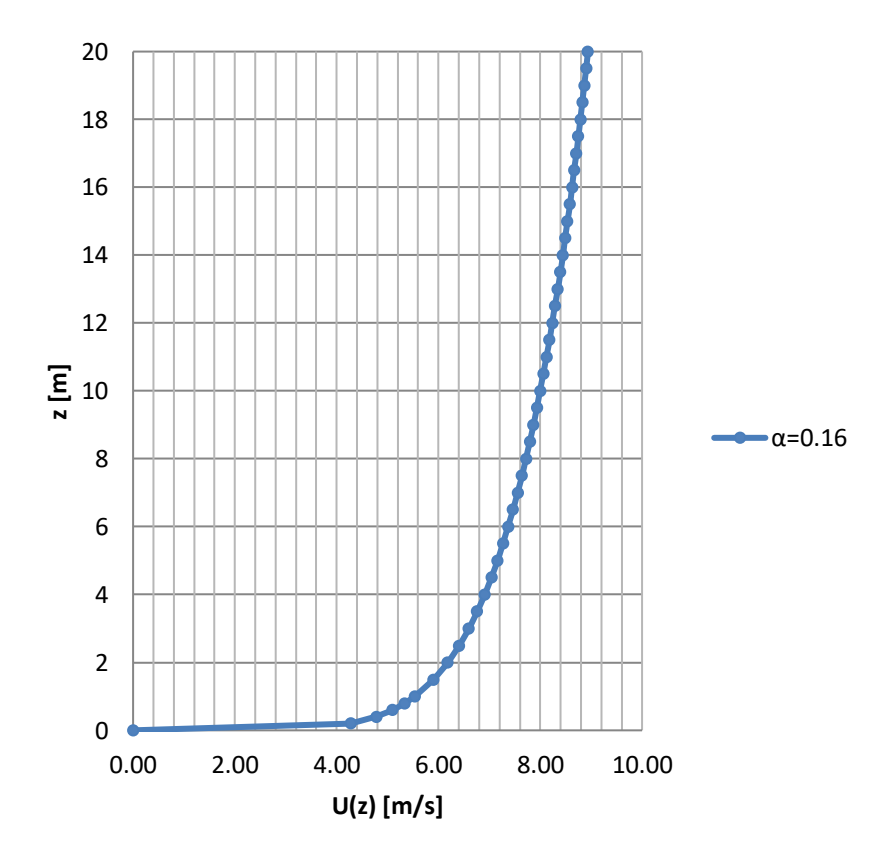


Fig. 1-1 - The incident wind speed profile upstream of the protection screens for the exponent $\alpha = 0.16$ and the reference speed U(10) = 8 m/s

Figure 1-2 shows the speed profile of the incident wind upstream of the protection screens for the exponent $\alpha = 0.16$ and the reference speed U(10) = 12 m/s.

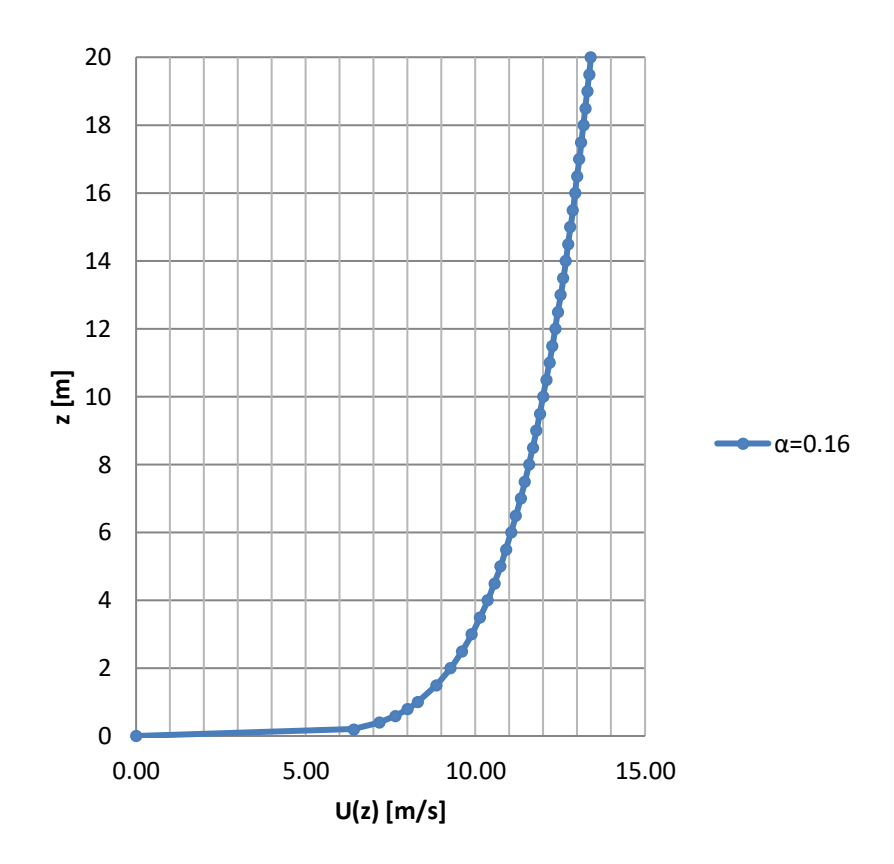


Fig. 1-2 - The incident wind speed profile upstream of the protection screens for the exponent α = 0.16 and the reference speed U(10) = 12 m/s

Figure 1-3 shows the speed profile of the incident wind upstream of the protection screens for the exponent $\alpha = 0.16$ and the reference speed U(10) = 16 m/s.

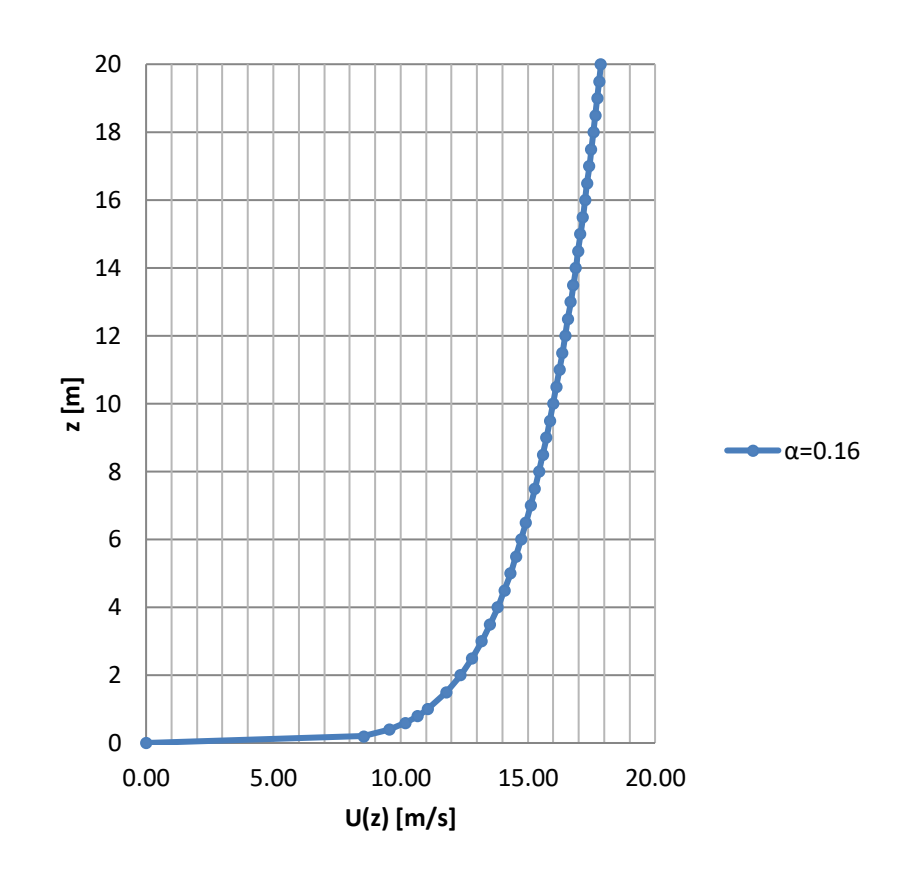


Fig. 1-3- The incident wind speed profile upstream of the protection screens for the exponent a = 0.16 and the reference speed U(10) = 16 m/s

d. Condition on exit from the computational domain

To exit the calculation range, the Outlet type condition was chosen, having the pressure set to 0.

e. Boundary condition for the protection screens

For the permeable protection screens, the screen-type limit condition was chosen, with a degree of permeability of 40%, with the diameter of the wires that make up the screen of 1 mm.

1.4 Discretization of the computational domain

For the discretization of the model, COMSOL Multiphysics® software uses different numerical techniques depending on the type of simulation studied. The predominant discretization methods are based on finite elements. Consequently, the general purpose placement algorithm creates a network with appropriate item types to match the associated numerical methods. For example, the default algorithm can use a tetrahedral network or a combination of a tetrahedral network and a network for boundary condition areas, with a combination of element types, to provide faster and more accurate results.

As the default element type for most application modes, COMSOL Multiphysics uses second-order Lagrange elements or shape functions. These and other higher order elements add additional degrees of freedom to the midpoints and inner nodes of the discretized elements. These degrees of freedom offer a more precise solution, but also require more memory due to the finesse of the discretized system. For

many fields of application, such as the study of loads in structural and solid mechanics, the increased accuracy of a second-order element is important. In modeling fluid flow using incompressible Navier-Stokes equations, a combination of element types that use an element for the higher-order velocity component than for the pressure component usually provides the best results. The default element for the Navier-Stokes Incompressible application mode is element P2-P1 using second-order elements for speed components and linear elements for pressure.

The discretization used in a fluid flow simulation depends on the flow pattern and the accuracy required in the simulation. A fluid flow pattern may inherently require fine discretization to converge, even if the results may not properly require high accuracy.

2. NUMERICAL TESTING, ORDERING, AND CODING OF TESTS

Numerical tests, a total of 48, were performed for 3 reference wind speeds, for 4 types of protection screens assemblies and for 4 downstream sections of the screens.

2.1 Numerical tests ordening

The 48 numerical tests (48TN) in this research are ordered as follows:

- 16 numerical tests grouped in 3 categories of numerical tests CTi, i = 1,2,3 (CT1, CT2, CT3), each of these categories corresponding to a reference speed of the upstream incident wind, U(10) (U(10)=8 m/s, U(10)=12 m/s, U(10)=16 m/s);
- each category of numerical CTi tests comprises 4 groups of tests GTi,j (GT1,1...GT3,4); each test group corresponds to the number of protection screens (n=1, 2, 3, 4);
- each group of tests GTi, j comprises 4 numerical tests TNi, j, k, corresponding to the 4 sections located at the distances d_{av} from the last row of protection screens (d_{av} =2H, d_{av} =4H, d_{av} =6H, d_{av} =8H).

Table 2.1 shows, schematically, the way in which the numerical tests are ordered by reference speeds, by the number of protection screens and by the position of the downstream sections..

Tab. 2.1. Numerical tests ordering

CT- Category	1CT=4GT=16TN	3CT i	CT1CT3	3CT=12GT=48TN
Tests		(i=13)		
GT- Group	1GT=4TN	12GT i,j	GT1,1GT3,4	12GT=48TN
Tests		(i=13, j=14)		
TN-	1TN=1TN	48TN i,j,k (i=13,	TN1,1,1TN3,4,4	48TN=48TN
Numerical		j=14, k=14)		
tests				

Table 2.2 shows the distribution of numerical TN tests related to downstream day distances, by groups of GT tests corresponding to the number of protection screens n and by categories of CT tests related to reference speeds U(10).

Tab. 2.2. Distribution of TN numerical tests by groups of GT tests and by categories of CT tests

	<i>U</i> (10)=	Γ1 =8 m/s		CT2 <i>U</i> (10)=12 m/s				CT3 <i>U</i> (10)=16 m/s			
GT1,1 n=1	GT1,2 n=2	GT1,3 n=3	GT1,4 n=4	GT2,1 n=1	GT2,2 n=2	GT2,3 n=3	GT2,4 n=4	GT3,1 n=1	GT3,2 n=2	GT3,3 n=3	GT3,4 n=4
TN1,1,1	TN1,2,1	TN1,3,1	TN1,4,1	TN2,1,1	TN2,2,1	TN2,3,1	TN2,4,1	TN3,1,1	TN3,2,1	TN3,3,1	TN3,4,1
d _{RX} =2H	d _{ax} =2H	d _{ax} =2H	d _{ax} =2H	d _{ax} =2H	d _{ax} =2H	d _{ax} =2H	d _{ax} =2H	d _{ax} =2H	d _{ax} =2H	d _{ax} =2H	d _{ax} =2H
TN1,1,2	TN1,2,2	TN1,3,2	TN1,4,2	TN2,1,2	TN2,2,2	TN2,3,2	TN2,4,2	TN3,1,2	TN3,2,2	TN3,3,2	TN3,4,2
d _{ax} =4H	d _{ax} =4H	d _{ax} =4H	d _{ax} =4H	d _{ax} =4H	d _{ax} =4H	d _{ax} =4H	d _{ax} =4H	d _{ax} =4H	d _{ax} =4H	d _{ax} =4H	d _{ax} =4H
TN1,1,3	TN1,2,3	TN1,3,3	TN1,4,3	TN2,1,3	TN2,2,3	TN2,3,3	TN2,4,3	TN3,1,3	TN3,2,3	TN3,3,3	TN3,4,3
d _{ax} =6H	d _{ax} =6H	d _{ax} =6H	d _{ax} =6H	d _{ax} =6H	d _{ax} =6H	d _{ax} =6H	d _{ax} =6H	d _{ax} =6H	d _{ax} =6H	d _{ax} =6H	d _{ax} =6H
TN1,1,4	TN1,2,4	TN1,3,4	TN1,4,4	TN2,1,4	TN2,2,4	TN2,3,4	TN2,4,4	TN3,1,4	TN3,2,4	TN3,3,4	TN3,4,4
d _{ax} =8H	<i>d</i> _{ax} =8H	<i>d</i> _{ex} =8H	d _{ax} =8H	<u>d</u> ,x=8H	d _{ax} =8H	d _{ax} =8H	d _{ax} =8H	d _{ax} =8H	d _{ax} =8H	<u>d</u> _{ax} =8H	d _{ax} =8H

2.2 Coding of numerical tests

For a better control over the numerical tests performed in this paper, they were coded by a basic code (CB) and a code specific to the numerical test performed (CT).

Basic Code CB:P-H-d-dam

Ex: CB:40-10-4-2H

where,

P – degree of penetrability (P=40 %)

H – the height of the protection screens (H=10 m)

d – the distance between the protection screens in the wind direction (d=4 m)

 d_{am} — distance measured upstream of the first row of protective screens at which the incident wind speed profile is considered (d_{am} =2H)

Aerodynamic Test Code (or Test Category) CT:U(10)-n-dav

Ex : CT:8-2-6H for U(10)=8 m/s, n=2 rows, $d_{av}=6$ H

where,

U(10) – incident wind speed, 10 m from the ground

n – the number of protection screens

 d_{av} – the distance measured downstream from the last row of protective screens



3. RESULTS OF NUMERICAL SIMULATIONS

In this chapter, the numerical tests performed for 3 reference speeds of the incident wind are presented (U(10)=8 m/s, U(10)=12 m/s, U(10)=16 m/s), for 4 types of protection screens (n=1, 2, 3, 4 screens) and for 4 downstream sections of the screens $(d_{av}=2H, d_{av}=4H, d_{av}=6H, d_{av}=8H)$.

3.1 Numerical testing for test category CT1 (U(10)=8m/s)

3.1.1 Numerical testing for the test group GT1,1 (n=1 screen) from the tests category CT1 (U(10)=8m/s)

These numerical tests were performed for the situations included in the group of numerical tests GT1,1 which refer to the movement of air over a sandy soil provided with 1 row of permeable protective screens. (n=1), group belonging to the category of numerical tests CT1 relating to a reference speed upstream of the protection screen (U(10)=8 m/s).

The calculation range corresponding to the GT1,1 numerical test group has a length of 100 m (10H) and a height of 20 m. At a distance of 2H = 20 m from the section entering the calculation range there is a protection screen with permeability of 40% and with height H = 10 m.

The following figure shows the diagram of the calculation range in the range of motion for the case of the location of n = 1 protection screens (CT1, GT1,1, CB:40-10-4-2H).

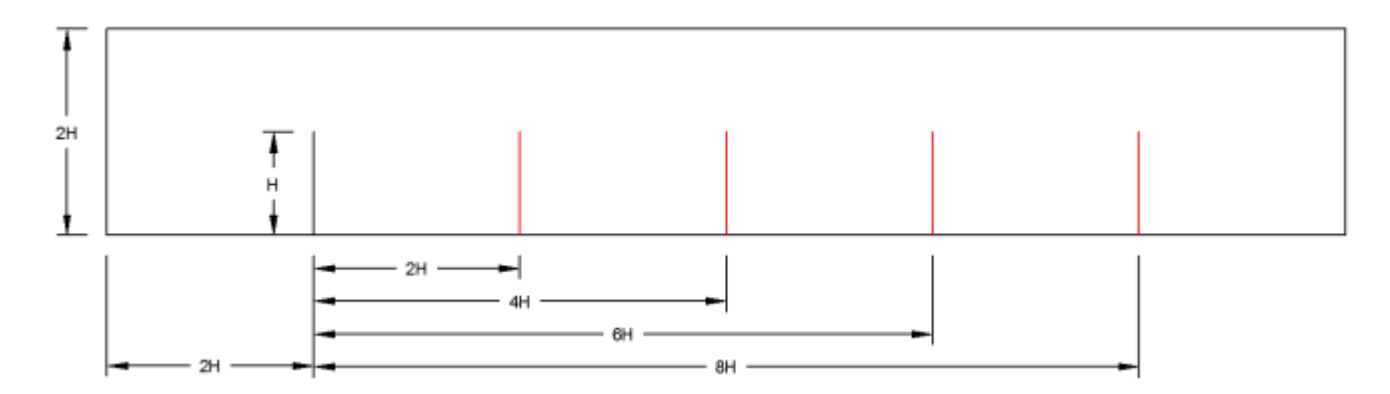


Fig. 3-1 - Schematic of the computational domain for the case of placing n = 1 protection screens (CT1, GT1,1, CB:40-10-4-2H)

The calculation domain from the computational domain thus established, was then meshed, generating the computing network for calculations, with the COMSOL Multiphysics program at a level of discretization that ensures the obtaining of a speed field, on the range of motion, with a convenient approximation.

Figure 3-2 shows the discretization of the computational domain in the area of the protection screens, for a number of protection screens n=1 (CT1, GT1,1, CB:40-10-4-2H).

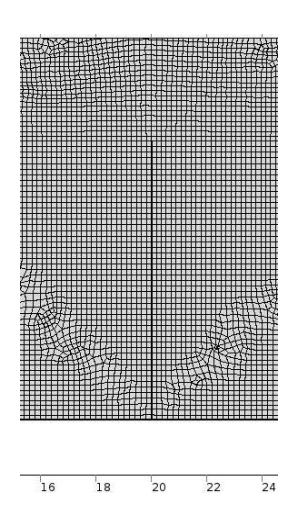


Fig. 3-2 - Discretization of the computational domain in the area of the protection screens, for a number of protection screens n=1 (CT1, GT1,1, CB:40-10-4-2H)

Applying, on the computational domain, the finite element model COMSOL Multiphysics, the velocity range in this calculation field is obtained.

Figure 3-3 shows the speed field in the computational domain for the reference speed U(10)=8 m/s and number of protection screens n=1 (CT1,GT1,1, CB:40-10-4-2H).

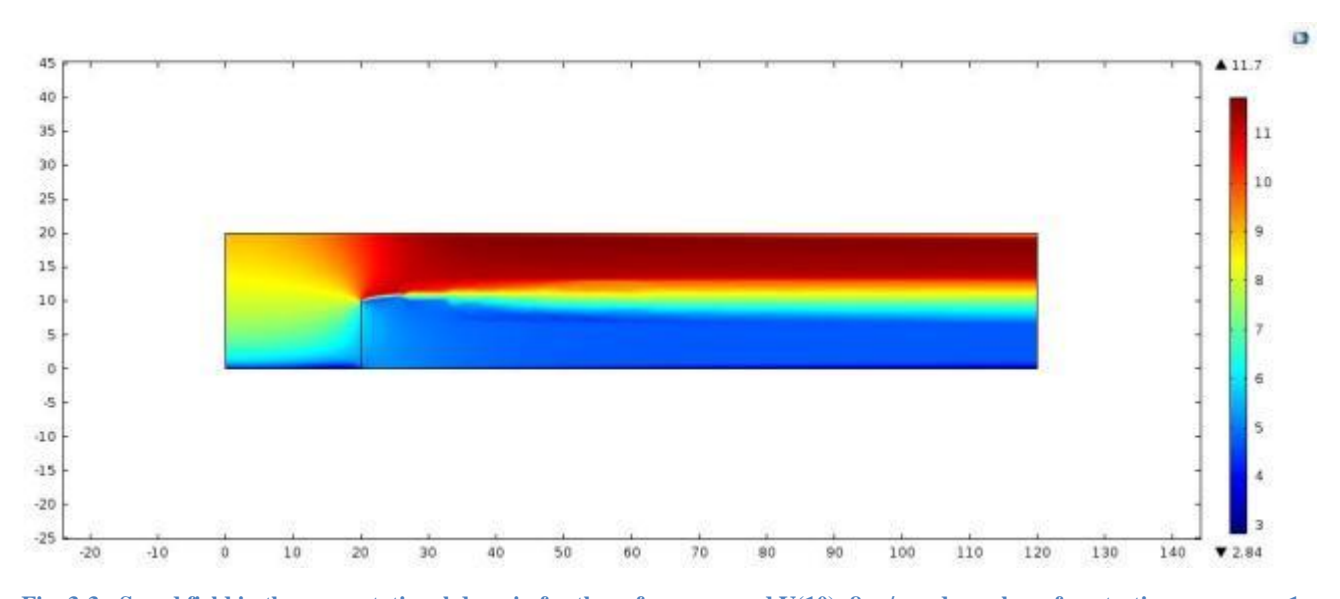
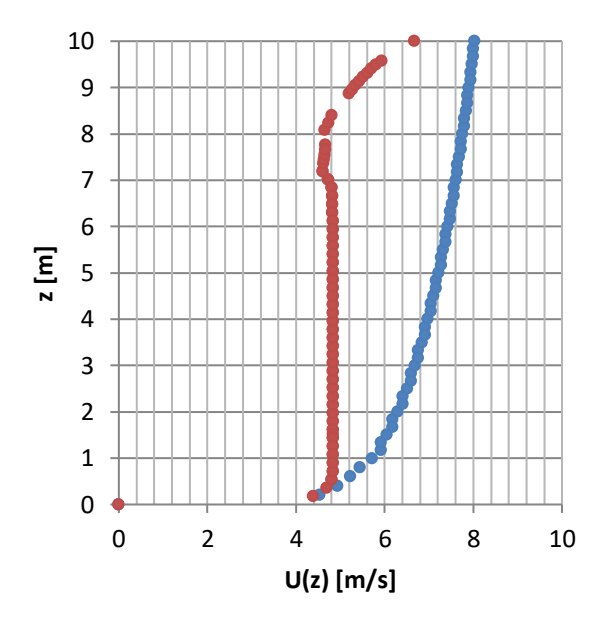


Fig. 3-3 - Speed field in the computational domain for the reference speed U(10)=8 m/s and number of protection screens n=1 (CT1, GT1,1, CB:40-10-4-2H)

From the speed field corresponding to the test group GT1,1, from the category of tests CT1, the speed profiles from 4 sections located at the downstream distances from the protection screens were extracted, $d_{av} = 2H$, $d_{av} = 4H$, $d_{av} = 6H$, $d_{av} = 8H$. These speed profiles were represented up to the height z = 10 m, because, for the present research, only the speeds at heights $z_1 = 0.20$ m, $z_2 = 1.00$ m and $z_3 = 2.00$ m are concerned, heights at which the phenomenon of sand entrainment produces.

The speed profiles in the 4 sections downstream of the protection screen ($d_{av} = 2H$, $d_{av} = 4H$, $d_{av} = 6H$, $d_{av} = 8H$), resulting from the reduction of the incident wind speed, were compared with the power law type speed profile in upstream of the protection screens, i.e. at heights $z_1 = 0.20$ m, $z_2 = 1.00$ m and $z_3 = 2.00$ m.

Figures 3-4, 3-5, 3-6, 3-7 show the speed profiles U(z) downstream of the screen, for the reference speed U(10)=8 m/s and number of protection screens n=1, at distances dav=2H (CT1, GT1,1, TN1,1,1, CB: 40-10-4-2H, CT: 8-1-2H), $d_{av}=4H$ (CT1, GT1,1, TN1,1,2, CB:40-10-4-2H, CT:8-1-4H), dav=6H (CT1, GT1,1, TN1,1,3, CB:40-10-4-2H, CT: 8-1-6H), dav=8H (CT1, GT1,1, TN1,1,4, CB:40-10-4-2H, CT:8-1-8H), compared to the speed profile of the incident wind.



• Profil viteza amonte • Profil viteza aval dav=2H

Fig. 3-4- Speed profile U(z) downstream of the screens, for reference speed U(10)=8m/s and number of protection screens n=1, at distance dav=2H (CT1, GT1,1, TN1,1, 1, CB:40-10-4-2H, CT:8-1-2H). Comparison with the incident wind speed profile.

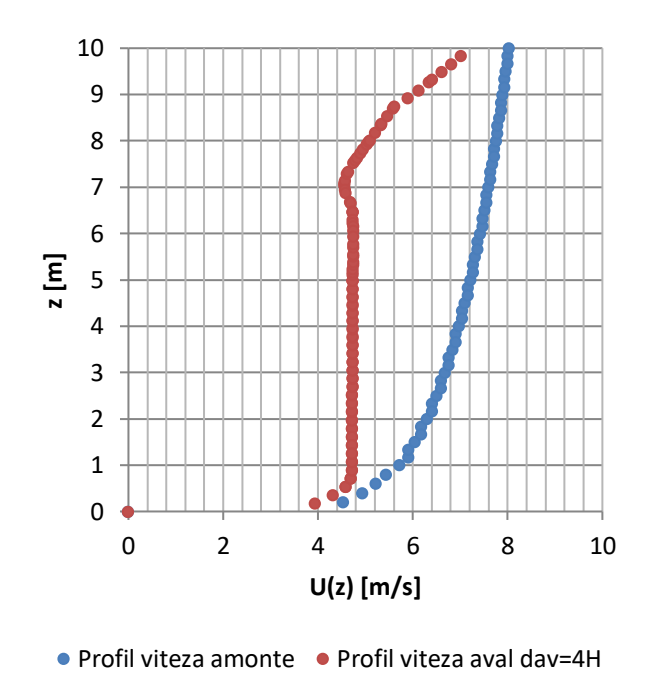


Fig. 3-5 - Speed profile U(z) downstream of the screens, for reference speed U(10)=8m/s and number of protection screens n=1, at distance dav=4H (CT1, GT1,1, TN1,1, 2, CB:40-10-4-2H, CT:8-1-4H). Comparison with the incident wind speed profile.

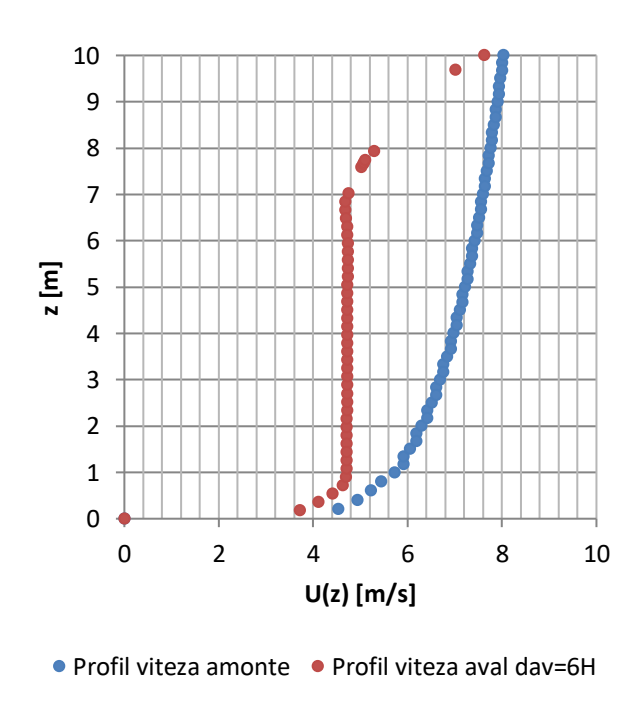


Fig. 3-6 - Speed profile U(z) downstream of the screens, for reference speed U(10)=8m/s and number of protection screens n=1, at distance dav=6H (CT1, GT1,1, TN1,1, 3, CB:40-10-4-2H, CT:8-1-6H). Comparison with the incident wind speed profile.

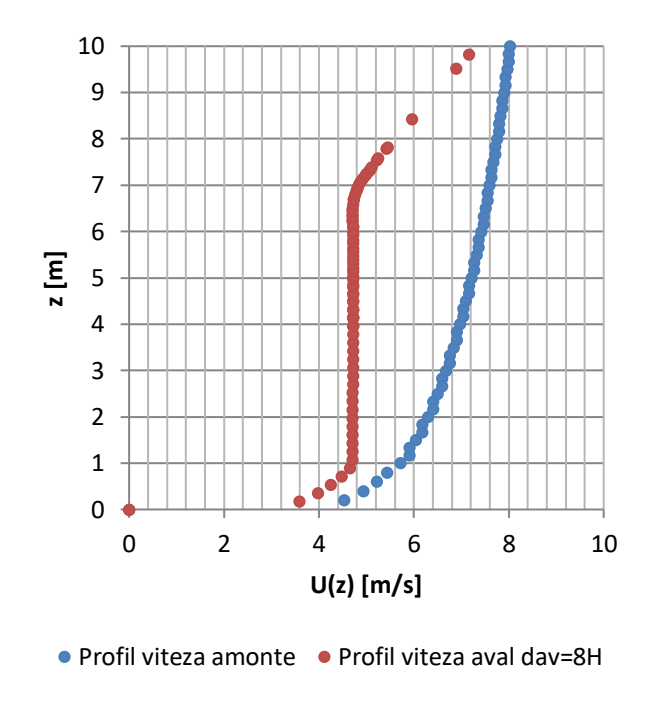


Fig. 3-7 - Speed profile U(z) downstream of the screens, for reference speed U(10)=8m/s and number of protection screens n=1, at distance dav=8H (CT1, GT1,1, TN1,1, 4, CB:40-10-4-2H, CT:8-1-8H). Comparison with the incident wind speed profile.

Next, wind speeds were determined at heights z_1 =0,20 m, z_2 =1,00 m si z_3 =2,00 m from the speed profiles corresponding to the downstream sections of the protection screens located at distances d_{av} =2H, d_{av} =4H, d_{av} =6H, d_{av} =8H.

Figure 3-8 shows the variation of U speeds at heights z_1 =0,20m, z_2 =1m şi z_3 =2m, depending on the downstream distance d_{av} for the reference speed U(10)=8 m/s and number of protection screens n=1 (CT1, GT1.1, CB:40-10-4-2H).

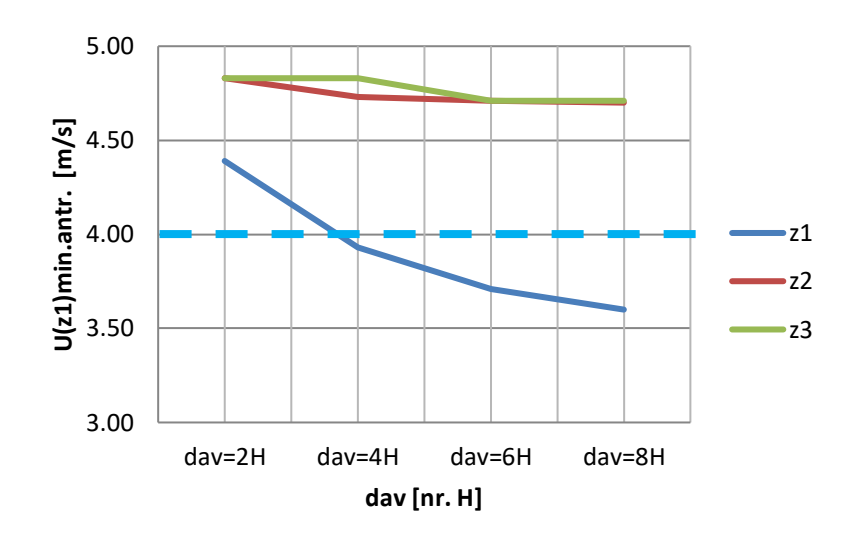


Fig. 3-8 - Variation of U speeds at heights z1=0,20m, z2=1m and z3=2m, depending on the downstream distance day for the reference speed U(10)=8 m/s and number of protection screens n=1 (CT1, GT1.1, CB:40-10-4-2H)

Then, for heights z_1 =0,20 m, z_2 =1,00 m și z_3 =2,00 m, for the sections downstream of the protection screens located at distances d_{av} =2H, d_{av} =4H, d_{av} =6H, d_{av} =8H, the differences were made between the speeds on the upstream speed profile located at d_{am} =2H and the speeds from the homologous points on the downstream speed profiles, ie ΔU =U(z)am-U(z)av.

Figure 3-9 shows the variation of the speed decrease $\Delta U = U(\mathbf{z})$ am- $U(\mathbf{z})$ av at the heights $z_1 = 0.20$ m, $z_2 = 1$ m și $z_3 = 2$ m, depending on the downstream distance d_{av} for the reference speed $U(\mathbf{10}) = \mathbf{8}$ m/s and number of protective screens n = 1 (CT1, GT1,1, CB:40-10-4-2H).

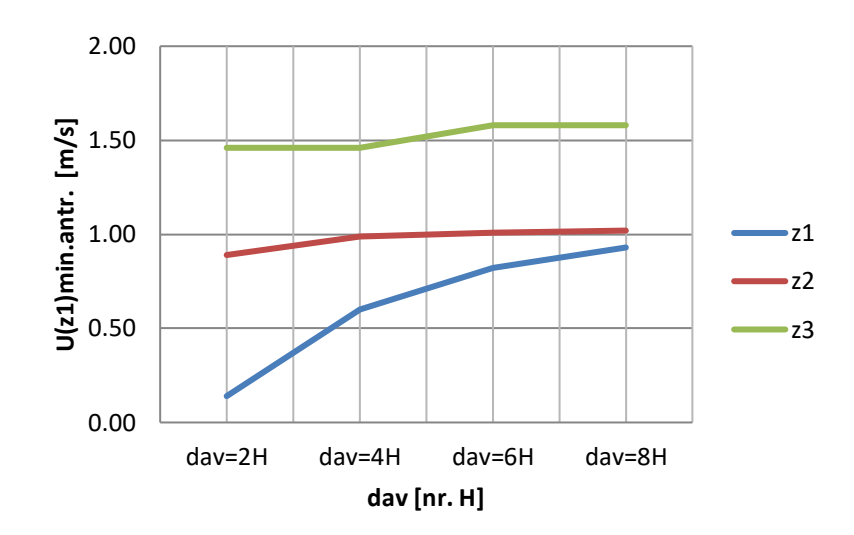


Fig. 3-9 - Variation of ΔU=U(z)am-U(z)av speeds at heights z1=0,20m, z2=1m and z3=2m, depending on the downstream distance day for the reference speed U(10)=8 m/s and number of protection screens n=1 (CT1, GT1.1, CB:40-10-4-2H)

3.1.2 Numerical testing for the test group GT1,2 (n=2 screens) from the tests category CT1 (U(10)=8m/s))

These numerical tests were performed for the situations included in the group of numerical tests GT1,2 which refer to the movement of air over a sandy soil provided with 2 rows of permeable protective screens. (n=2), group belonging to the category of numerical tests CT1 relating to a reference speed upstream of the protection screen (U(10)=8 m/s).

The calculation range corresponding to the GT1,2 numerical test group has a length of 100 m (10H) and a height of 20 m. At a distance of 2H = 20 m from the section entering the calculation range there are 2 protection screens with permeability of 40% and with height H = 10 m.

Figure 3-10 shows the diagram of the calculation range in the range of motion for the case of the location of n = 2 protection screens (CT1, GT1,2, CB:40-10-4-2H).

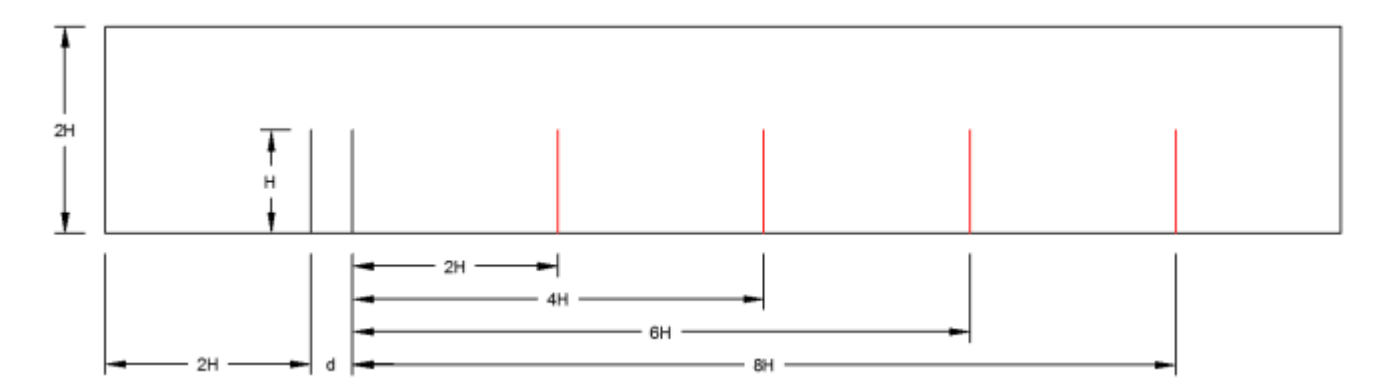


Fig. 3-10 - Schematic of the computational domain for the case of placing n = 2 protection screens (CT1, GT1,2, CB:40-10-4-2H)

The calculation domain from the computational domain thus established, was then meshed, generating the computing network for calculations, with the COMSOL Multiphysics program at a level of discretization that ensures the obtaining of a speed field, on the range of motion, with a convenient approximation

Figure 3-11 shows the discretization of the computational domain in the area of the protection screens, for a number of protection screens n=2 (CT1, GT1,2, CB:40-10-4-2H).

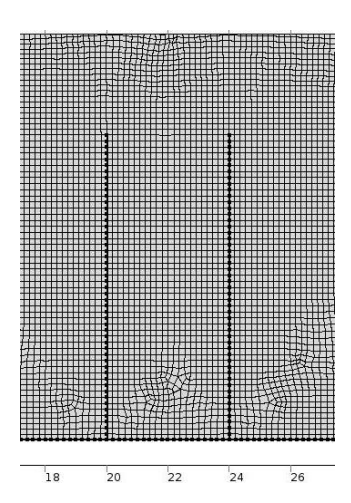


Fig. 3-11 - Discretization of the computational domain in the area of the protection screens, for a number of protection screens n=2 (CT1, GT1,2, CB:40-10-4-2H)

Applying, on the computational domain, the finite element model COMSOL Multiphysics, the velocity range in this calculation field is obtained.

Figure 3-12 shows the speed field in the computational domain for the reference speed U(10)=8 m/s and number of protection screens n=2 (CT1,GT1,2, CB:40-10-4-2H).

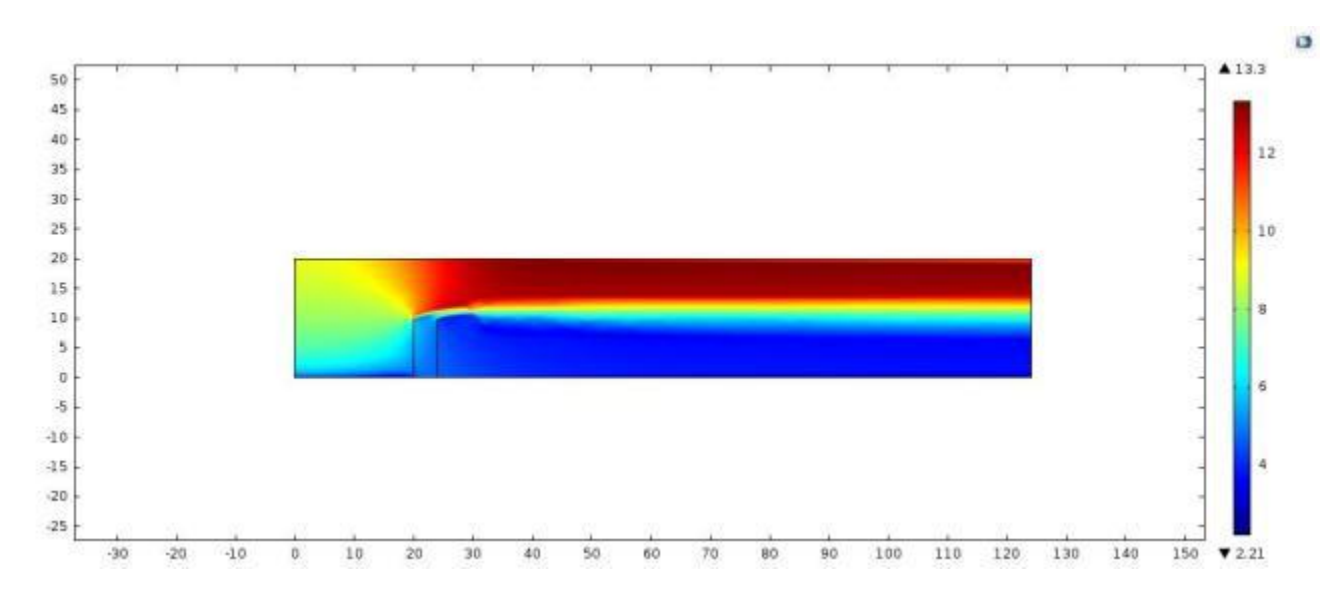


Fig. 3-12 - Speed field in the computational domain for the reference speed U(10)=8 m/s and number of protection screens n=2 (CT1, GT1,2, CB:40-10-4-2H)

From the speed field corresponding to the test group GT1,2, from the category of tests CT1, the speed profiles from 4 sections located at the downstream distances from the protection screens were extracted, $d_{av} = 2H$, $d_{av} = 4H$, $d_{av} = 6H$, $d_{av} = 8H$. These speed profiles were represented up to the height z = 10 m, because, for the present research, only the speeds at heights $z_1 = 0.20$ m, $z_2 = 1.00$ m and $z_3 = 2.00$ m are concerned, heights at which the phenomenon of sand entrainment produces.

The speed profiles in the 4 sections downstream of the protection screens ($d_{av} = 2H$, $d_{av} = 4H$, $d_{av} = 6H$, $d_{av} = 8H$), resulting from the reduction of the incident wind speed, were compared with the power law type speed profile in upstream of the protection screens, i.e. at heights $z_1 = 0.20$ m, $z_2 = 1.00$ m and $z_3 = 2.00$ m.

Figures 3-13, 3-14, 3-15, 3-16 show the speed profiles U(z) downstream of the screens, for the reference speed U(10)=8 m/s and number of protection screens n=2, at distances dav=2H (CT1, GT1,2, TN1,2,1, CB: 40-10-4-2H, CT: 8-2-2H), dav=4H (CT1, GT1,2, TN1,2,2, CB:40-10-4-2H, CT:8-2-4H), dav=6H (CT1, GT1,2, TN1,2,3, CB:40-10-4-2H, CT:8-2-6H), dav=8H (CT1, GT1,2, TN1,2,4, CB:40-10-4-2H, CT:8-2-8H), compared to the speed profile of the incident wind.

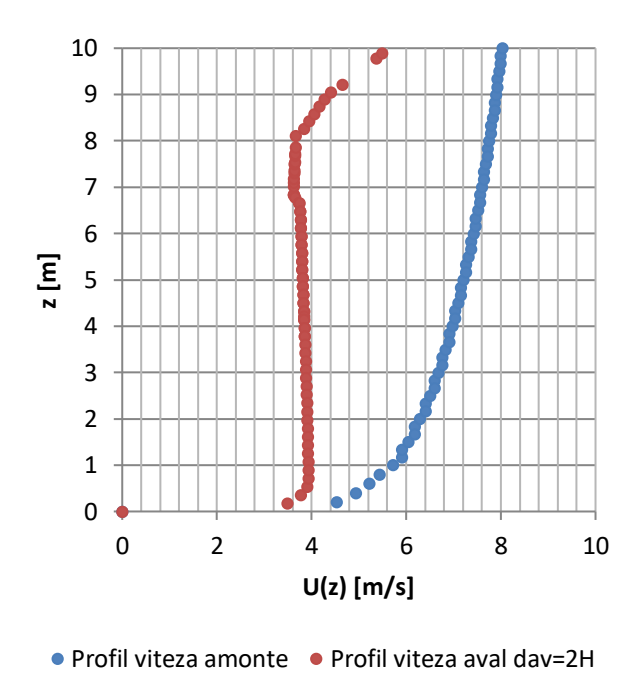


Fig. 3-13 - Speed profile U(z) downstream of the screens, for reference speed U(10)=8m/s and number of protection screens n=2, at distance day=2H (CT1, GT1,2, TN1,2,1, CB:40-10-4-2H, CT:8-2-2H). Comparison with the incident wind speed profile.

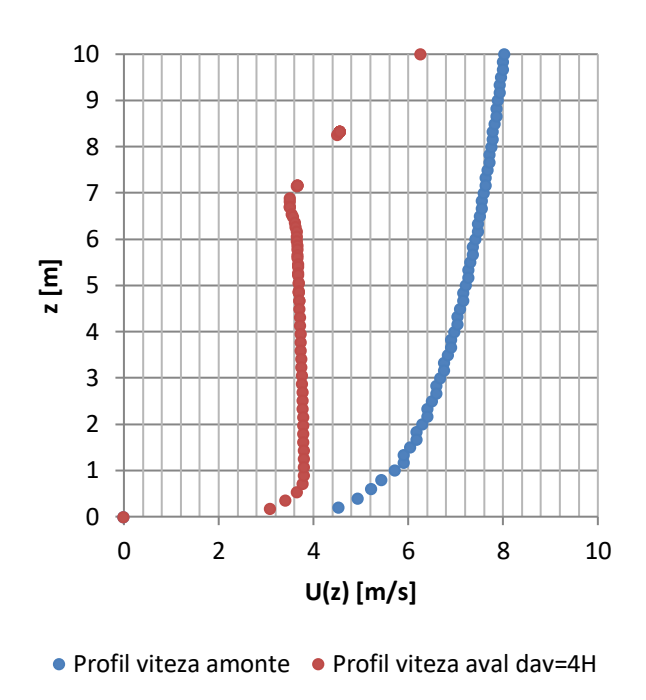


Fig. 3-14 - Speed profile U(z) downstream of the screens, for reference speed U(10)=8m/s and number of protection screens n=2, at distance dav=4H (CT1, GT1,2, TN1,2,2, CB:40-10-4-2H, CT:8-2-4H). Comparison with the incident wind speed profile.

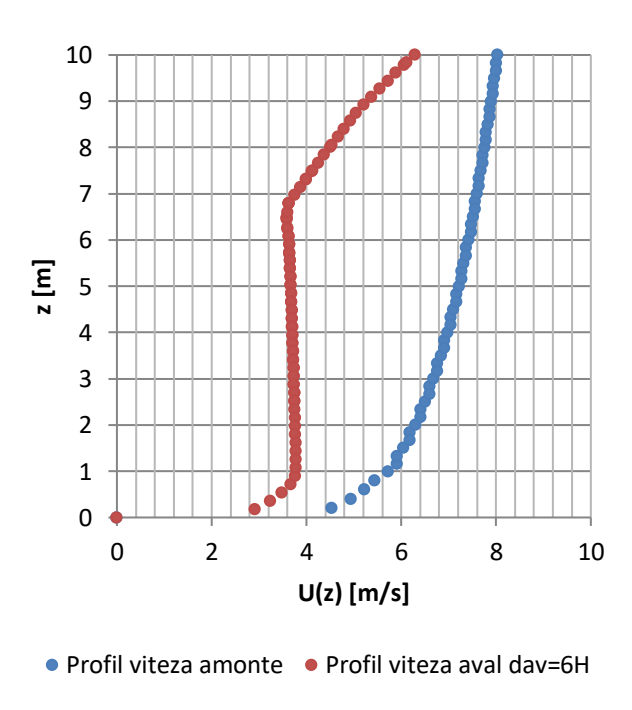


Fig. 3-15 - Speed profile U(z) downstream of the screens, for reference speed U(10)=8m/s and number of protection screens n=2, at distance dav=6H (CT1, GT1,2, TN1,2,3, CB:40-10-4-2H, CT:8-2-6H). Comparison with the incident wind speed profile.

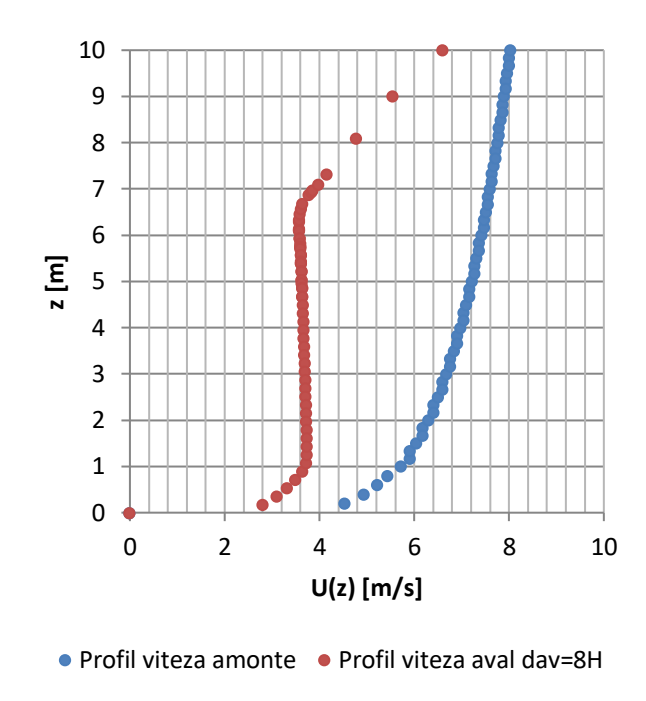


Fig. 3-16 - Speed profile U(z) downstream of the screens, for reference speed U(10)=8m/s and number of protection screens n=2, at distance dav=4H (CT1, GT1,2, TN1,2,4, CB:40-10-4-2H, CT:8-2-8H). Comparison with the incident wind speed profile.

Next, wind speeds were determined at heights z_1 =0,20 m, z_2 =1,00 m si z_3 =2,00 m from the speed profiles corresponding to the downstream sections of the protection screens located at distances d_{av} =2H, d_{av} =4H, d_{av} =6H, d_{av} =8H.

Figure 3-17 shows the variation of U speeds at heights z_1 =0,20m, z_2 =1m şi z_3 =2m, depending on the downstream distance d_{av} for the reference speed U(10)=8 m/s and number of protection screens n=2 (CT1, GT1.2, CB:40-10-4-2H).

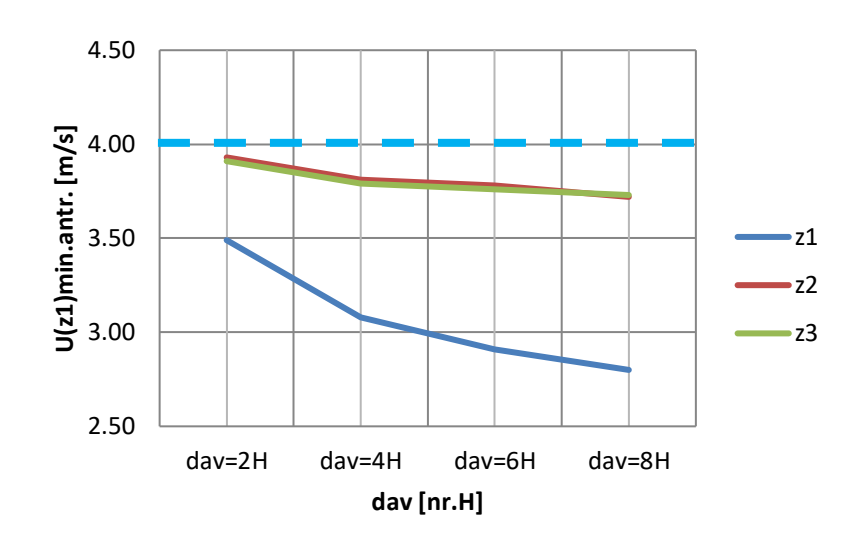


Fig. 3-17 - Variation of U speeds at heights z1=0,20m, z2=1m \pm i z3=2m, depending on the downstream distance day for the reference speed U(10)=8 m/s and number of protection screens n=2 (CT1, GT1.2, CB:40-10-4-2H)

Then, for heights z_1 =0,20 m, z_2 =1,00 m și z_3 =2,00 m, for the sections downstream of the protection screens located at distances d_{av} =2H, d_{av} =4H, d_{av} =6H, d_{av} =8H, the differences were made between the speeds on the upstream speed profile located at d_{am} =2H and the speeds from the homologous points on the downstream speed profiles, ie ΔU =U(z)am-U(z)av.

Figure 3-18 shows the variation of the speed decrease $\Delta U = U(\mathbf{z})\mathbf{am} - U(\mathbf{z})\mathbf{av}$ at the heights $z_1 = 0.20$ m, $z_2 = 1$ m şi $z_3 = 2$ m, depending on the downstream distance d_{av} for the reference speed U(10) = 8 m/s and number of protective screens n = 2 (CT1, GT1,2, CB:40-10-4-2H).

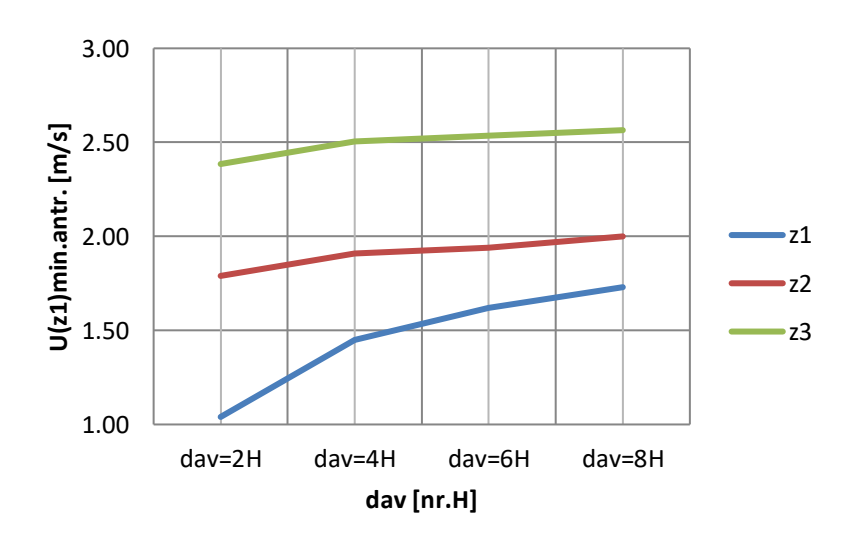


Fig. 3-18 - Variația scăderii de viteză ΔU=U(z)am-U(z)av la înălțimile z1=0,20 m, z2=1m și z3=2m, funcție de distanța aval dav pentru viteza de referință U(10)=8 m/s și număr de ecrane de protecție n=2 (CT1,GT1,2, CB:40-10-4-2H)



3.1.3 Numerical testing for the test group GT1,3 (n=3 screens) from the tests category CT1 (U(10)=8 m/s)

These numerical tests were performed for the situations included in the group of numerical tests GT1,3 which refer to the movement of air over a sandy soil provided with 3 rows of permeable protective screens. (n=3), group belonging to the category of numerical tests CT1 relating to a reference speed upstream of the protection screen (U(10)=8 m/s).

The calculation range corresponding to the GT1,3 numerical test group has a length of 100 m (10H) and a height of 20 m. At a distance of 2H = 20 m from the section entering the calculation range there is a protection screen with permeability of 40% and with height H = 10 m.

Figure 3-19 shows the diagram of the calculation range in the range of motion for the case of the location of n = 3 protection screens (CT1, GT1,3, CB:40-10-4-2H).

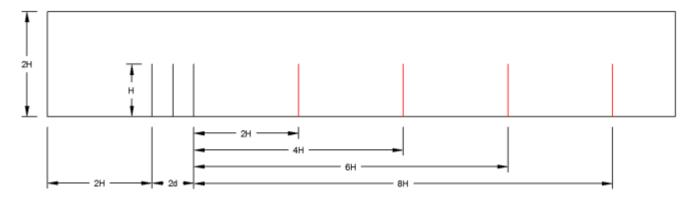


Fig. 3-19 - Schematic of the computational domain for the case of placing n = 3 protection screens (CT1, GT1,3, CB:40-10-4-2H)

The calculation domain from the computational domain thus established, was then meshed, generating the computing network for calculations, with the COMSOL Multiphysics program at a level of discretization that ensures the obtaining of a speed field, on the range of motion, with a convenient approximation.

Figure 3-20 shows the discretization of the computational domain in the area of the protection screens, for a number of protection screens n=3 (CT1, GT1,3, CB:40-10-4-2H).

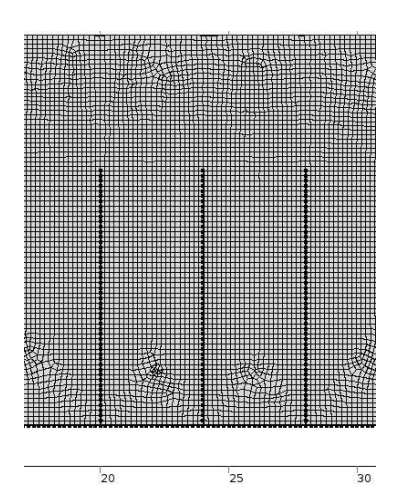


Fig. 3-20 - Discretization of the computational domain in the area of the protection screens, for a number of protection screens n=3 (CT1, GT1,3, CB:40-10-4-2H)

Applying, on the computational domain, the finite element model COMSOL Multiphysics, the velocity range in this calculation field is obtained.

Figure 3-21 shows the speed field in the computational domain for the reference speed U(10)=8 m/s and number of protection screens n=3 (CT1,GT1,3, CB:40-10-4-2H).

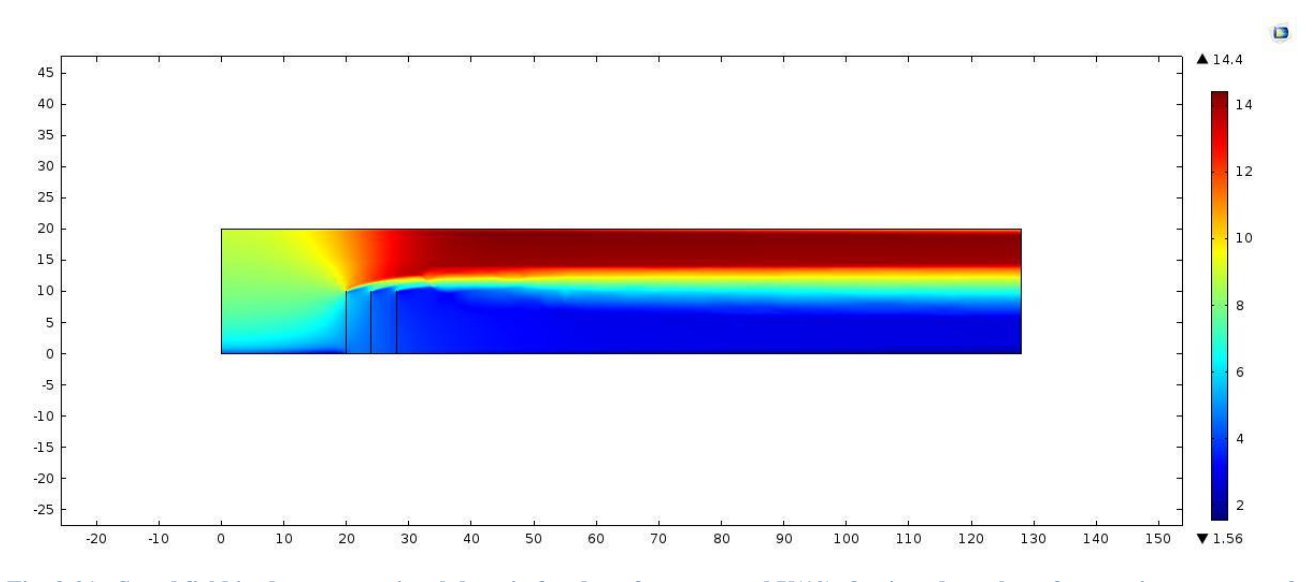
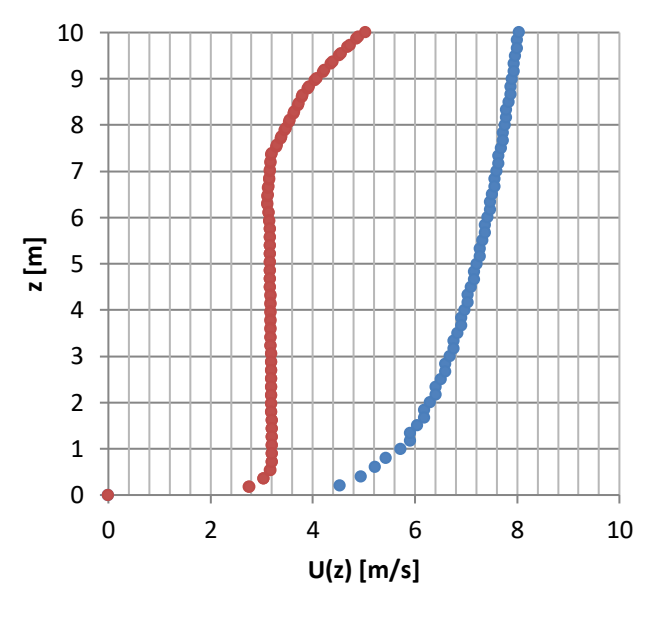


Fig. 3-21 - Speed field in the computational domain for the reference speed U(10)=8 m/s and number of protection screens n=3 (CT1,GT1,3, CB:40-10-4-2H)

From the speed field corresponding to the test group GT1,3, from the category of tests CT1, the speed profiles from 4 sections located at the downstream distances from the protection screens were extracted, $d_{av} = 2H$, $d_{av} = 4H$, $d_{av} = 6H$, $d_{av} = 8H$. These speed profiles were represented up to the height z = 10 m, because, for the present research, only the speeds at heights $z_1 = 0.20$ m, $z_2 = 1.00$ m and $z_3 = 2.00$ m are concerned, heights at which the phenomenon of sand entrainment produces.

The speed profiles in the 4 sections downstream of the protection screens ($d_{av} = 2H$, $d_{av} = 4H$, $d_{av} = 6H$, $d_{av} = 8H$), resulting from the reduction of the incident wind speed, were compared with the power law type speed profile in upstream of the protection screens, i.e. at heights $z_1 = 0.20$ m, $z_2 = 1.00$ m and $z_3 = 2.00$ m.

Figures 3-22, 3-23, 3-24, 3-25 show the speed profiles U(z) downstream of the screens, for the reference speed U(10)=8 m/s and number of protection screens n=3, at distances dav=2H (CT1, GT1,3, TN1,3,1, CB: 40-10-4-2H, CT:8-3-2H), dav=4H (CT1, GT1,3, TN1,3,2, CB:40-10-4-2H, CT:8-3-4H), dav=6H (CT1, GT1,3, TN1,3,3, CB:40-10-4-2H, CT:8-3-6H), dav=8H (CT1, GT1,3, TN1,3,4, CB:40-10-4-2H, CT:8-3-8H), compared to the speed profile of the incident wind.



Profil de viteza amonte
 Profil de viteza aval dav=2H

Fig. 3-22 - Speed profile U(z) downstream of the screens, for reference speed U(10)=8m/s and number of protection screens n=3, at distance dav= 2H (CT1,GT1,3, TN1,3,1,CB:40-10-4-2H, CT:8-3-2H). Comparison with the incident wind speed profile.

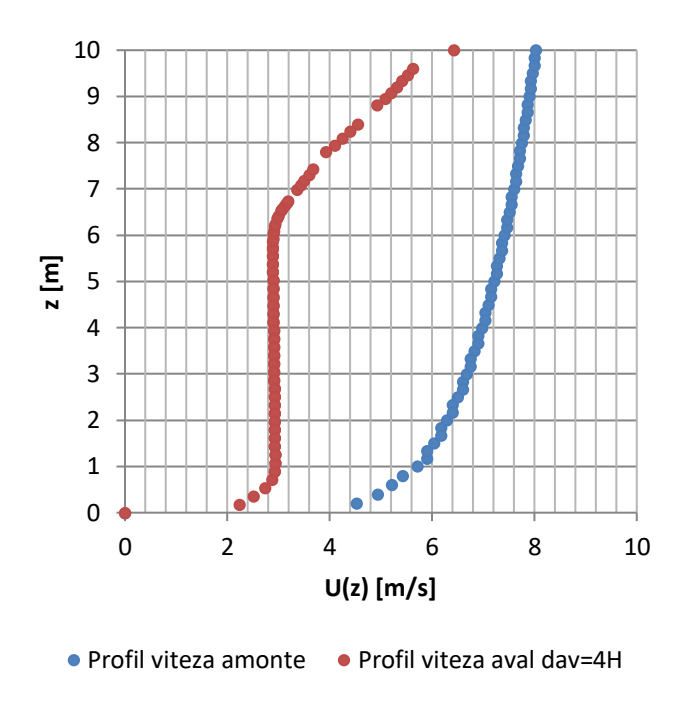


Fig. 3-23 - Speed profile U(z) downstream of the screens, for reference speed U(10)=8m/s and number of protection screens n=3, at distance dav= 4H (CT1,GT1,3, TN1,3,2,CB:40-10-4-2H, CT:8-3-4H). Comparison with the incident wind speed profile.

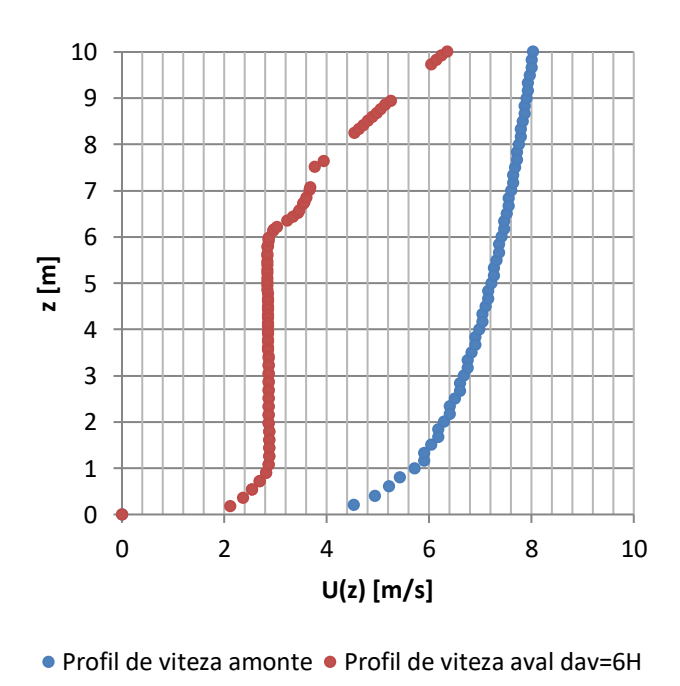


Fig. 3-24 - Speed profile U(z) downstream of the screens, for reference speed U(10)=8m/s and number of protection screens n=3, at distance dav= 6H (CT1,GT1,3, TN1,3,3, CB:40-10-4-2H, CT:8-3-6H). Comparison with the incident wind speed profile.

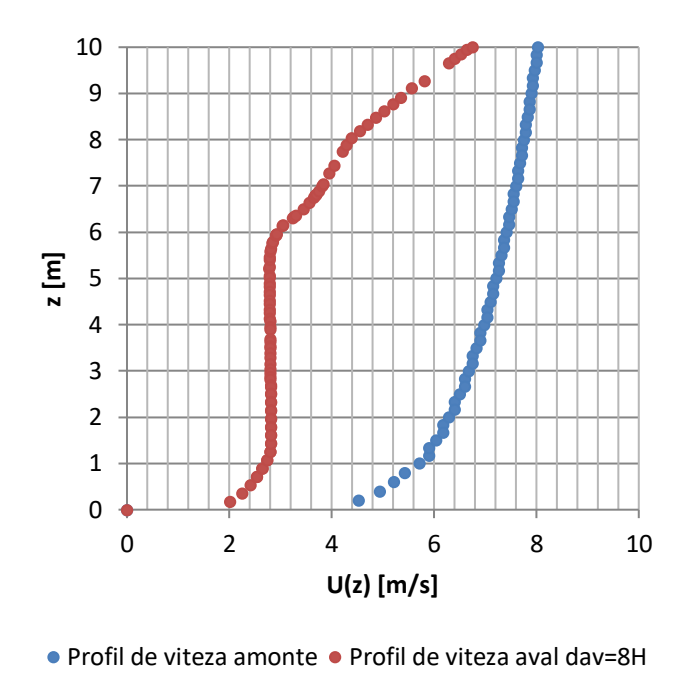


Fig. 3-25 - Speed profile U(z) downstream of the screens, for reference speed U(10)=8m/s and number of protection screens n=3, at distance day= 8H (CT1,GT1,3, TN1,3,4,CB:40-10-4-2H, CT:8-3-8H). Comparison with the incident wind speed profile.

Next, wind speeds were determined at heights z_1 =0,20 m, z_2 =1,00 m si z_3 =2,00 m from the speed profiles corresponding to the downstream sections of the protection screens located at distances d_{av} =2H, d_{av} =4H, d_{av} =6H, d_{av} =8H.

Figure 3-26 shows the variation of U speeds at heights z_1 =0,20m, z_2 =1m şi z_3 =2m, depending on the downstream distance d_{av} for the reference speed U(10)=8 m/s and number of protection screens n=3 (CT1, GT1.3, CB:40-10-4-2H).

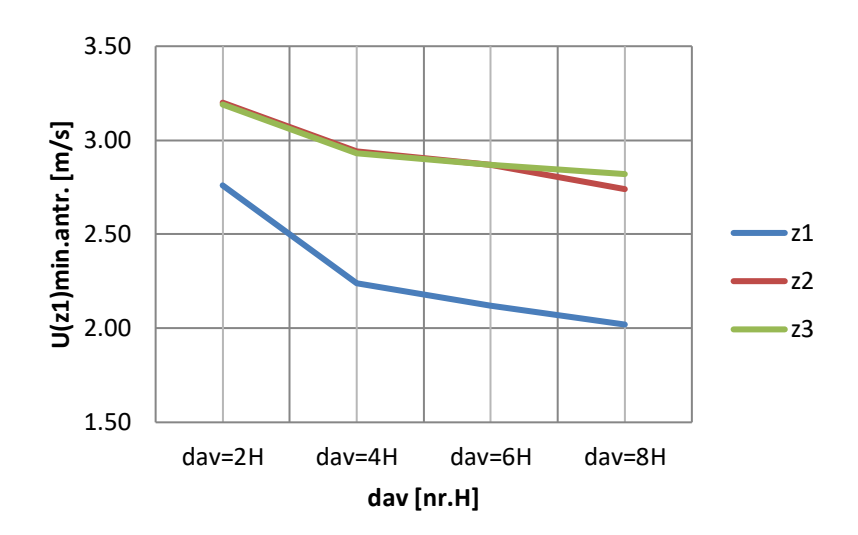


Fig. 3-26 - Variation of U speeds at heights z1=0,20m, z2=1m \pm i z3=2m, depending on the downstream distance day for the reference speed U(10)=8 m/s and number of protection screens n=3 (CT1,GT1,3, CB:40-10-4-2H)

Then, for heights z_1 =0,20 m, z_2 =1,00 m si z_3 =2,00 m, for the sections downstream of the protection screens located at distances d_{av} =2H, d_{av} =4H, d_{av} =6H, d_{av} =8H, the differences were made between the speeds on the upstream speed profile located at d_{am} =2H and the speeds from the homologous points on the downstream speed profiles, ie ΔU =U(z)am-U(z)av.

Figure 3-27 shows the variation of the speed decrease $\Delta U = U(\mathbf{z})\mathbf{am} - U(\mathbf{z})\mathbf{av}$ at the heights $z_1 = 0.20$ m, $z_2 = 1$ m şi $z_3 = 2$ m, depending on the downstream distance d_{av} for the reference speed U(10) = 8 m/s and number of protective screens n = 3 (CT1, GT1,3, CB:40-10-4-2H).

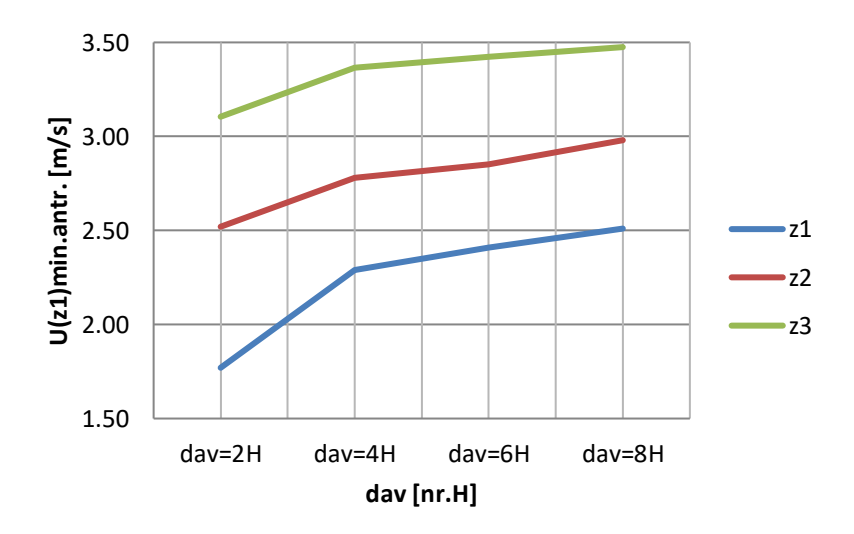


Fig. 3-27 - Variation of ΔU=U(z)am-U(z)av speeds at heights z1=0,20m, z2=1m şi z3=2m, depending on the downstream distance day for the reference speed U(10)=8 m/s and number of protection screens n=3 (CT1,GT1,3, CB:40-10-4-2H)



3.1.4 Numerical testing for the test group GT1,4 (n=4 screens) from the tests category CT1 (U(10)=8 m/s)

These numerical tests were performed for the situations included in the group of numerical tests GT1,4 which refer to the movement of air over a sandy soil provided with 4 rows of permeable protective screens. (n=4), group belonging to the category of numerical tests CT1 relating to a reference speed upstream of the protection screen (U(10)=8 m/s).

The calculation range corresponding to the GT1,4 numerical test group has a length of 100 m (10H) and a height of 20 m. At a distance of 2H = 20 m from the section entering the calculation range there is a protection screen with permeability of 40% and with height H = 10 m.

Figure 3-28 shows the diagram of the calculation range in the range of motion for the case of the location of n = 4 protection screens (CT1, GT1,4, CB:40-10-4-2H).

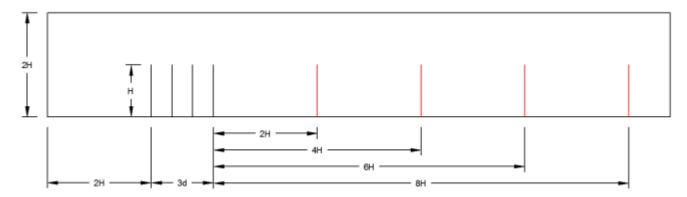


Fig. 3-28 - Schematic of the computational domain for the case of placing n = 4 protection screens (CT1, GT1,4, CB:40-10-4-2H)

The calculation domain from the computational domain thus established, was then meshed, generating the computing network for calculations, with the COMSOL Multiphysics program at a level of discretization that ensures the obtaining of a speed field, on the range of motion, with a convenient approximation.

Figure 3-29 shows the discretization of the computational domain in the area of the protection screens, for a number of protection screens n=4 (CT1, GT1,4, CB:40-10-4-2H).

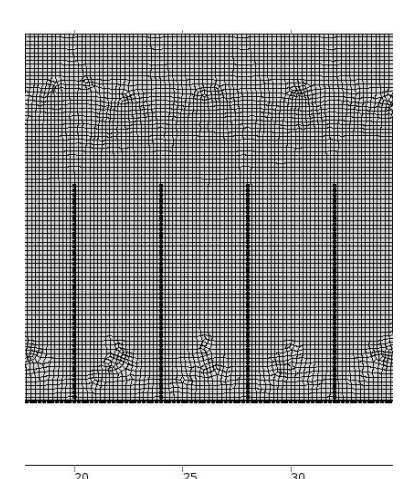


Fig. 3-29 - Discretization of the computational domain in the area of the protection screens, for a number of protection screens n=4 (CT1, GT1,4, CB:40-10-4-2H)

Applying, on the computational domain, the finite element model COMSOL Multiphysics, the velocity range in this calculation field is obtained.

Figure 3-30 shows the speed field in the computational domain for the reference speed U(10)=8 m/s and number of protection screens n=4 (CT1,GT1,4, CB:40-10-4-2H).

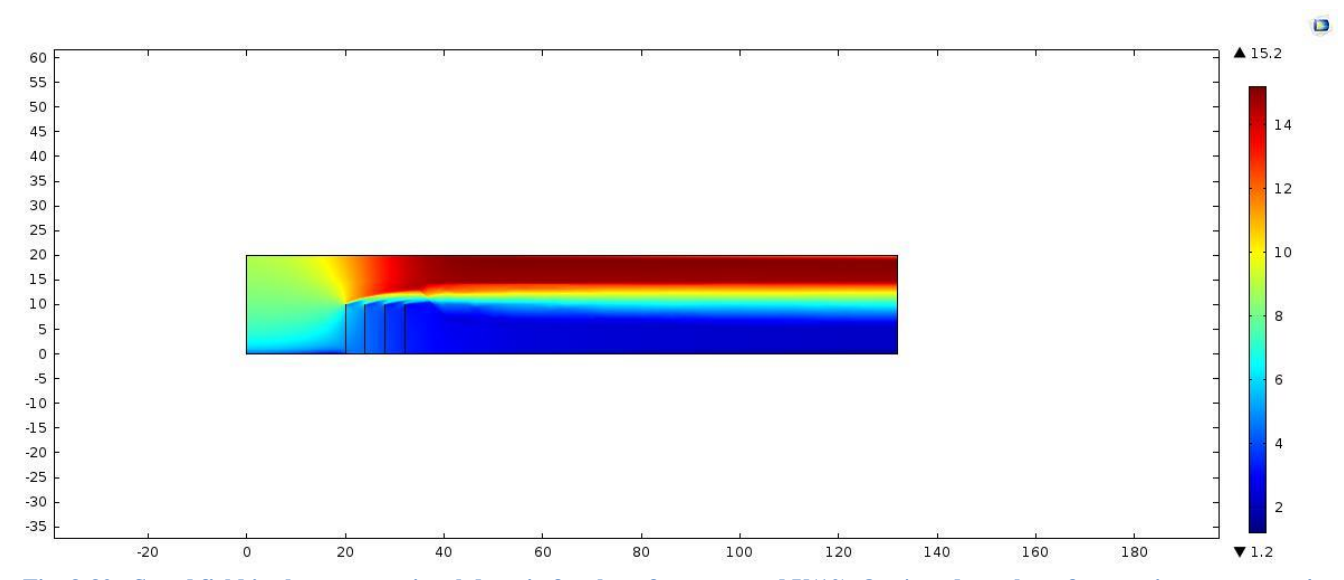


Fig. 3-30 - Speed field in the computational domain for the reference speed U(10)=8 m/s and number of protection screens n=4 (CT1,GT1,4, CB:40-10-4-2H)

From the speed field corresponding to the test group GT1,4, from the category of tests CT1, the speed profiles from 4 sections located at the downstream distances from the protection screens were extracted, $d_{av} = 2H$, $d_{av} = 4H$, $d_{av} = 6H$, $d_{av} = 8H$. These speed profiles were represented up to the height z = 10 m, because, for the present research, only the speeds at heights $z_1 = 0.20$ m, $z_2 = 1.00$ m and $z_3 = 2.00$ m are concerned, heights at which the phenomenon of sand entrainment produces.

The speed profiles in the 4 sections downstream of the protection screens (dav = 2H, dav = 4H, dav = 6H, dav = 8H), resulting from the reduction of the incident wind speed, were compared with the power law type speed profile in upstream of the protection screens, i.e. at heights z1 = 0.20 m, z2 = 1.00 m and z3 = 2.00 m.

Figures 3-31, 3-32, 3-33, 3-34 show the speed profiles U(z) downstream of the screens, for the reference speed U(10)=8 m/s and number of protection screens n=4, at distances $d_{av}=2H$ (CT1,GT1,4, TN1,4,1,CB:40-10-4-2H, CT:8-4-2H), $d_{av}=4H$ (CT1,GT1,4, TN1,4,2,CB:40-10-4-2H, CT:8-4-4H), $d_{av}=6H$ (CT1,GT1,4, TN1,4,3, CB:40-10-4-2H, CT:8-4-6H), $d_{av}=8H$ (CT1,GT1,4, TN1,3,4,CB:40-10-4-2H, CT:8-4-8H), compared to the speed profile of the incident wind.

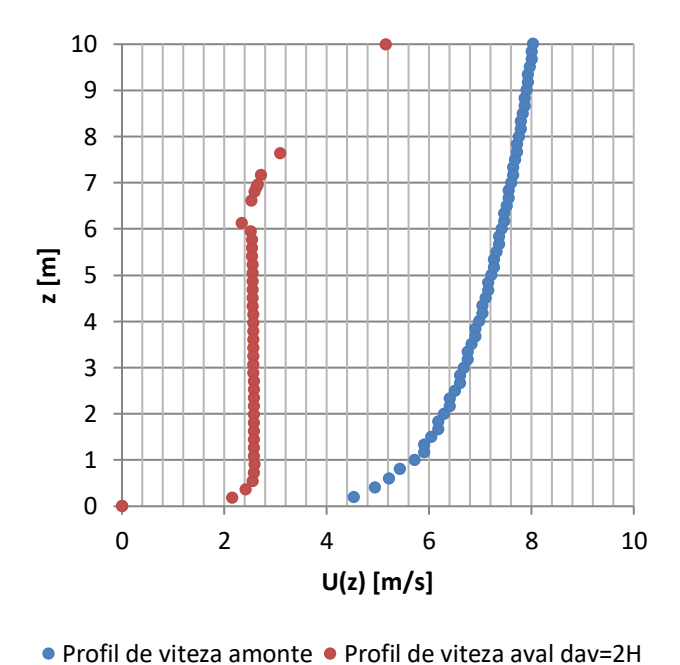


Fig. 3-31 - Speed profile U(z) downstream of the screens, for reference speed U(10)=8m/s and number of protection screens n=4, at distance dav= 2H (CT1,GT1,4, TN1,4,1,CB:40-10-4-2H, CT:8-4-2H). Comparison with the incident wind speed profile.

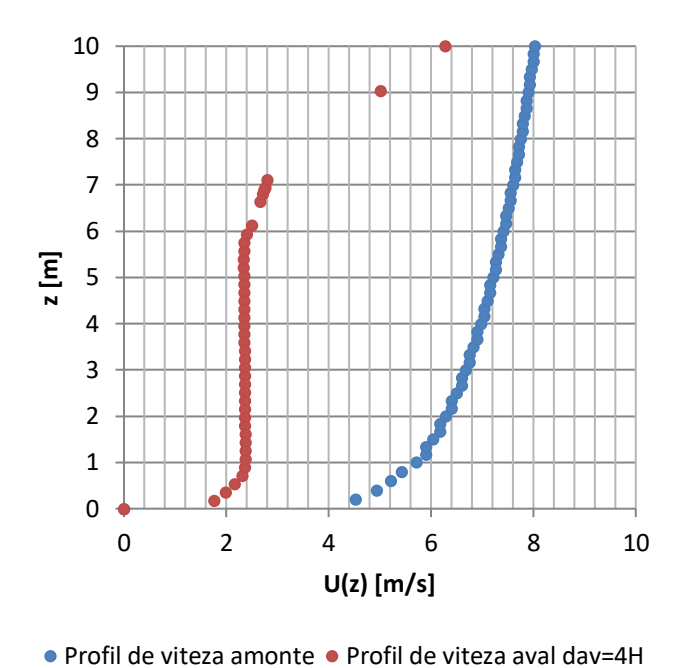


Fig. 3-32 - Speed profile U(z) downstream of the screens, for reference speed U(10)=8m/s and number of protection screens n=4, at distance day = 4H (CT1,GT1,4, TN1,4,2,CB:40-10-4-2H, CT:8-4-4H). Comparison with the incident wind speed profile.

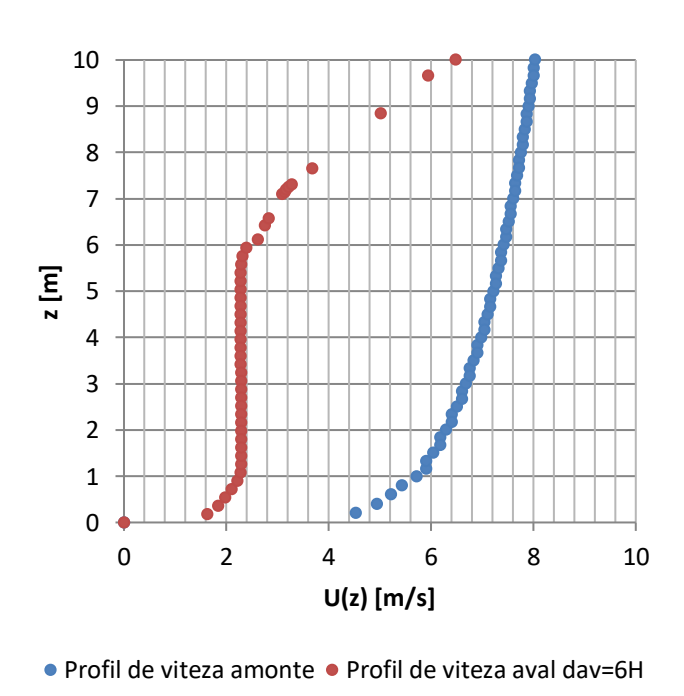


Fig. 3-33 - Speed profile U(z) downstream of the screens, for reference speed U(10)=8m/s and number of protection screens n=4, at distance dav= 6H (CT1,GT1,4, TN1,4,3, CB:40-10-4-2H, CT:8-4-6H). Comparison with the incident wind speed profile.

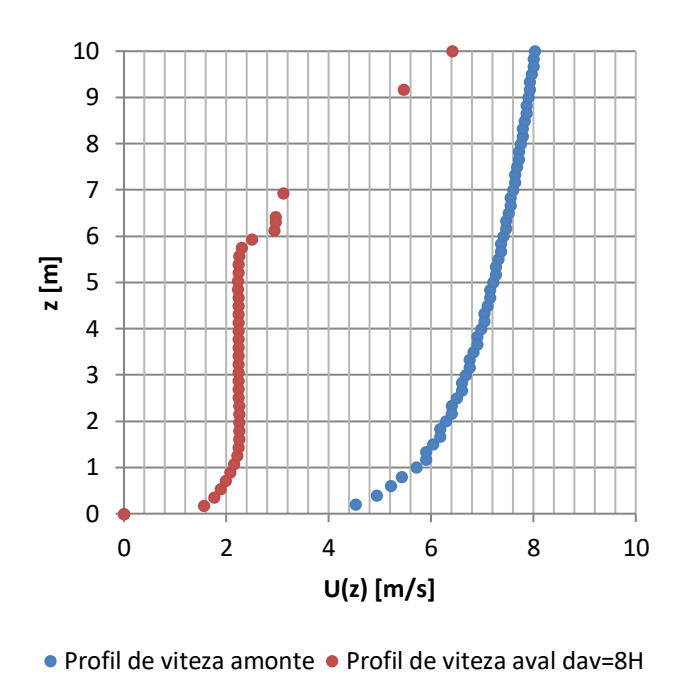


Fig. 3-34 - Speed profile U(z) downstream of the screens, for reference speed U(10)=8m/s and number of protection screens n=4, at distance dav= 8H (CT1,GT1,4, TN1,4,4,CB:40-10-4-2H, CT:8-4-8H). Comparison with the incident wind speed profile.

Next, wind speeds were determined at heights z_1 =0,20 m, z_2 =1,00 m si z_3 =2,00 m from the speed profiles corresponding to the downstream sections of the protection screens located at distances d_{av} =2H, d_{av} =4H, d_{av} =6H, d_{av} =8H.

Figure 3-35 shows the variation of U speeds at heights z_1 =0,20m, z_2 =1m şi z_3 =2m, depending on the downstream distance d_{av} for the reference speed U(10)=8 m/s and number of protection screens n=4 (CT1,GT1,4, CB:40-10-4-2H).

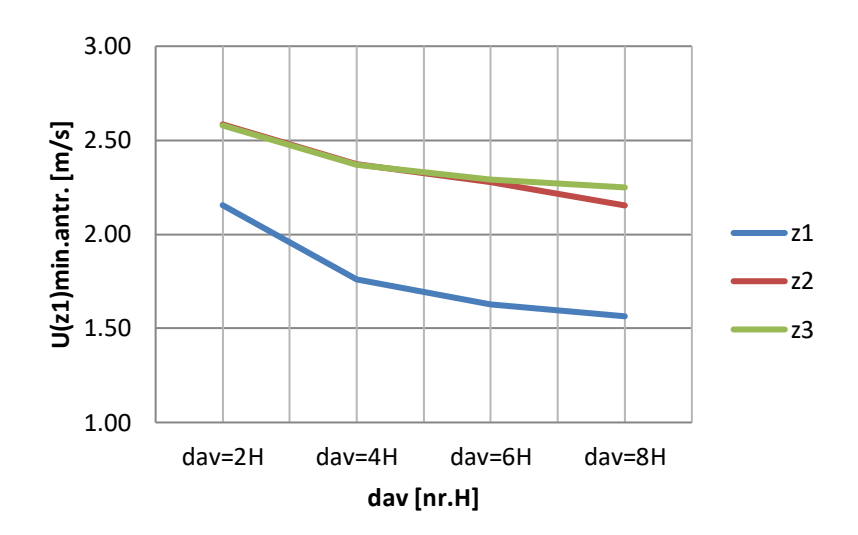


Fig. 3-35 - Variation of U speeds at heights z1=0,20m, z2=1m şi z3=2m, depending on the downstream distance day for the reference speed U(10)=8 m/s and number of protection screens n=4 (CT1,GT1,4, CB:40-10-4-2H)

Figure 3-36 shows the variation of the speed decrease $\Delta U = U(\mathbf{z})\mathbf{am} - U(\mathbf{z})\mathbf{av}$ at the heights $z_1 = 0.20$ m, $z_2 = 1$ m şi $z_3 = 2$ m, depending on the downstream distance d_{av} for the reference speed U(10) = 8 m/s and number of protective screens n = 4 (CT1,GT1,4, CB:40-10-4-2H).

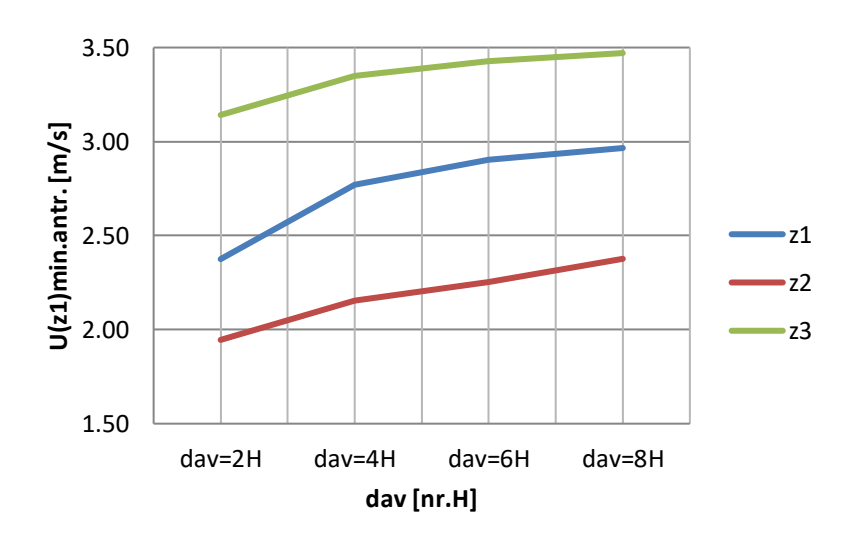


Fig. 3-36 - Variation of $\Delta U=U(z)$ am-U(z)aw speeds at heights z1=0,20m, z2=1m și z3=2m, depending on the downstream distance day for the reference speed U(10)=8 m/s and number of protection screens n=4 (CT1,GT1,4, CB:40-10-4-2H)



3.2 Numerical testing for test category CT2 (U(10)=12 m/s)

3.2.1 Numerical testing for the test group GT2,1 (n=1 screen) from the tests category CT2 (U(10)=12 m/s)

These numerical tests were performed for the situations included in the group of numerical tests GT2,1 which refer to the movement of air over a sandy soil provided with 1 row of permeable protective screens. (n=1), group belonging to the category of numerical tests CT2 relating to a reference speed upstream of the protection screen (U(10)=12 m/s).

The calculation range corresponding to the GT2,1 numerical test group has a length of 100 m (10H) and a height of 20 m. At a distance of 2H = 20 m from the section entering the calculation range there is a protection screen with permeability of 40% and with height H = 10 m.

Figure 3-37 shows the diagram of the calculation range in the range of motion for the case of the location of n = 1 protection screens (CT2, GT2,1, CB:40-10-4-2H).

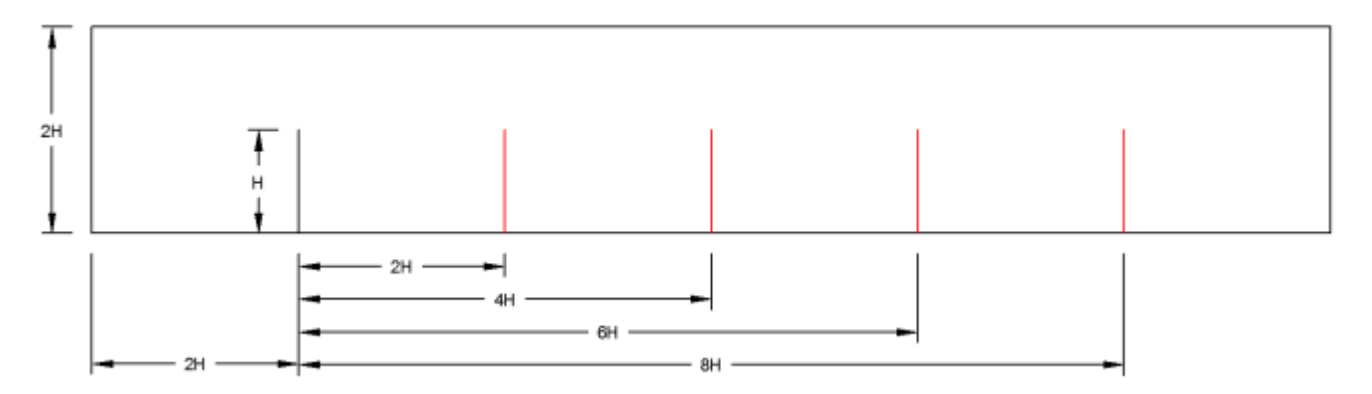


Fig. 3-37 - Schematic of the computational domain for the case of placing n = 1 protection screens (CT2, GT2,1, CB:40-10-4-2H)

The calculation domain from the computational domain thus established, was then meshed, generating the computing network for calculations, with the COMSOL Multiphysics program at a level of discretization that ensures the obtaining of a speed field, on the range of motion, with a convenient approximation.

Figure 3-38 shows the discretization of the computational domain in the area of the protection screens, for a number of protection screens n=1 (CT2, GT2,1, CB:40-10-4-2H).

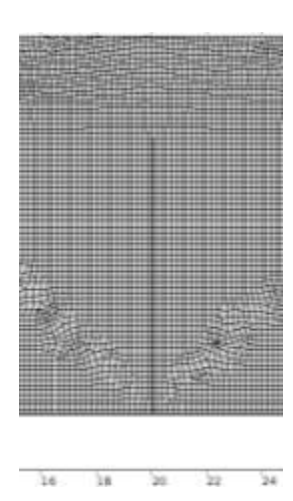


Fig. 3-38 - Discretization of the computational domain in the area of the protection screens, for a number of protection screens n=1 (CT2, GT2,1, CB:40-10-4-2H)

Figure 3-39 shows the speed field in the computational domain for the reference speed U(10)=12 m/s and number of protection screens n=1(CT2,GT2,1,CB:40-10-4-2H).

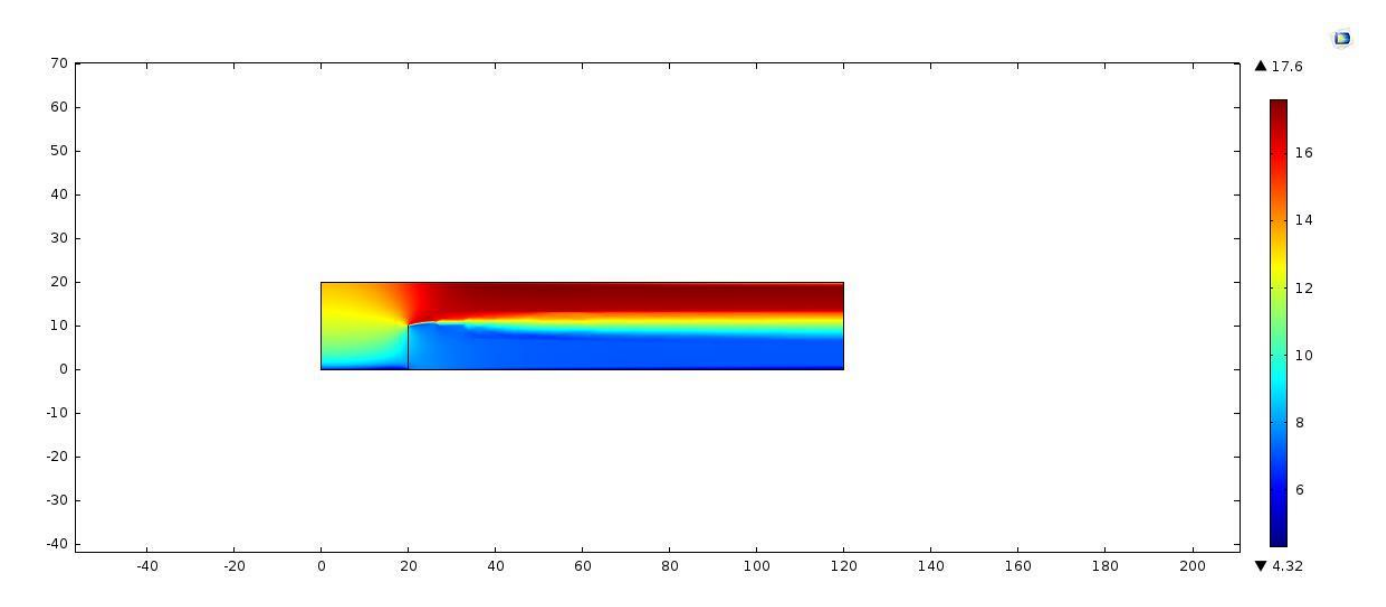
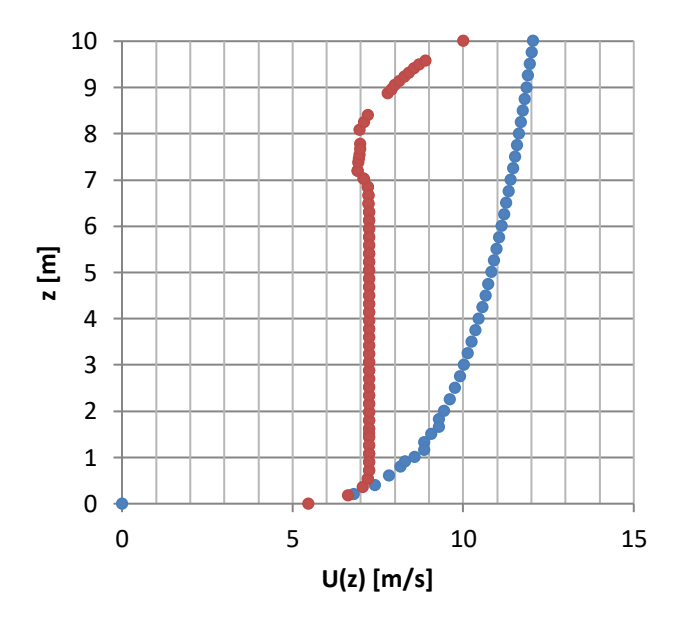


Fig. 3-39 - Speed field in the computational domain for the reference speed U(10)=12 m/s and number of protection screens n=1 (CT2,GT2,1, CB:40-10-4-2H)

From the speed field corresponding to the test group GT2,1, from the category of tests CT2, the speed profiles from 4 sections located at the downstream distances from the protection screens were extracted, $d_{av} = 2H$, $d_{av} = 4H$, $d_{av} = 6H$, $d_{av} = 8H$. These speed profiles were represented up to the height z = 10 m, because, for the present research, only the speeds at heights $z_1 = 0.20$ m, $z_2 = 1.00$ m and $z_3 = 2.00$ m are concerned, heights at which the phenomenon of sand entrainment produces.

Figures 3-40, 3-41, 3-42, 3-43 show the speed profiles U(z) downstream of the screens, for the reference speed U(10)=12 m/s and number of protection screens n=1, at distances $d_{av}=2H$ (CT2,GT2,1, TN2,1,1,CB:40-10-4-2H, CT:12-1-2H), $d_{av}=4H$ (CT2,GT2,1, TN2,1,2,CB:40-10-4-2H, CT:12-1-4H), $d_{av}=6H$ (CT2,GT2,1, TN2,1,3, CB:40-10-4-2H, CT:12-1-6H), $d_{av}=8H$ (CT2,GT2,1, TN2,1,4,CB:40-10-4-2H, CT:12-1-8H), compared to the speed profile of the incident wind.



Profil de viteza amonte
 Profil de viteza aval dav=2H

Fig. 3-40 - Speed profile U(z) downstream of the screens, for reference speed U(10)=12 m/s and number of protection screens n=1, at distance dav= 2H (CT2,GT2,1, TN2,1,1,CB:40-10-4-2H, CT:12-1-2H). Comparison with the incident wind speed profile.

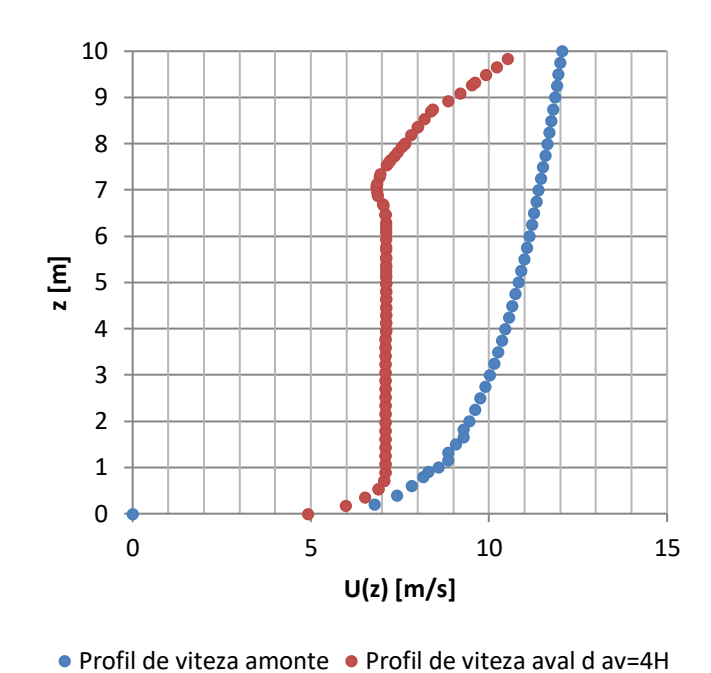


Fig. 3-41 - Speed profile U(z) downstream of the screens, for reference speed U(10)=12 m/s and number of protection screens n=1, at distance dav= 4H (CT2,GT2,1, TN2,1,2,CB:40-10-4-2H, CT:12-1-4H). Comparison with the incident wind speed profile.

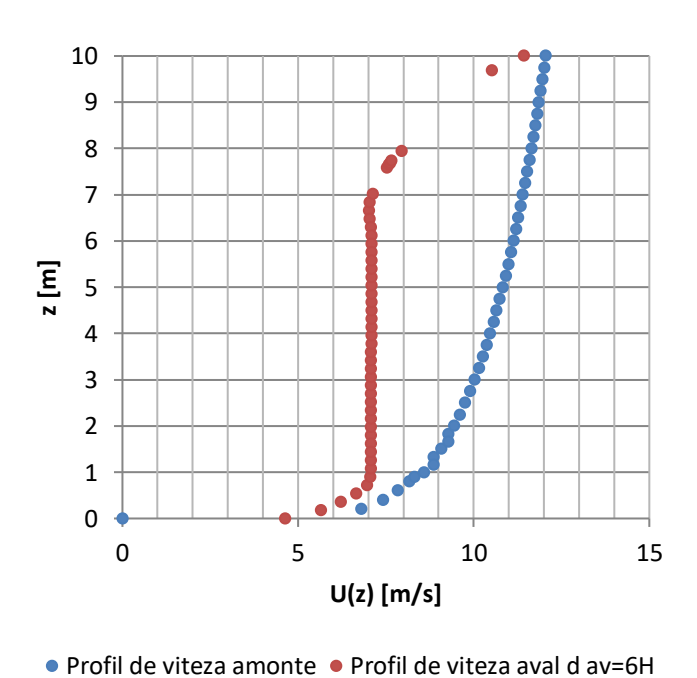


Fig. 3-42 - Speed profile U(z) downstream of the screens, for reference speed U(10)=12 m/s and number of protection screens n=1, at distance dav= 6H (CT2,GT2,1, TN2,1,3, CB:40-10-4-2H, CT:12-1-6H). Comparison with the incident wind speed profile.

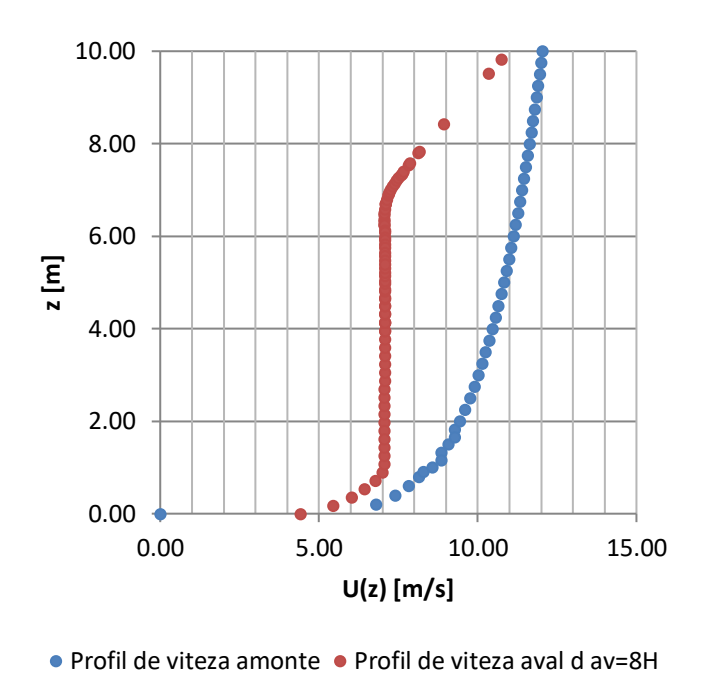


Fig. 3-43 - Speed profile U(z) downstream of the screens, for reference speed U(10)=12 m/s and number of protection screens n=1, at distance dav= 8H (CT2,GT2,1, TN2,1,4,CB:40-10-4-2H, CT:12-1-8H). Comparison with the incident wind speed profile.

Figure 3-44 shows the variation of U speeds at heights z_1 =0,20m, z_2 =1m şi z_3 =2m, depending on the downstream distance d_{av} for the reference speed U(10)=12 m/s and number of protection screens n=1 (CT2,GT2,1, CB:40-10-4-2H).

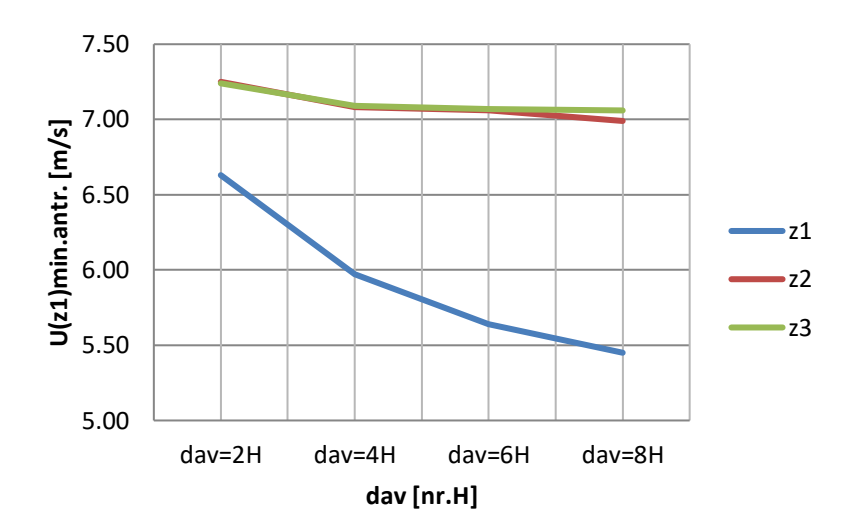


Fig. 3-44 - Variation of U speeds at heights z1=0,20m, z2=1m şi z3=2m, depending on the downstream distance day for the reference speed U(10)=12 m/ and number of protection screens n=1 (CT2,GT2,1, CB:40-10-4-2H)

Figure 3-45 shows the variation of the speed decrease $\Delta U = U(\mathbf{z})\mathbf{am} - U(\mathbf{z})\mathbf{av}$ at the heights $z_1 = 0.20$ m, $z_2 = 1$ m şi $z_3 = 2$ m, depending on the downstream distance d_{av} for the reference speed U(10) = 12 m/s and number of protective screens n = 1 (CT2,GT2,1, CB:40-10-4-2H).

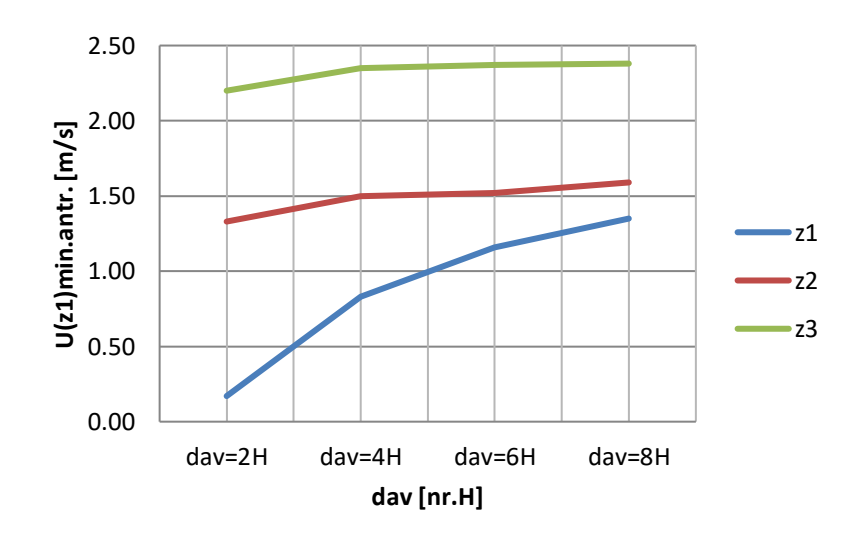


Fig. 3-45 - Variation of $\Delta U=U(z)$ am-U(z)aw speeds at heights z1=0,20m, z2=1m și z3=2m, depending on the downstream distance day for the reference speed U(10)=12 m/s and number of protection screens n=1 (CT2,GT2,1, CB:40-10-4-2H)



3.2.2 Numerical testing for the test group GT2,2 (n=2 screens) from the tests category CT2 (U(10)=12 m/s)

These numerical tests were performed for the situations included in the group of numerical tests GT2,2 which refer to the movement of air over a sandy soil provided with 2 rows of permeable protective screens. (n=2), group belonging to the category of numerical tests CT2 relating to a reference speed upstream of the protection screen (U(10)=12 m/s).

The calculation range corresponding to the GT2,2 numerical test group has a length of 100 m (10H) and a height of 20 m. At a distance of 2H = 20 m from the section entering the calculation range there is a protection screen with permeability of 40% and with height H = 10 m.

Figure 3-46 shows the diagram of the calculation range in the range of motion for the case of the location of n=2 protection screens (CT2, GT2,2, CB:40-10-4-2H).

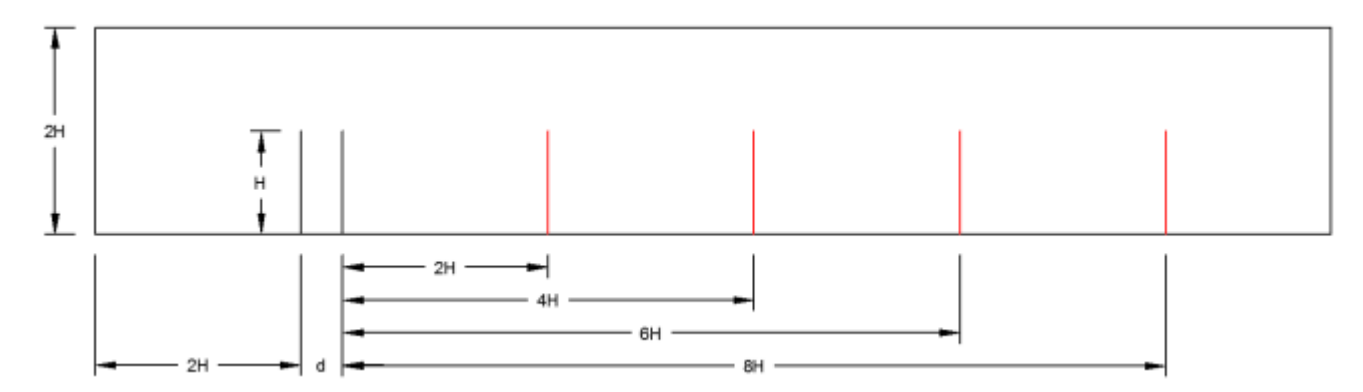


Fig. 3-46 - Schematic of the computational domain for the case of placing n = 1 protection screens (CT2, GT2,2, CB:40-10-4-2H)

The calculation domain from the computational domain thus established, was then meshed, generating the computing network for calculations, with the COMSOL Multiphysics program at a level of discretization that ensures the obtaining of a speed field, on the range of motion, with a convenient approximation.

Figure 3-47 shows the discretization of the computational domain in the area of the protection screens, for a number of protection screens n=2 (CT2, GT2,2, CB:40-10-4-2H).

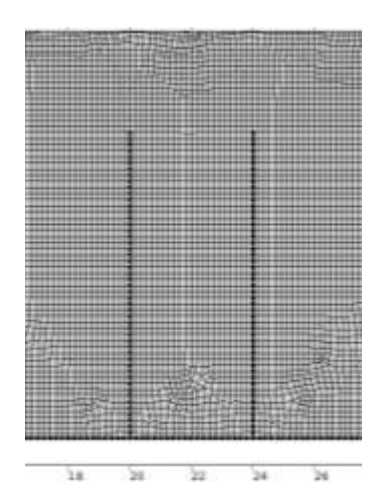


Fig. 3-47 - Discretization of the computational domain in the area of the protection screens, for a number of protection screens n=2 (CT2, GT2,2, CB:40-10-4-2H)

Figure 3-48 shows the speed field in the computational domain for the reference speed U(10)=12 m/s and number of protection screens n=2 (CT2,GT2,2, CB:40-10-4-2H).

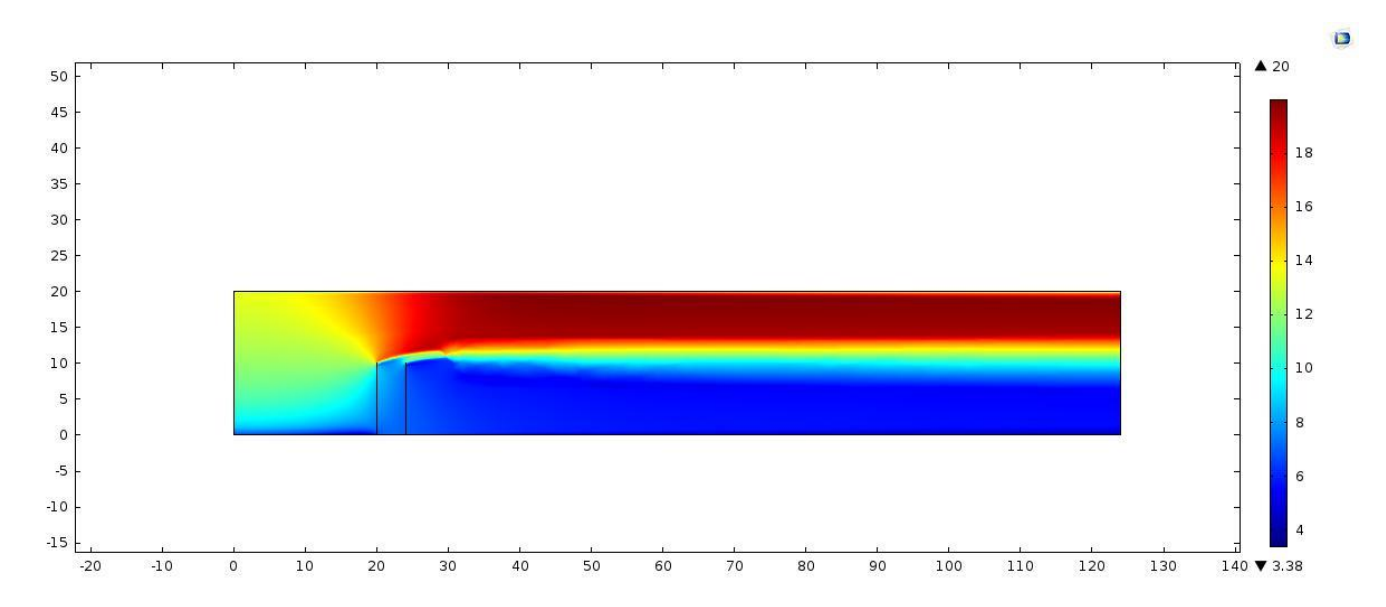


Fig. 3-48 - Speed field in the computational domain for the reference speed U(10)=12 m/s and number of protection screens n=2 (CT2,GT2,2, CB:40-10-4-2H)

From the speed field corresponding to the test group GT2,2, from the category of tests CT2, the speed profiles from 4 sections located at the downstream distances from the protection screens were extracted, $d_{av} = 2H$, $d_{av} = 4H$, $d_{av} = 6H$, $d_{av} = 8H$. These speed profiles were represented up to the height z = 10 m, because, for the present research, only the speeds at heights $z_1 = 0.20$ m, $z_2 = 1.00$ m and $z_3 = 2.00$ m are concerned, heights at which the phenomenon of sand entrainment produces.

Figures 3-49, 3-50, 3-51, 3-52 show the speed profiles U(z) downstream of the screens, for the reference speed U(10)=12 m/s and number of protection screens n=2, at distances $d_{av}=2H$ (CT2,GT2,2, TN2,2,1,CB:40-10-4-2H, CT:12-2-2H), $d_{av}=4H$ (CT2,GT2,2, TN2,2,2,CB:40-10-4-2H, CT:12-2-4H), $d_{av}=6H$ (CT2,GT2,2, TN2,2,3, CB:40-10-4-2H, CT:12-2-6H), $d_{av}=8H$ (CT2,GT2,2, TN2,2,4,CB:40-10-4-2H, CT:12-2-8H), compared to the speed profile of the incident wind.

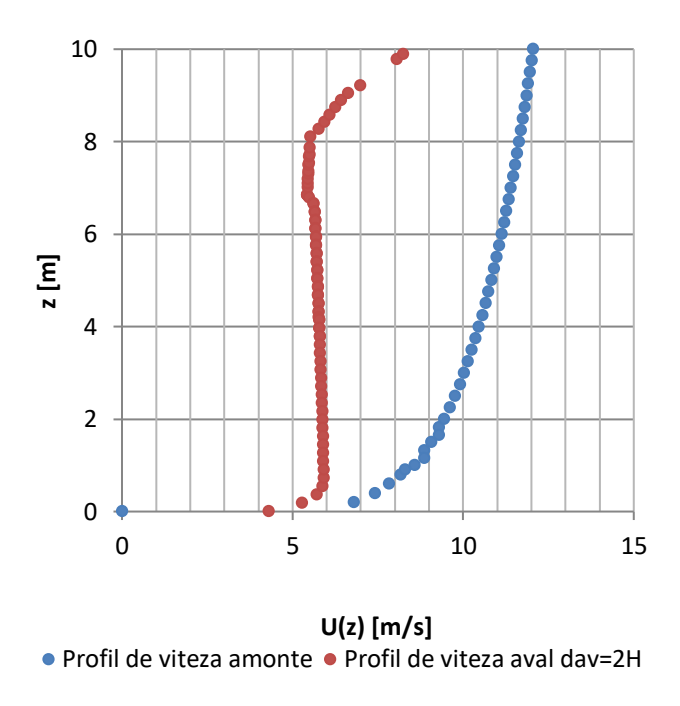


Fig. 3-49 - Speed profile U(z) downstream of the screens, for reference speed U(10)=12 m/s and number of protection screens n=2, at distance dav= 2H (CT2,GT2,2, TN2,2,1,CB:40-10-4-2H, CT:12-2-2H). Comparison with the incident wind speed profile.

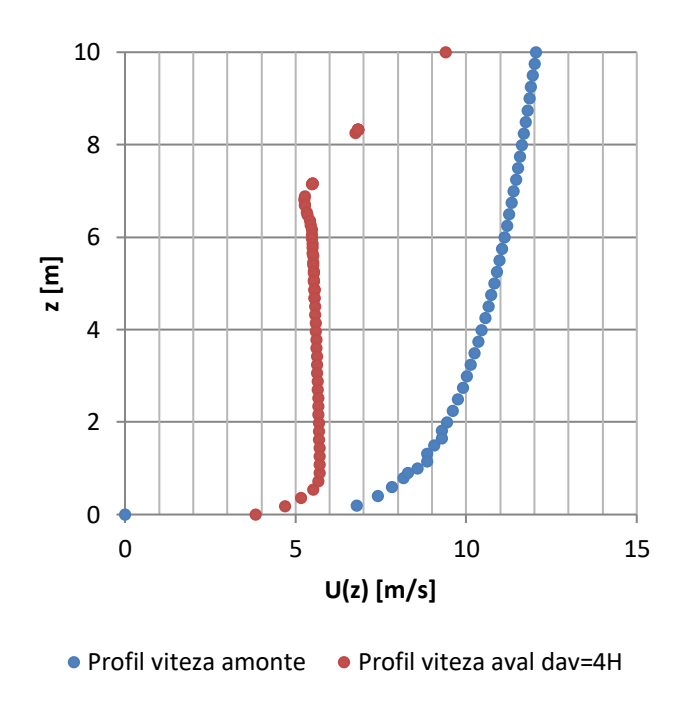


Fig. 3-50 - Speed profile U(z) downstream of the screens, for reference speed U(10)=12 m/s and number of protection screens n=2, at distance dav= 4H (CT2,GT2,2, TN2,2,2,CB:40-10-4-2H, CT:12-2-4H). Comparison with the incident wind speed profile.

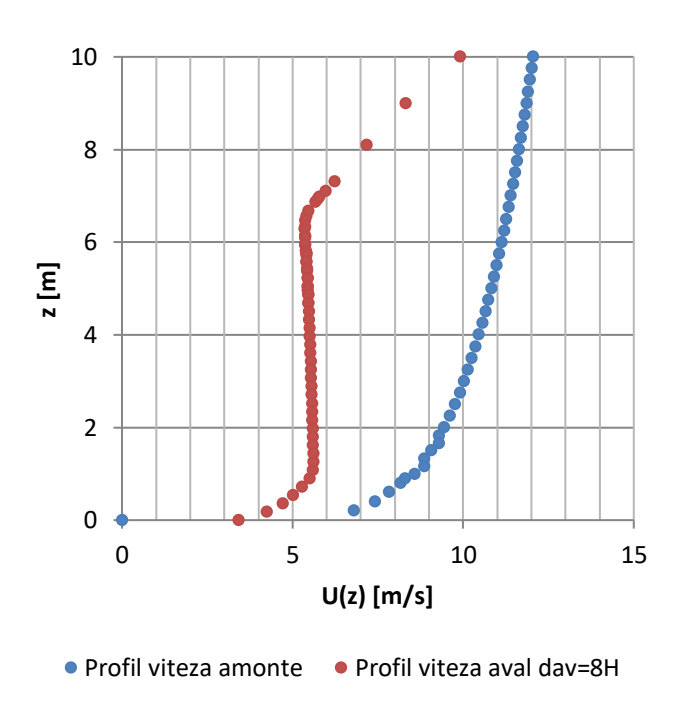


Fig. 3-51 - Speed profile U(z) downstream of the screens, for reference speed U(10)=12 m/s and number of protection screens n=2, at distance dav= 6H (CT2,GT2,2, TN2,2,3, CB:40-10-4-2H, CT:12-2-6H). Comparison with the incident wind speed profile.

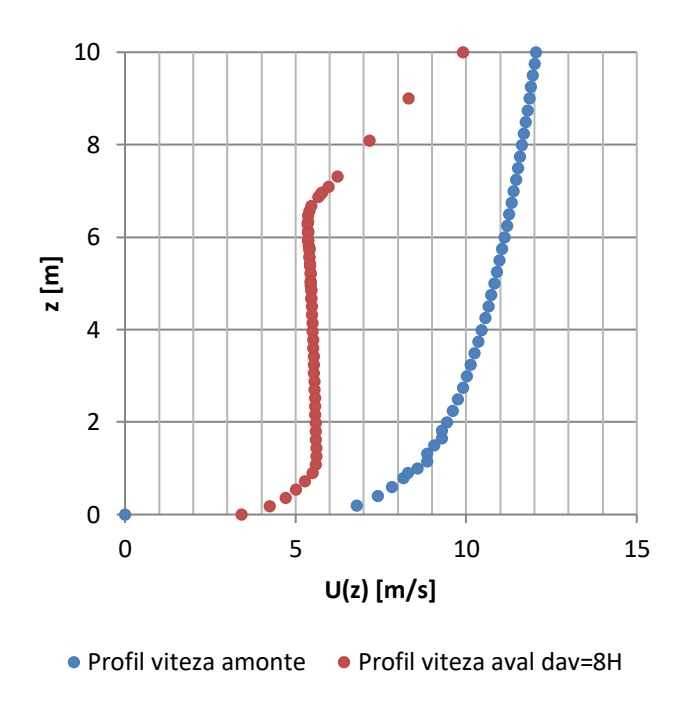


Fig. 3-52 - Speed profile U(z) downstream of the screens, for reference speed U(10)=12 m/s and number of protection screens n=2, at distance dav= 8H (CT2,GT2,2, TN2,2,4,CB:40-10-4-2H, CT:12-2-8H). Comparison with the incident wind speed profile.

Figure 3-53 shows the variation of U speeds at heights z_1 =0,20m, z_2 =1m şi z_3 =2m, depending on the downstream distance d_{av} for the reference speed U(10)=12 m/s and number of protection screens n=2 (CT2,GT2,2, CB:40-10-4-2H).

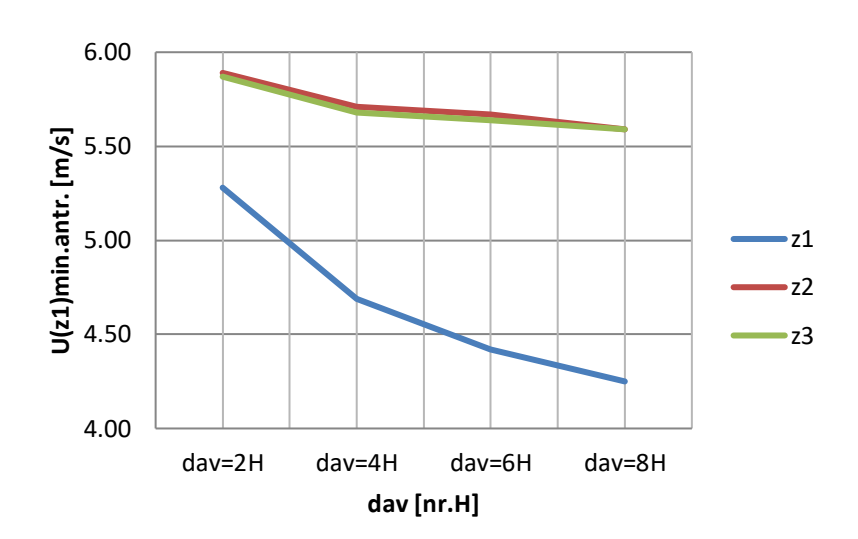


Fig. 3-53 - Variation of U speeds at heights z1=0,20m, z2=1m \pm i z3=2m, depending on the downstream distance day for the reference speed U(10)=12 m/s and number of protection screens n=2 (CT2,GT2,2, CB:40-10-4-2H)

Figure 3-54 shows the variation of the speed decrease $\Delta U = U(\mathbf{z})\mathbf{am} - U(\mathbf{z})\mathbf{av}$ at the heights $z_1 = 0.20$ m, $z_2 = 1$ m şi $z_3 = 2$ m, depending on the downstream distance d_{av} for the reference speed U(10) = 12 m/s and number of protective screens n = 2 (CT2,GT2,2, CB:40-10-4-2H).

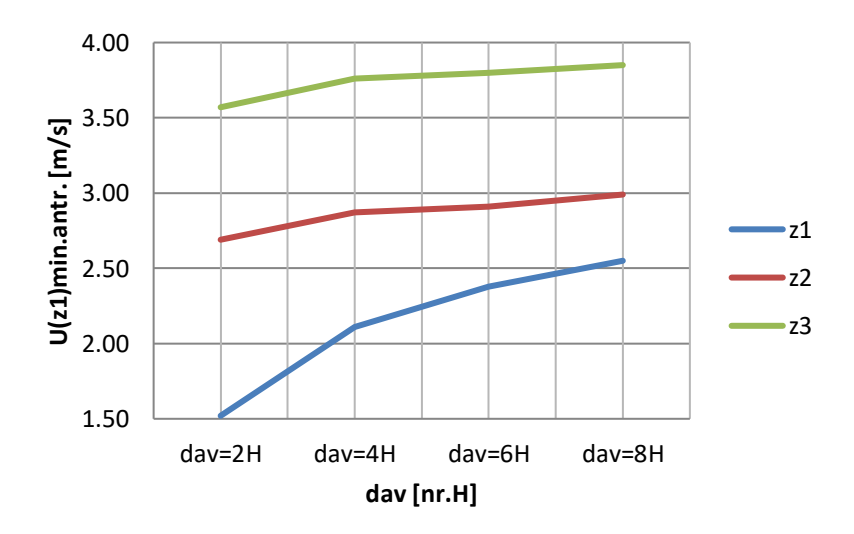


Fig. 3-54 - Variation of $\Delta U=U(z)$ am-U(z)aw speeds at heights z1=0,20m, z2=1m și z3=2m, depending on the downstream distance day for the reference speed U(10)=12 m/s and number of protection screens n=2 (CT2,GT2,2, CB:40-10-4-2H)



3.2.3 Numerical testing for the test group GT2,3 (n=3 screens) from the tests category CT2 (U(10)=12 m/s)

These numerical tests were performed for the situations included in the group of numerical tests GT2,3 which refer to the movement of air over a sandy soil provided with 3 rows of permeable protective screens. (n=3), group belonging to the category of numerical tests CT2 relating to a reference speed upstream of the protection screen (U(10)=12 m/s).

The calculation range corresponding to the GT2,3 numerical test group has a length of 100 m (10H) and a height of 20 m. At a distance of 2H = 20 m from the section entering the calculation range there is a protection screen with permeability of 40% and with height H = 10 m.

Figure 3-55 shows the diagram of the calculation range in the range of motion for the case of the location of n=3 protection screens (CT2, GT2,3, CB:40-10-4-2H).

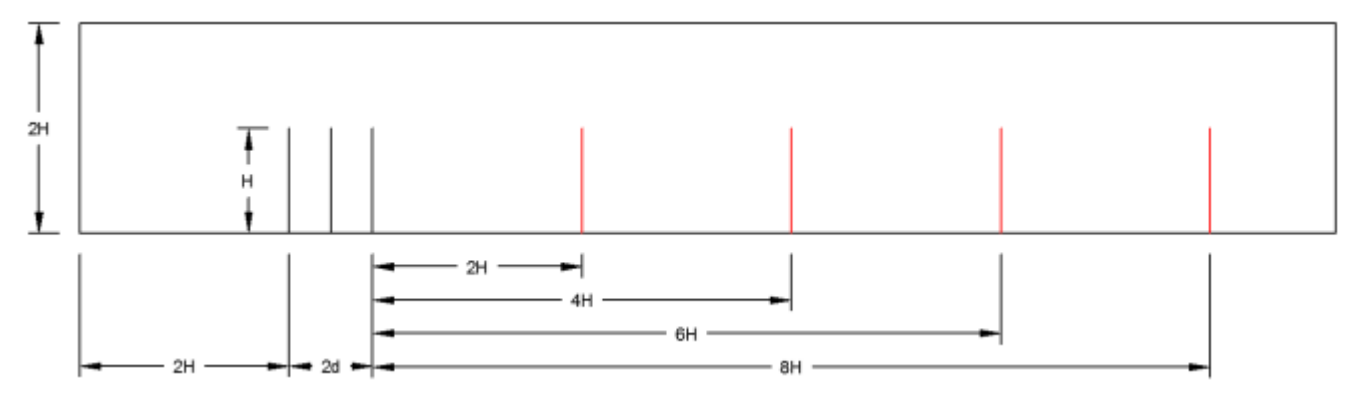


Fig. 3-55 - Schematic of the computational domain for the case of placing n = 2 protection screens (CT2, GT2,3, CB:40-10-4-2H)

The calculation domain from the computational domain thus established, was then meshed, generating the computing network for calculations, with the COMSOL Multiphysics program at a level of discretization that ensures the obtaining of a speed field, on the range of motion, with a convenient approximation.

Figure 3-56 shows the discretization of the computational domain in the area of the protection screens, for a number of protection screens n=3 (CT2, GT2,3, CB:40-10-4-2H).

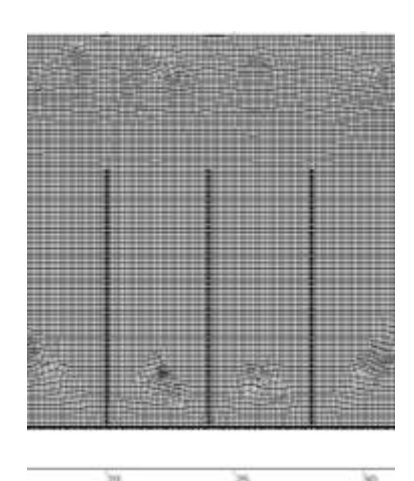


Fig. 3-56 - Discretization of the computational domain in the area of the protection screens, for a number of protection screens n=3 (CT2, GT2,3, CB:40-10-4-2H)

Figure 3-57 shows the speed field in the computational domain for the reference speed U(10)=12 m/s and number of protection screens n=3 (CT2,GT2,3, CB:40-10-4-2H).

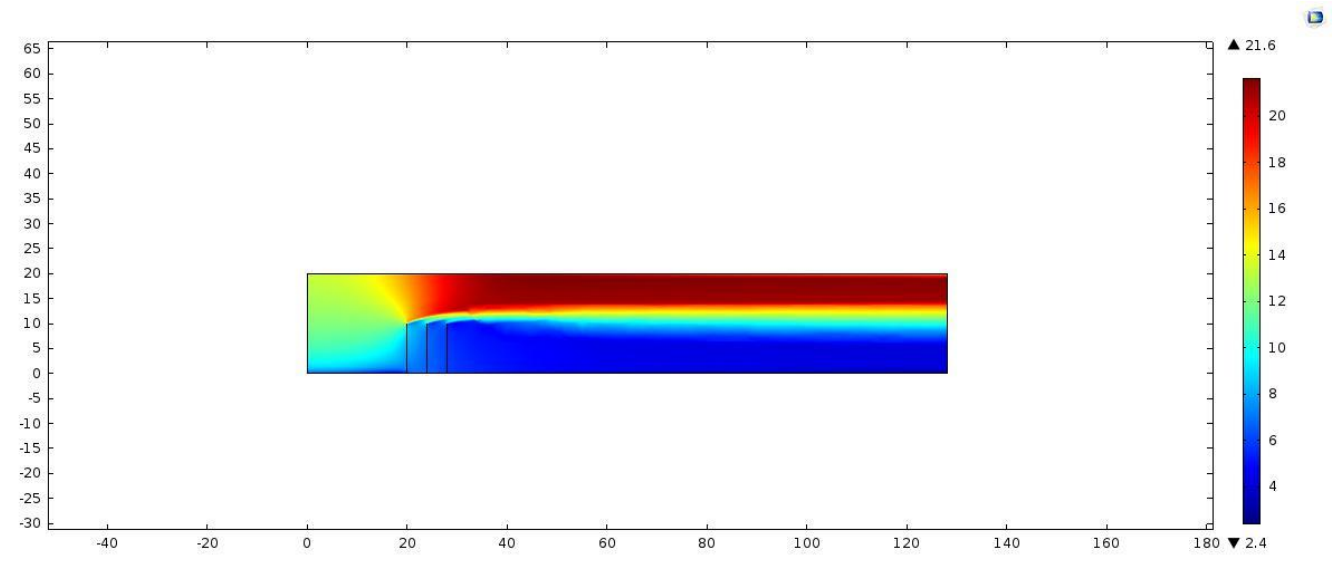


Fig. 3-57 - Speed field in the computational domain for the reference speed U(10)=12 m/s and number of protection screens n=3 (CT2,GT2,3, CB:40-10-4-2H)

From the speed field corresponding to the test group GT2,3, from the category of tests CT2, the speed profiles from 4 sections located at the downstream distances from the protection screens were extracted, $d_{av} = 2H$, $d_{av} = 4H$, $d_{av} = 6H$, $d_{av} = 8H$. These speed profiles were represented up to the height z = 10 m, because, for the present research, only the speeds at heights $z_1 = 0.20$ m, $z_2 = 1.00$ m and $z_3 = 2.00$ m are concerned, heights at which the phenomenon of sand entrainment produces.

Figures 3-58, 3-59, 3-60, 3-61 show the speed profiles U(z) downstream of the screens, for the reference speed U(10)=12 m/s and number of protection screens n=3, at distances $d_{av}=2H$ (CT2,GT2,3, TN2,3,1,CB:40-10-4-2H, CT:12-3-2H), $d_{av}=4H$ (CT2,GT2,3, TN2,3,2,CB:40-10-4-2H, CT:12-3-4H), $d_{av}=6H$ (CT2,GT2,3, TN2,3,3, CB:40-10-4-2H, CT:12-3-6H), $d_{av}=8H$ (CT2,GT2,3, TN2,3,4,CB:40-10-4-2H, CT:12-3-8H), compared to the speed profile of the incident wind.

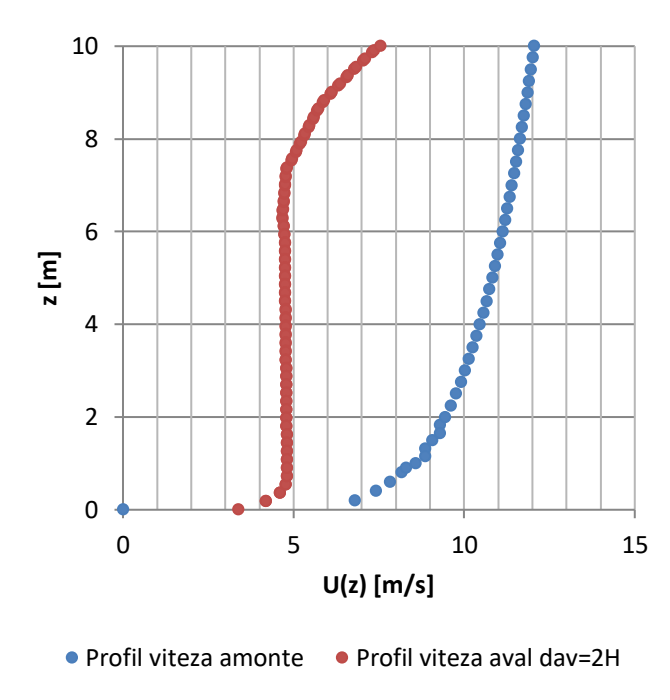


Fig. 3-58 - Speed profile U(z) downstream of the screens, for reference speed U(10)=12 m/s and number of protection screens n=3, at distance dav= 2H (CT2,GT2,3, TN2,3,1,CB:40-10-4-2H, CT:12-3-2H). Comparison with the incident wind speed profile.

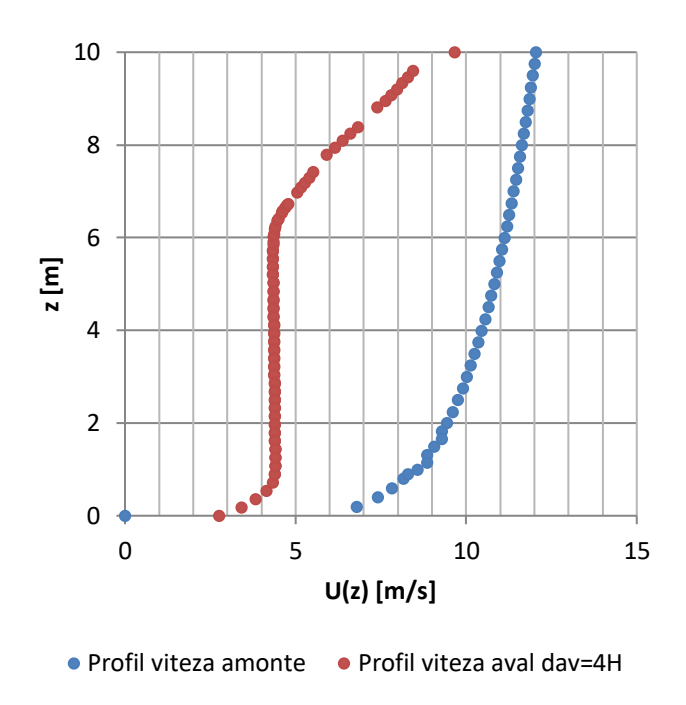


Fig. 3-59 - Speed profile U(z) downstream of the screens, for reference speed U(10)=12 m/s and number of protection screens n=3, at distance dav= 4H (CT2,GT2,3, TN2,3,2,CB:40-10-4-2H, CT:12-3-4H). Comparison with the incident wind speed profile.

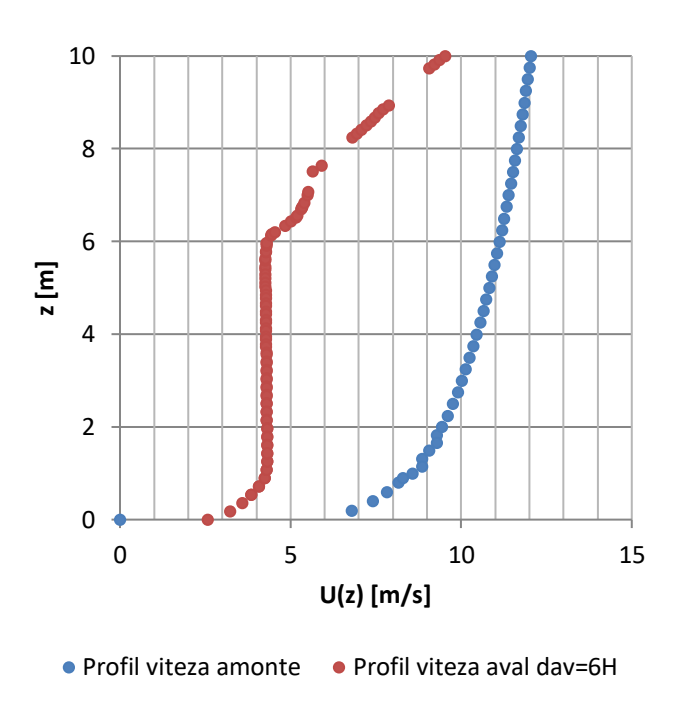


Fig. 3-60 - Speed profile U(z) downstream of the screens, for reference speed U(10)=12 m/s and number of protection screens n=3, at distance dav= 6H (CT2,GT2,3, TN2,3,3, CB:40-10-4-2H, CT:12-3-6H). Comparison with the incident wind speed profile.

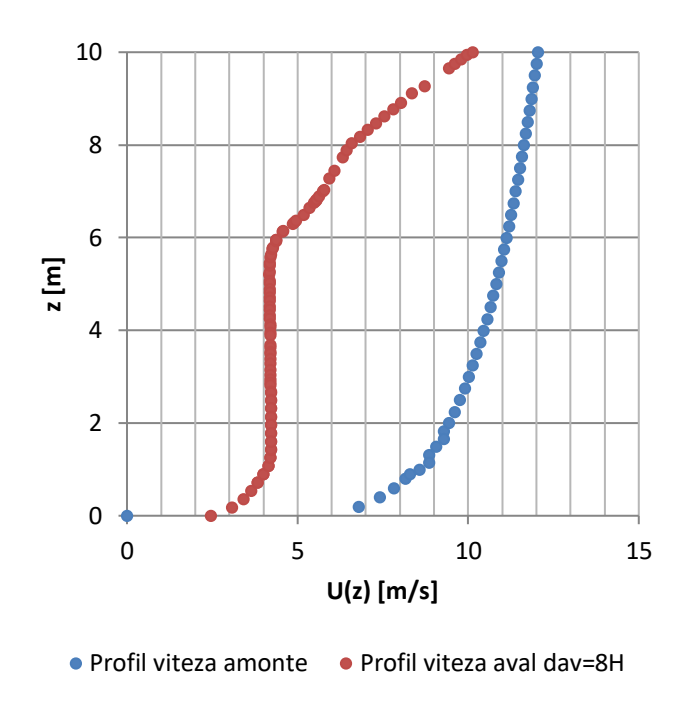


Fig. 3-61 - Speed profile U(z) downstream of the screens, for reference speed U(10)=12 m/s and number of protection screens n=3, at distance dav= 8H (CT2,GT2,3, TN2,3,4,CB:40-10-4-2H, CT:12-3-8H). Comparison with the incident wind speed profile.

Figure 3-62 shows the variation of U speeds at heights z_1 =0,20m, z_2 =1m şi z_3 =2m, depending on the downstream distance d_{av} for the reference speed U(10)=12 m/s and number of protection screens n=3 (CT2,GT2,3, CB:40-10-4-2H).

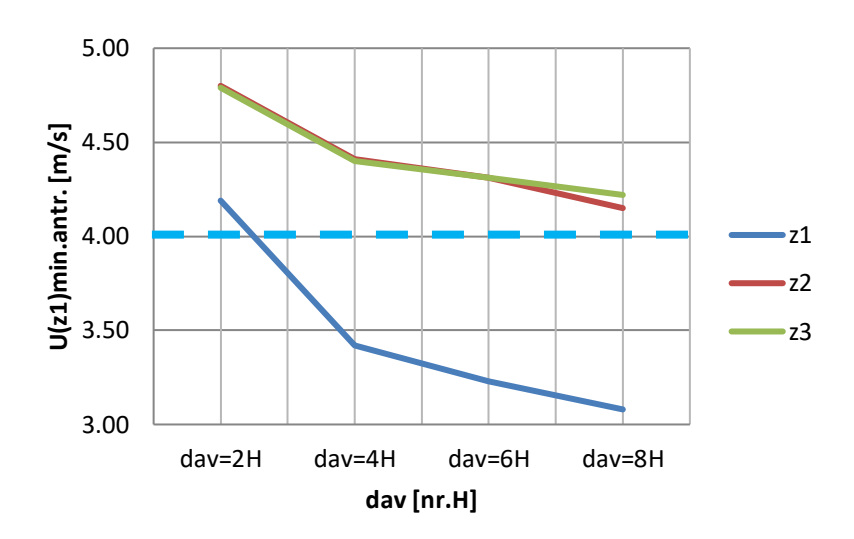


Fig. 3-62 - Variation of U speeds at heights z1=0,20m, z2=1m \pm i z3=2m, depending on the downstream distance day for the reference speed U(10)=12 m/s and number of protection screens n=3 (CT2,GT2,3, CB:40-10-4-2H)

Figure 3-63 shows the variation of the speed decrease $\Delta U = U(\mathbf{z})\mathbf{am} - U(\mathbf{z})\mathbf{av}$ at the heights $z_1 = 0.20$ m, $z_2 = 1$ m şi $z_3 = 2$ m, depending on the downstream distance d_{av} for the reference speed U(10) = 12 m/s and number of protection screens n = 3 (CT2,GT2,3, CB:40-10-4-2H).

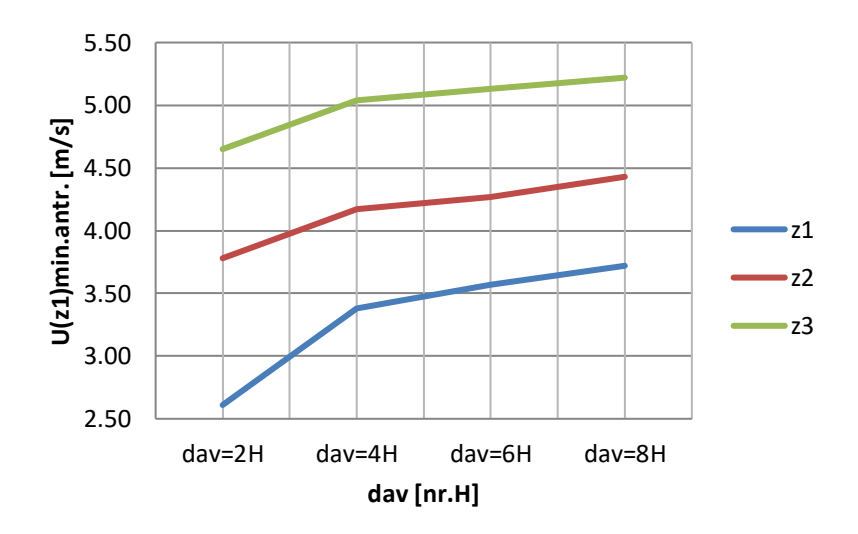


Fig. 3-63 - Variation of ΔU=U(z)am-U(z)av speeds at heights z1=0,20m, z2=1m şi z3=2m, depending on the downstream distance day for the reference speed U(10)=12 m/s and number of protection screens n=3 (CT2,GT2,3, CB:40-10-4-2H)



3.2.4 Numerical testing for the test group GT2,4 (n=4 screens) from the tests category CT2 (U(10)=12 m/s)

These numerical tests were performed for the situations included in the group of numerical tests GT2,4 which refer to the movement of air over a sandy soil provided with 4 rows of permeable protective screens. (n=4), group belonging to the category of numerical tests CT2 relating to a reference speed upstream of the protection screen (U(10)=12 m/s).

The calculation range corresponding to the GT2,4 numerical test group has a length of 100 m (10H) and a height of 20 m. At a distance of 2H = 20 m from the section entering the calculation range there is a protection screen with permeability of 40% and with height H = 10 m.

Figure 3-64 shows the diagram of the calculation range in the range of motion for the case of the location of n=4 protection screens (CT2, GT2,4, CB:40-10-4-2H).

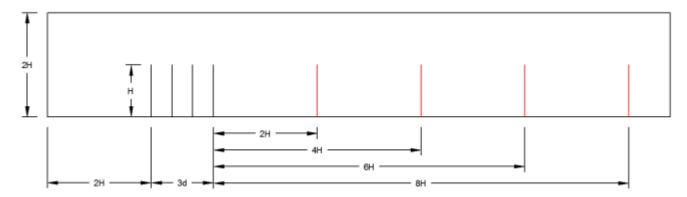


Fig. 3-64 - Schematic of the computational domain for the case of placing a n=4 protection screens (CT2, GT2,4, CB:40-10-4-2H)

The calculation domain from the computational domain thus established, was then meshed, generating the computing network for calculations, with the COMSOL Multiphysics program at a level of discretization that ensures the obtaining of a speed field, on the range of motion, with a convenient approximation.

Figure 3-65 shows the discretization of the computational domain in the area of the protection screens, for a number of protection screens n=4 (CT2, GT2,4, CB:40-10-4-2H).

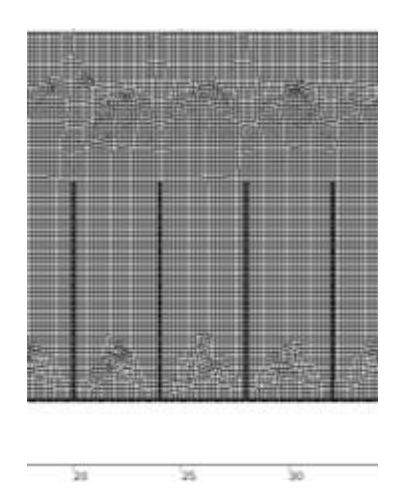


Fig. 3-65 - Discretization of the computational domain in the area of the protection screens, for a number of protection screens n=4 (CT2, GT2,4, CB:40-10-4-2H)

Figure 3-66 shows the speed field in the computational domain for the reference speed U(10)=12 m/s and number of protection screens n=4 (CT2,GT2,4, CB:40-10-4-2H).

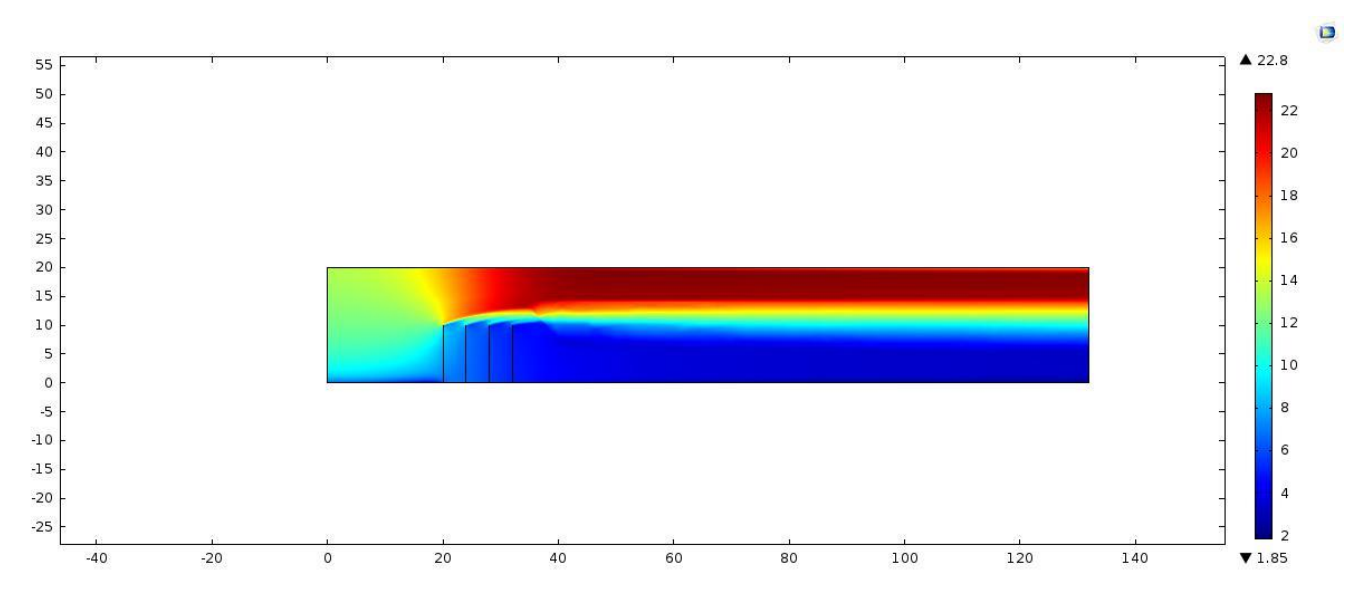


Fig. 3-66 - Speed field in the computational domain for the reference speed U(10)=12 m/s and number of protection screens n=4 (CT2,GT2,4, CB:40-10-4-2H)

From the speed field corresponding to the test group GT2,4, from the category of tests CT2, the speed profiles from 4 sections located at the downstream distances from the protection screens were extracted, $d_{av} = 2H$, $d_{av} = 4H$, $d_{av} = 6H$, $d_{av} = 8H$. These speed profiles were represented up to the height z = 10 m, because, for the present research, only the speeds at heights $z_1 = 0.20$ m, $z_2 = 1.00$ m and $z_3 = 2.00$ m are concerned, heights at which the phenomenon of sand entrainment produces.

Figures 3-67, 3-68, 3-69, 3-70 show the speed profiles U(z) downstream of the screens, for the reference speed U(10)=12 m/s and number of protection screens n=4, at distances $d_{av}=2H$ (CT2,GT2,4, TN2,4,1,CB:40-10-4-2H, CT:12-4-2H), $d_{av}=4H$ (CT2,GT2,4, TN2,4,2,CB:40-10-4-2H, CT:12-4-4H), $d_{av}=6H$ (CT2,GT2,4, TN2,4,3, CB:40-10-4-2H, CT:12-4-6H), $d_{av}=8H$ (CT2,GT2,4, TN2,3,4,CB:40-10-4-2H, CT:12-4-8H), compared to the speed profile of the incident wind.

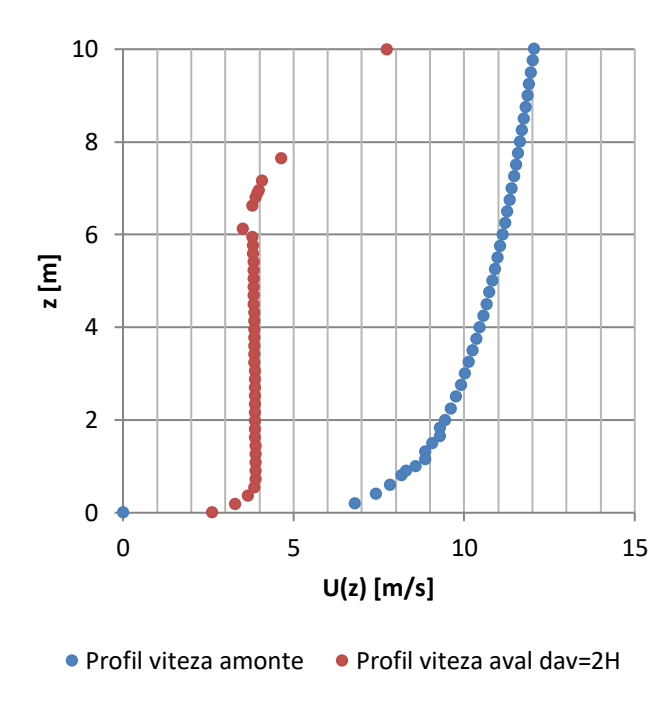


Fig. 3-67 - Speed profile U(z) downstream of the screens, for reference speed U(10)=12 m/s and number of protection screens n=4, at distance dav= 2H (CT2,GT2,4, TN2,4,1,CB:40-10-4-2H, CT:12-4-2H). Comparison with the incident wind speed profile.

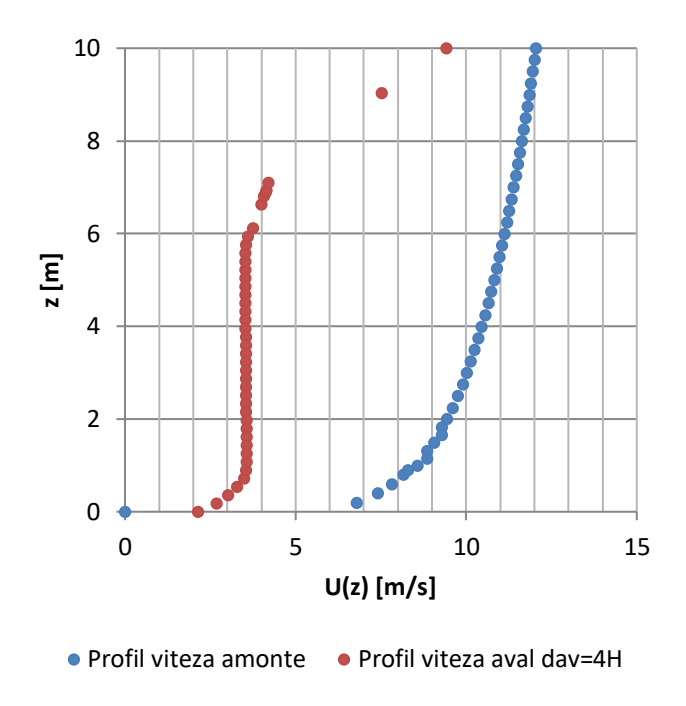


Fig. 3-68 - Speed profile U(z) downstream of the screens, for reference speed U(10)=12 m/s and number of protection screens n=4, at distance dav= 4H (CT2,GT2,4, TN2,4,2,CB:40-10-4-2H, CT:12-4-4H). Comparison with the incident wind speed profile.

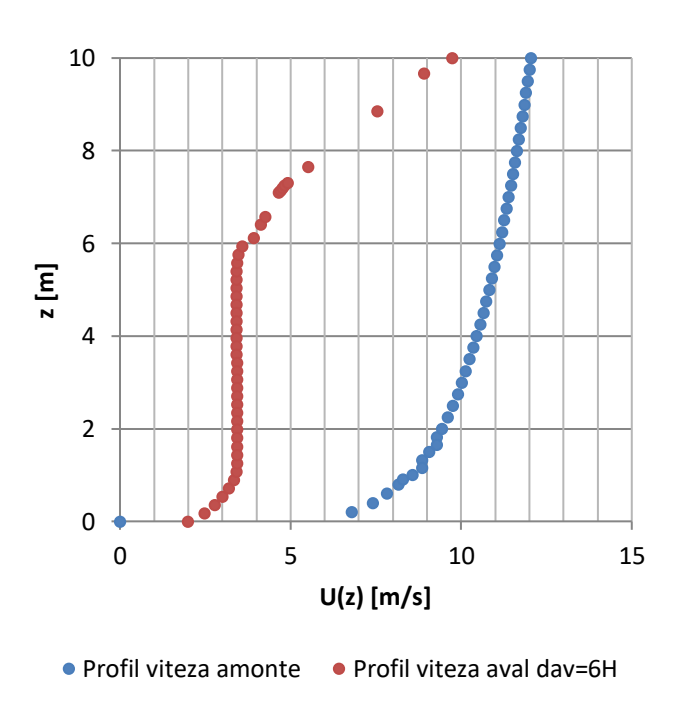


Fig. 3-69 - Speed profile U(z) downstream of the screens, for reference speed U(10)=12 m/s and number of protection screens n=4, at distance dav= 6H (CT2,GT2,4, TN2,4,3, CB:40-10-4-2H, CT:12-4-6H). Comparison with the incident wind speed profile.

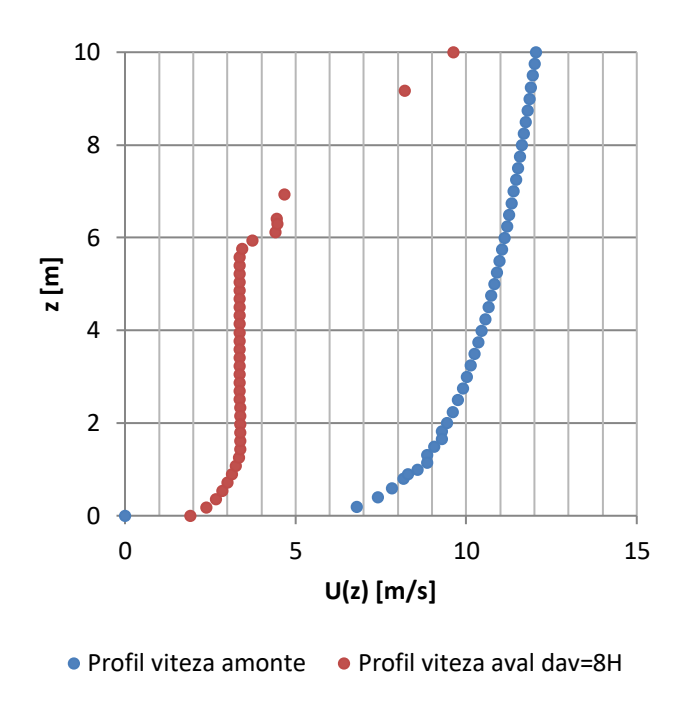


Fig. 3-70 - Speed profile U(z) downstream of the screens, for reference speed U(10)=12 m/s and number of protection screens n=4, at distance dav= 8H (CT2,GT2,4, TN2,4,4,CB:40-10-4-2H, CT:12-4-8H). Comparison with the incident wind speed profile.

Figure 3-71 shows the variation of U speeds at heights z_1 =0,20m, z_2 =1m şi z_3 =2m, depending on the downstream distance d_{av} for the reference speed U(10)=12 m/s and number of protection screens n=4 (CT2,GT2,4, CB:40-10-4-2H).

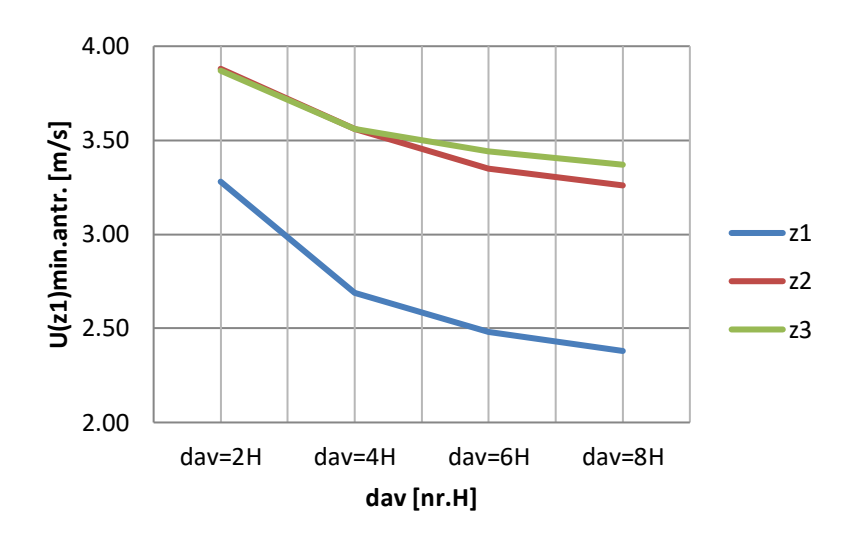


Fig. 3-71 - Variation of U speeds at heights z1=0,20m, z2=1m \pm i z3=2m, depending on the downstream distance day for the reference speed U(10)=12 m/s and number of protection screens n=4 (CT2,GT2,4, CB:40-10-4-2H)

Figure 3-72 shows the variation of the speed decrease $\Delta U = U(\mathbf{z})\mathbf{am} - U(\mathbf{z})\mathbf{av}$ at the heights $z_1 = 0.20$ m, $z_2 = 1$ m şi $z_3 = 2$ m, depending on the downstream distance d_{av} for the reference speed U(10) = 12 m/s and number of protection screens n = 4 (CT2,GT2,4, CB:40-10-4-2H).

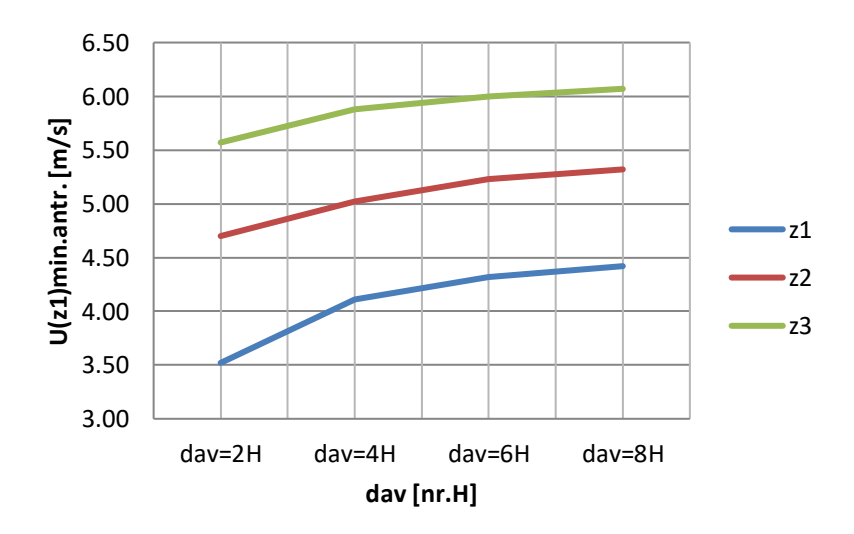


Fig. 3-72 - Variation of $\Delta U=U(z)$ am-U(z)av speeds at heights z1=0,20m, z2=1m și z3=2m, depending on the downstream distance day for the reference speed U(10)=12 m/s and number of protection screens n=4 (CT2,GT2,4, CB:40-10-4-2H)



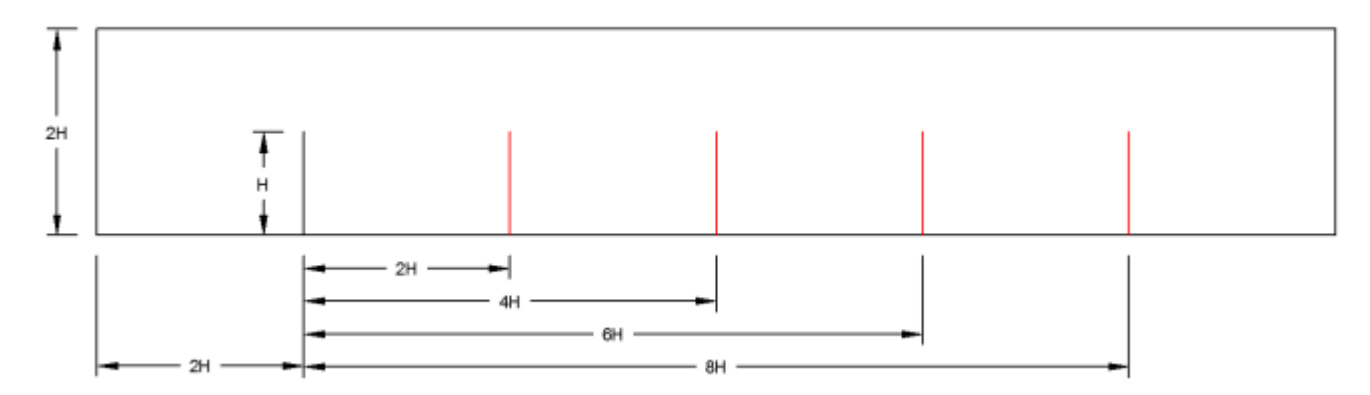
3.3 Numerical testing for test category CT3 (U(10)=16 m/s)

3.3.1 Numerical testing for the test group GT3,1 (n=1 ecran) from the tests category CT3 (U(10)=16 m/s)

These numerical tests were performed for the situations included in the group of numerical tests GT3,1 which refer to the movement of air over a sandy soil provided with 1 row of permeable protective screens. (n=1), group belonging to the category of numerical tests CT3 relating to a reference speed upstream of the protection screen (U(10)=16 m/s).

The calculation range corresponding to the GT3,1 numerical test group has a length of 100 m (10H) and a height of 20 m. At a distance of 2H = 20 m from the section entering the calculation range there is a protection screen with permeability of 40% and with height H = 10 m.

Figure 3-73 shows the diagram of the calculation range in the range of motion for the case of the location of n = 1 protection screens (CT3, GT3,1, CB:40-10-4-2H).



 $Fig. \ 3-73-Schematic \ of the \ computational \ domain \ for \ the \ case \ of \ placing \ n=1 \ protection \ screens \ (CT3, GT3,1, CB:40-10-4-2H)$

The calculation domain from the computational domain thus established, was then meshed, generating the computing network for calculations, with the COMSOL Multiphysics program at a level of discretization that ensures the obtaining of a speed field, on the range of motion, with a convenient approximation.

Figure 3-74 shows the discretization of the computational domain in the area of the protection screens, for a number of protection screens n=1 (CT3, GT3,1, CB:40-10-4-2H).

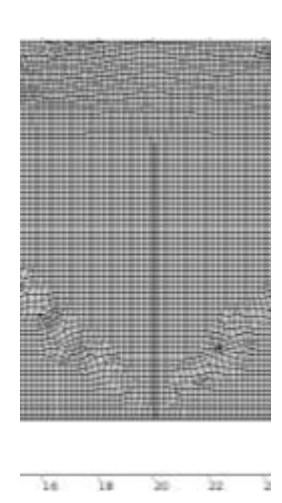


Fig. 3-74 - Discretization of the computational domain in the area of the protection screens, for a number of protection screens n=1 (CT3, GT3,1, CB:40-10-4-2H)

Figure 3-75 shows the speed field in the computational domain for the reference speed U(10)=16 m/s and number of protection screens n=1 (CT3,GT3,1, CB:40-10-4-2H).

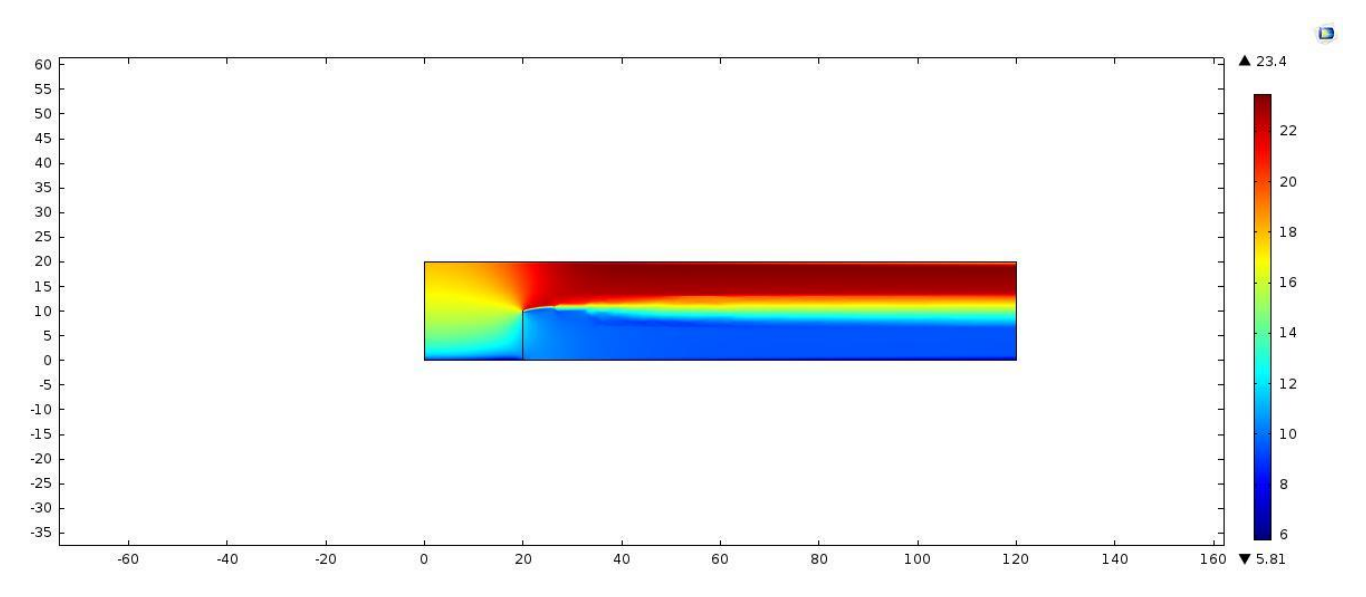


Fig. 3-75 - Speed field in the computational domain for the reference speed U(10)=16 m/s and number of protection screens n=1 (CT3,GT3,1, CB:40-10-4-2H)

From the speed field corresponding to the test group GT3,1, from the category of tests CT3, the speed profiles from 4 sections located at the downstream distances from the protection screens were extracted, $d_{av} = 2H$, $d_{av} = 4H$, $d_{av} = 6H$, $d_{av} = 8H$. These speed profiles were represented up to the height z = 10 m, because, for the present research, only the speeds at heights $z_1 = 0.20$ m, $z_2 = 1.00$ m and $z_3 = 2.00$ m are concerned, heights at which the phenomenon of sand entrainment produces.

Figures 3-76, 3-77, 3-78, 3-79 show the speed profiles U(z) downstream of the screens, for the reference speed U(10)=16 m/s and number of protection screens n=1, la distanțele $d_{av}=2H$ (CT3,GT3,1, TN3,1,1,CB:40-10-4-2H, CT:16-1-2H), $d_{av}=4H$ (CT3,GT3,1, TN3,1,2,CB:40-10-4-2H, CT:16-1-4H), $d_{av}=6H$ (CT3,GT3,1, TN3,1,3, CB:40-10-4-2H, CT:16-1-6H), $d_{av}=8H$ (CT3,GT3,1, TN3,1,4,CB:40-10-4-2H, CT:16-1-8H), compared to the speed profile of the incident wind.

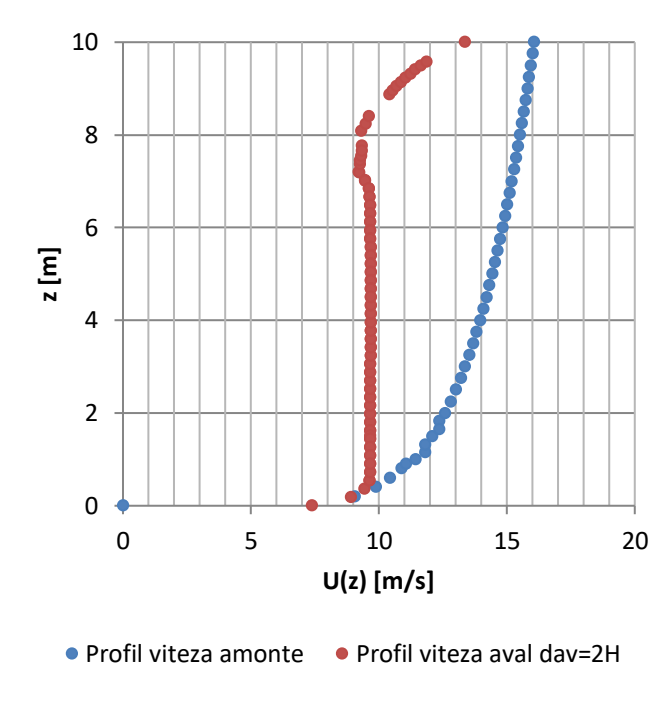


Fig. 3-76 - Speed profile U(z) downstream of the screens, for reference speed U(10)=16 m/s and number of protection screens n=1, at distance dav= 2H (CT3,GT3,1, TN3,1,1,CB:40-10-4-2H, CT:16-1-2H). Comparison with the incident wind speed profile

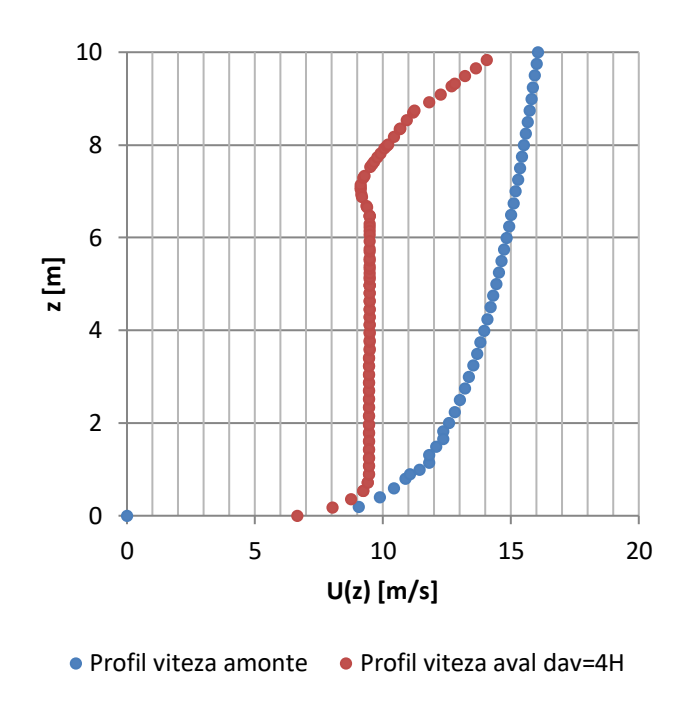


Fig. 3-77 - Speed profile U(z) downstream of the screens, for reference speed U(10)=16 m/s and number of protection screens n=1, at distance day= 4H (CT3,GT3,1, TN3,1,2,CB:40-10-4-2H, CT:16-1-4H). Comparison with the incident wind speed profile

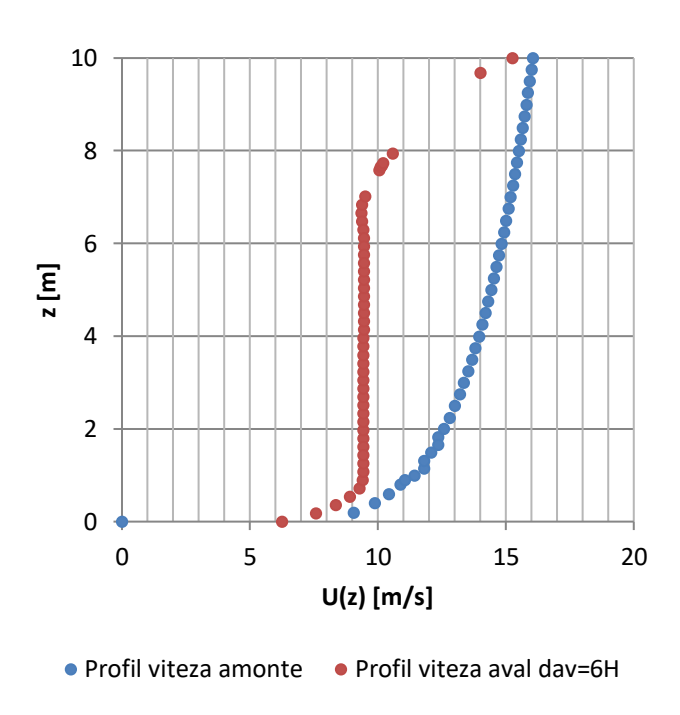


Fig. 3-78 - Speed profile U(z) downstream of the screens, for reference speed U(10)=16 m/s and number of protection screens n=1, at distance dav= 6H (CT3,GT3,1, TN3,1,3, CB:40-10-4-2H, CT:16-1-6H). Comparison with the incident wind speed profile

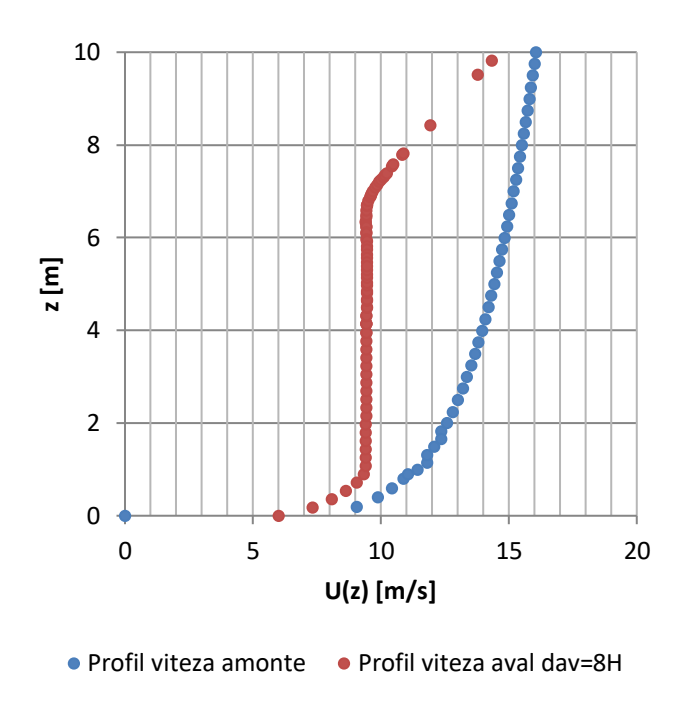


Fig. 3-79 - Speed profile U(z) downstream of the screens, for reference speed U(10)=16 m/s and number of protection screens n=1, at distance day= 8H (CT3,GT3,1, TN3,1,4,CB:40-10-4-2H, CT:16-1-8H). Comparison with the incident wind speed profile

Figure 3-80 shows the variation of U speeds at heights z_1 =0,20m, z_2 =1m şi z_3 =2m, depending on the downstream distance d_{av} for the reference speed U(10)=16 m/s and number of protection screens n=1 (CT3,GT3,1, CB:40-10-4-2H).

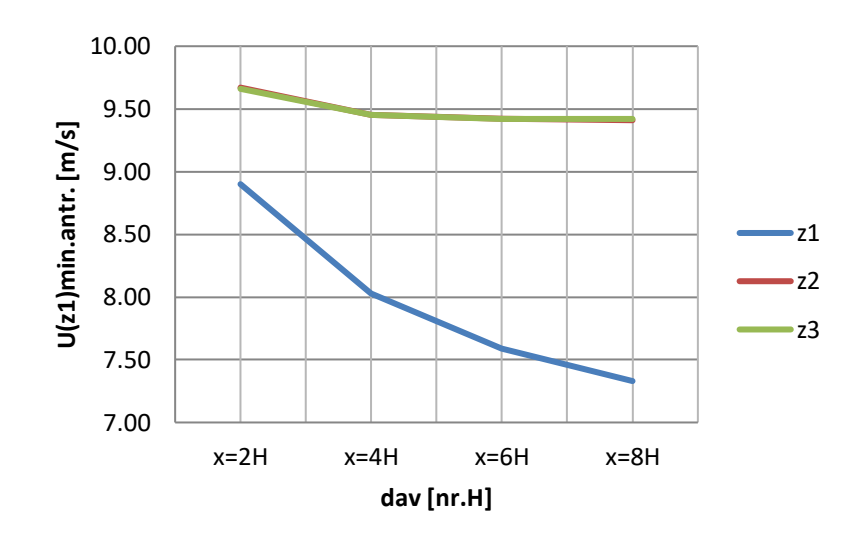


Fig. 3-80 - Variation of U speeds at heights z1=0,20m, z2=1m \pm i z3=2m, depending on the downstream distance day for the reference speed U(10)=16 m/s and number of protection screens n=1 (CT3,GT3,1, CB:40-10-4-2H)

Figure 3-81 the variation of the speed decrease $\Delta U = U(\mathbf{z})$ am- $U(\mathbf{z})$ av at the heights $z_1 = 0.20$ m, $z_2 = 1$ m şi $z_3 = 2$ m, depending on the downstream distance d_{av} for the reference speed U(10) = 16 m/s and number of protection screens n = 1 (CT3,GT3,1, CB:40-10-4-2H).

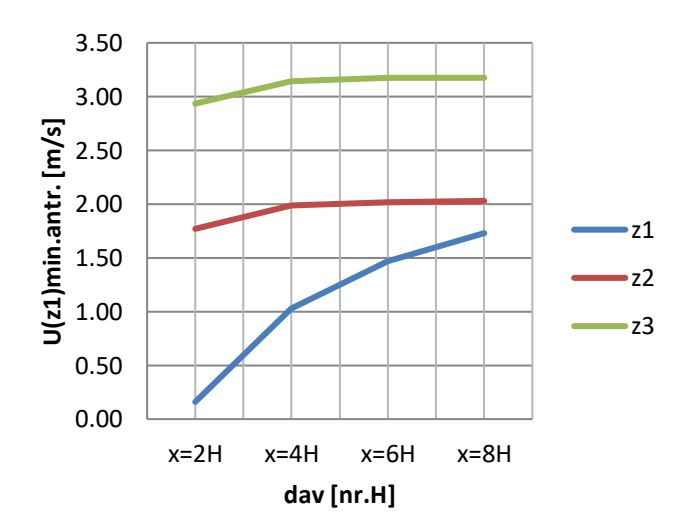


Fig. 3-81 - Variation of $\Delta U=U(z)$ am-U(z)aw speeds at heights z1=0,20m, z2=1m și z3=2m, depending on the downstream distance day for the reference speed U(10)=16 m/s and number of protection screens n=1 (CT3,GT3,1, CB:40-10-4-2H)



3.3.2 Numerical testing for the test group GT3,2 (n=2 ecrane) from the tests category CT3 (U(10)=16 m/s)

These numerical tests were performed for the situations included in the group of numerical tests GT3,2 which refer to the movement of air over a sandy soil provided with 2 rows of permeable protective screens. (n=2), group belonging to the category of numerical tests CT3 relating to a reference speed upstream of the protection screen (U(10)=16 m/s).

The calculation range corresponding to the GT3,2 numerical test group has a length of 100 m (10H) and a height of 20 m. At a distance of 2H = 20 m from the section entering the calculation range there is a protection screen with permeability of 40% and with height H = 10 m

Figure 3-82 shows the diagram of the calculation range in the range of motion for the case of the location of n=2 protection screens (CT3, GT3,2, CB:40-10-4-2H).

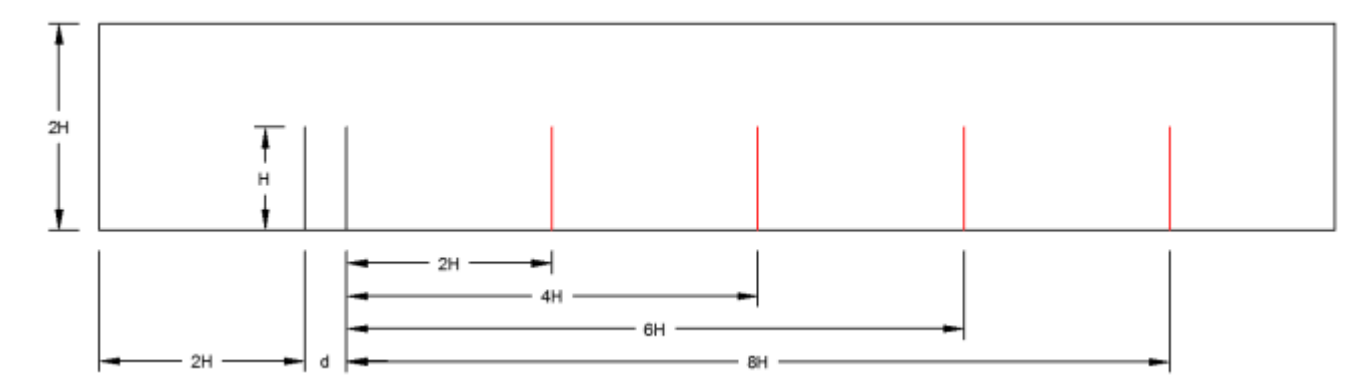


Fig. 3-82 - Schematic of the computational domain for the case of placing n = 2 protection screens (CT3, GT3,2, CB:40-10-4-2H)

The calculation domain from the computational domain thus established, was then meshed, generating the computing network for calculations, with the COMSOL Multiphysics program at a level of discretization that ensures the obtaining of a speed field, on the range of motion, with a convenient approximation.

Figure 3-83 shows the discretization of the computational domain in the area of the protection screens, for a number of protection screens n=2 (CT3, GT3,2, CB:40-10-4-2H).

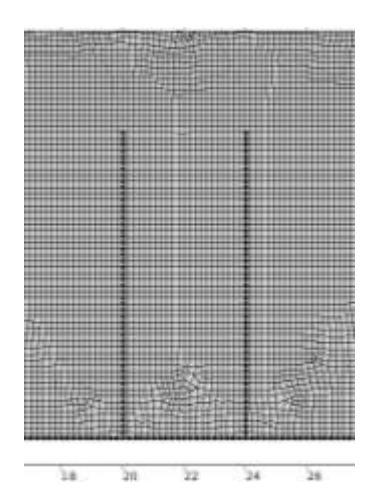


Fig. 3-83 - Discretization of the computational domain in the area of the protection screens, for a number of protection screens n=2 (CT3, GT3,2, CB:40-10-4-2H)

Figure 3-84 shows the speed field in the computational domain for the reference speed U(10)=16 m/s and number of protection screens n=2 (CT31,GT3,2, CB:40-10-4-2H).

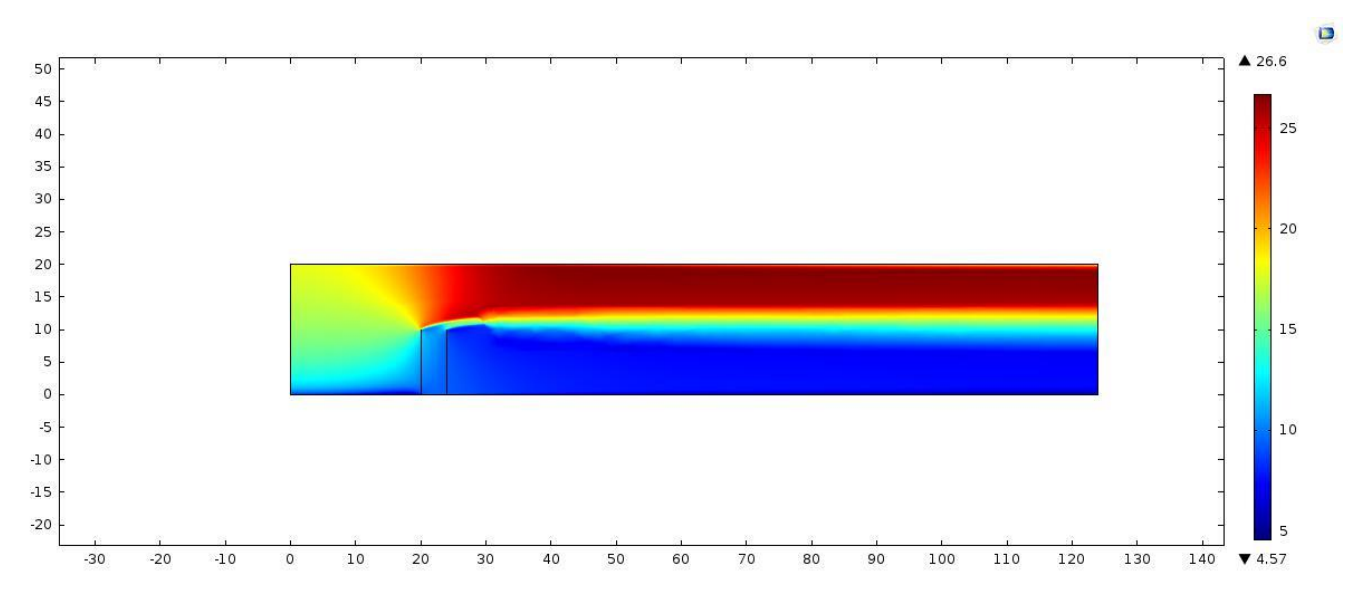


Fig. 3-84 - Speed field in the computational domain for the reference speed U(10)=16 m/s and number of protection screens n=2 (CT3,GT3,2, CB:40-10-4-2H)

From the speed field corresponding to the test group GT3,2, from the category of tests CT3, the speed profiles from 4 sections located at the downstream distances from the protection screens were extracted, $d_{av} = 2H$, $d_{av} = 4H$, $d_{av} = 6H$, $d_{av} = 8H$. These speed profiles were represented up to the height z = 10 m, because, for the present research, only the speeds at heights $z_1 = 0.20$ m, $z_2 = 1.00$ m and $z_3 = 2.00$ m are concerned, heights at which the phenomenon of sand entrainment produces.

Figures 3-85, 3-86, 3-87, 3-88 show the speed profiles U(z) downstream of the screens, for the reference speed U(10)=16 m/s and number of protection screens n=2, at distances $d_{av}=2H$ (CT3,GT3,2, TN3,2,1,CB:40-10-4-2H, CT:16-2-2H), $d_{av}=4H$ (CT3,GT3,2, TN3,2,2,CB:40-10-4-2H, CT:16-2-4H), $d_{av}=6H$ (CT3,GT3,2, TN3,2,3, CB:40-10-4-2H, CT:16-2-6H), $d_{av}=8H$ (CT3,GT3,2, TN3,2,4,CB:40-10-4-2H, CT:16-2-8H), compared to the speed profile of the incident wind.

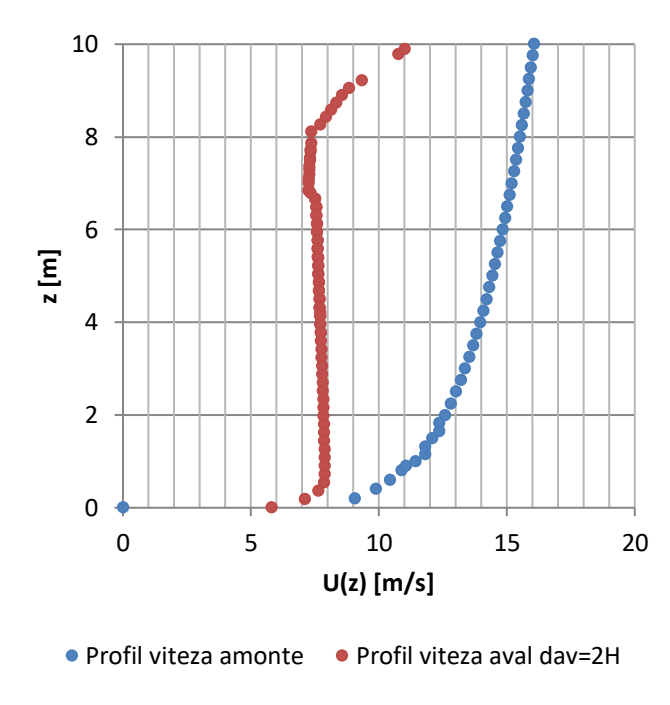


Fig. 3-85 - Speed profile U(z) downstream of the screens, for reference speed U(10)=16 m/s şi and number of protection screens n=2, at distance day= 2H (CT3,GT3,2, TN3,2,1,CB:40-10-4-2H, CT:16-2-2H). Comparison with the incident wind speed profile

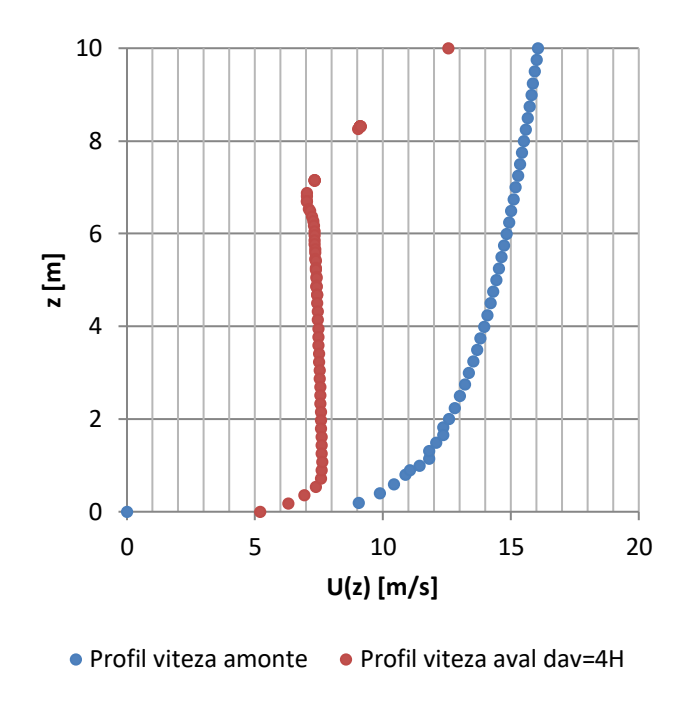


Fig. 3-86 - Speed profile U(z) downstream of the screens, for reference speed U(10)=16 m/s şi and number of protection screens n=2, at distance dav= 4H (CT3,GT3,2, TN3,2,2,CB:40-10-4-2H, CT:16-2-4H). Comparison with the incident wind speed profile

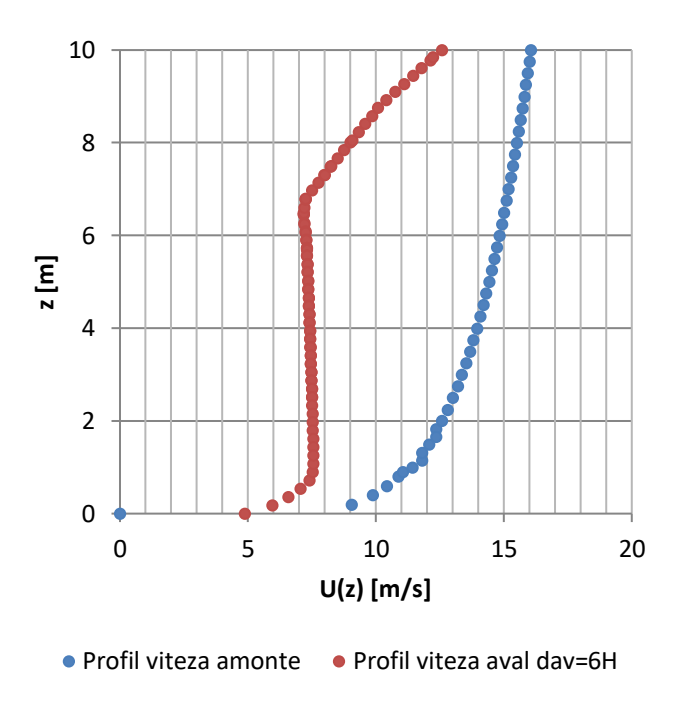


Fig. 3-87 - Speed profile U(z) downstream of the screens, for reference speed U(10)=16 m/s şi and number of protection screens n=2, at distance dav= 6H (CT3,GT3,2, TN3,2,3, CB:40-10-4-2H, CT:16-2-6H). Comparison with the incident wind speed profile

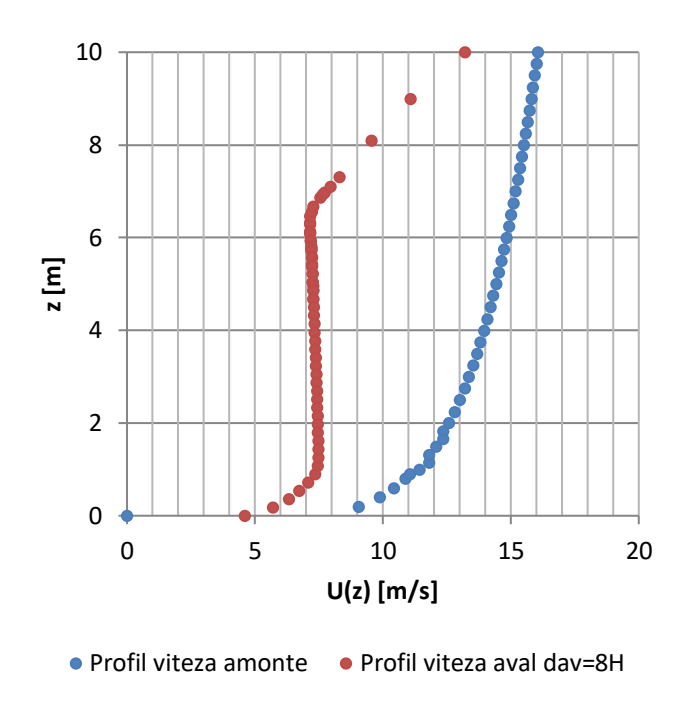


Fig. 3-88 - Speed profile U(z) downstream of the screens, for reference speed U(10)=16 m/s şi and number of protection screens n=2, at distance dav= 8H (CT3,GT3,2, TN3,2,4,CB:40-10-4-2H, CT:16-2-8H). Comparison with the incident wind speed profile

Figure 3-89 shows the variation of U speeds at heights z_1 =0,20m, z_2 =1m şi z_3 =2m, depending on the downstream distance d_{av} for the reference speed U(10)=16 m/s and number of protection screens n=2 (CT3,GT3,2, CB:40-10-4-2H).

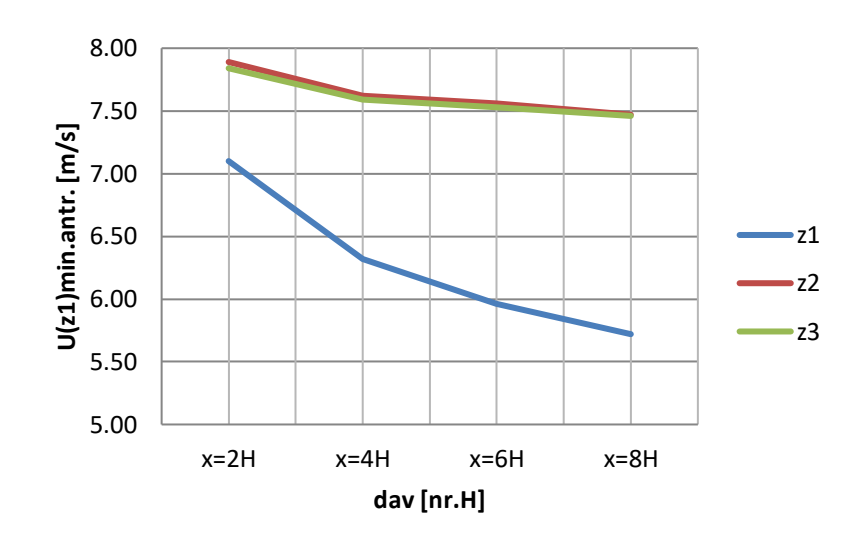


Fig. 3-89 - Variation of U speeds at heights z1=0,20m, z2=1m \pm i z3=2m, depending on the downstream distance day for the reference speed U(10)=16 m/s and number of protection screens n=2 (CT3,GT3,2, CB:40-10-4-2H)

Then, for heights z_1 =0,20 m, z_2 =1,00 m și z_3 =2,00 m, for the sections downstream of the protection screens located at distances d_{av} =2H, d_{av} =4H, d_{av} =6H, d_{av} =8H, the differences were made between the speeds on the upstream speed profile located at d_{am} =2H and the speeds from the homologous points on the downstream speed profiles, ie ΔU =U(z)am-U(z)av.

Figure 3-90 shows the variation of the speed decrease $\Delta U = U(\mathbf{z})\mathbf{am} - U(\mathbf{z})\mathbf{av}$ at the heights $z_1 = 0.20$ m, $z_2 = 1$ m şi $z_3 = 2$ m, depending on the downstream distance d_{av} for the reference speed U(10) = 16 m/s and number of protective screens n = 2 (CT3,GT3,2, CB:40-10-4-2H).

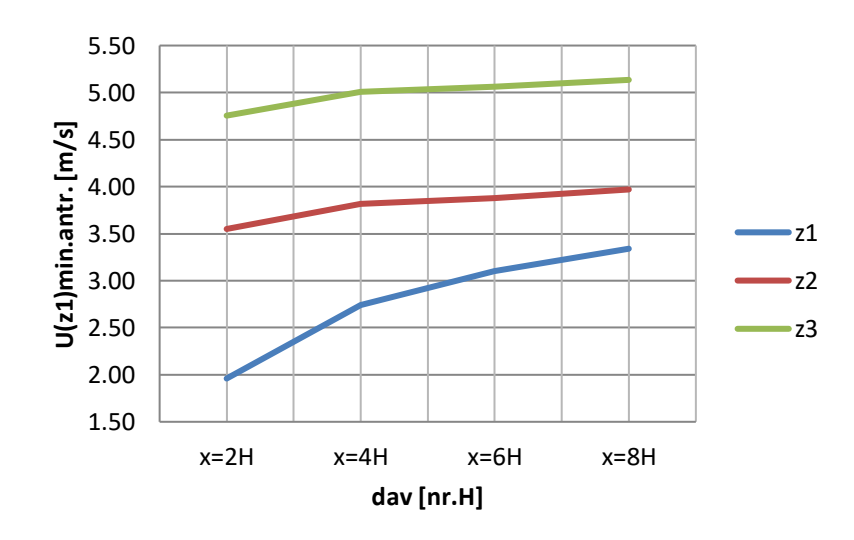


Fig. 3-90 - Variation of $\Delta U=U(z)$ am-U(z)aw speeds at heights z1=0,20m, z2=1m și z3=2m, depending on the downstream distance day for the reference speed U(10)=16 m/s and number of protection screens n=2 (CT3,GT3,2, CB:40-10-4-2H)



3.3.3 Numerical testing for the test group GT3,3 (n=3 screens) from the tests category CT3 (U(10)=16 m/s)

These numerical tests were performed for the situations included in the group of numerical tests GT3,3 which refer to the movement of air over a sandy soil provided with 3 rows of permeable protective screens. (n=3), group belonging to the category of numerical tests CT3 relating to a reference speed upstream of the protection screen (U(10)=16 m/s).

The calculation range corresponding to the GT3,3 numerical test group has a length of 100 m (10H) and a height of 20 m. At a distance of 2H = 20 m from the section entering the calculation range there is a protection screen with permeability of 40% and with height H = 10 m.

Figure 3-91 shows the diagram of the calculation range in the range of motion for the case of the location of n = 3 protection screens (CT3, GT3,3, CB:40-10-4-2H).

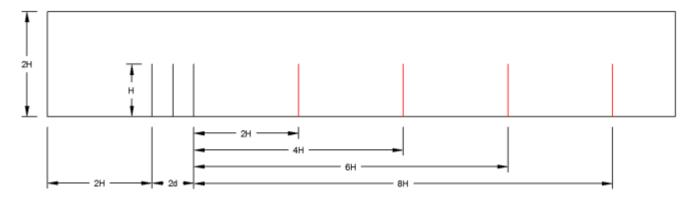


Fig. 3-91 - Schematic of the computational domain for the case of placing n = 3 protection screens (CT3, GT3,3, CB:40-10-4-2H)

The calculation domain from the computational domain thus established, was then meshed, generating the computing network for calculations, with the COMSOL Multiphysics program at a level of discretization that ensures the obtaining of a speed field, on the range of motion, with a convenient approximation.

Figure 3-92 shows the discretization of the computational domain in the area of the protection screens, for a number of protection screens n=3 (CT3, GT3,3, CB:40-10-4-2H).

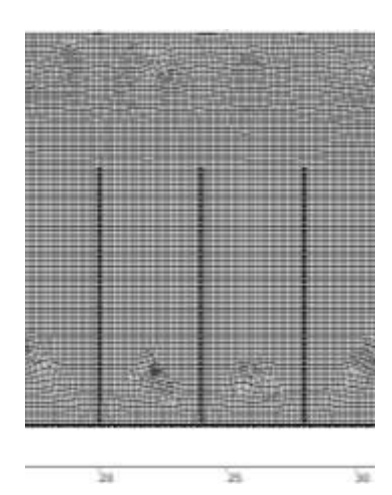


Fig. 3-92 - Discretization of the computational domain in the area of the protection screens, for a number of protection screens n=3 (CT3, GT3,3, CB:40-10-4-2H)

Applying, on the computational domain, the finite element model COMSOL Multiphysics, the velocity range in this calculation field is obtained.

Figure 3-93 shows the speed field in the computational domain for the reference speed U(10)=16 m/s and number of protection screens n=3 (CT3,GT3,3, CB:40-10-4-2H).

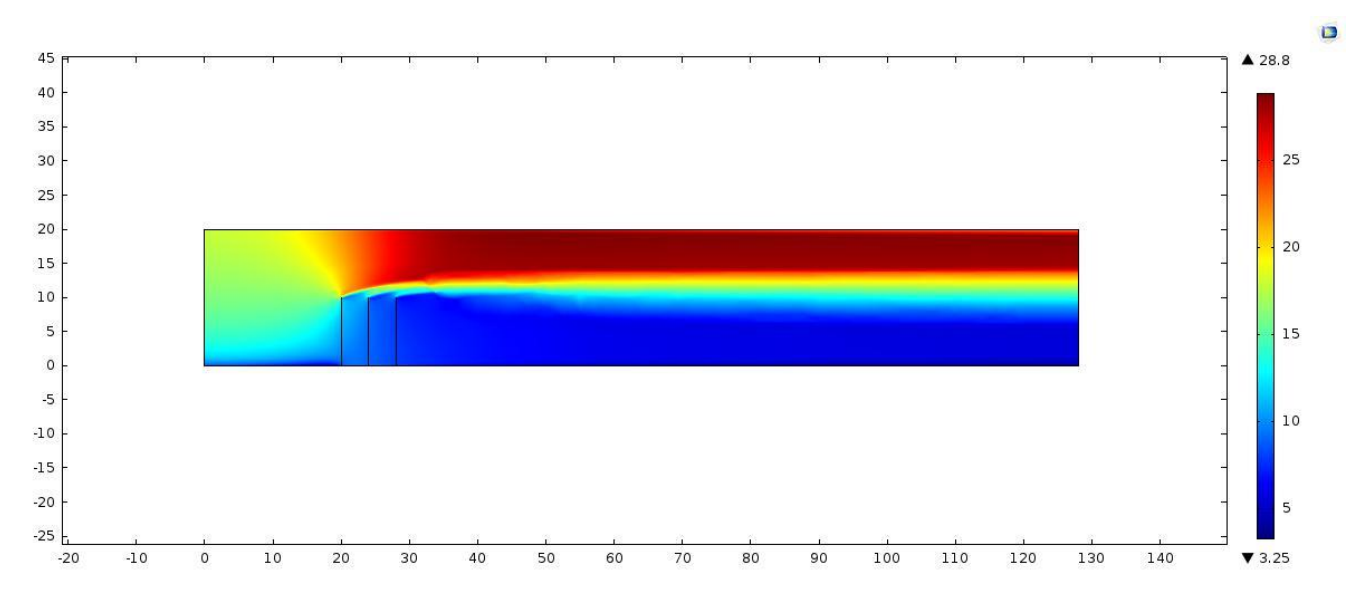


Fig. 3-93 - Speed field in the computational domain for the reference speed U(10)=16 m/s and number of protection screens n=3 (CT3,GT3,3, CB:40-10-4-2H)

From the speed field corresponding to the test group GT3,3, from the category of tests CT3, the speed profiles from 4 sections located at the downstream distances from the protection screens were extracted, $d_{av} = 2H$, $d_{av} = 4H$, $d_{av} = 6H$, $d_{av} = 8H$. These speed profiles were represented up to the height z = 10 m, because, for the present research, only the speeds at heights $z_1 = 0.20$ m, $z_2 = 1.00$ m and $z_3 = 2.00$ m are concerned, heights at which the phenomenon of sand entrainment produces.

The speed profiles in the 4 sections downstream of the protection screens ($d_{av} = 2H$, $d_{av} = 4H$, $d_{av} = 6H$, $d_{av} = 8H$), resulting from the reduction of the incident wind speed, were compared with the power law type speed profile in upstream of the protection screens, i.e. at heights $z_1 = 0.20$ m, $z_2 = 1.00$ m and $z_3 = 2.00$ m.

Figures 3-94, 3-95, 3-96, 3-97 show the speed profiles U(z) downstream of the screens, for the reference speed U(10)=16 m/s and number of protection screens n=3, at distances $d_{av}=2H$ (CT3,GT3,3, TN3,3,1,CB:40-10-4-2H, CT:16-3-2H), $d_{av}=4H$ (CT3,GT3,3, TN3,3,2,CB:40-10-4-2H, CT:16-3-4H), $d_{av}=6H$ (CT3,GT3,3, TN3,3,3, CB:40-10-4-2H, CT:16-3-6H), $d_{av}=8H$ (CT3,GT3,3, TN3,3,4,CB:40-10-4-2H, CT:16-3-8H), compared to the speed profile of the incident wind.

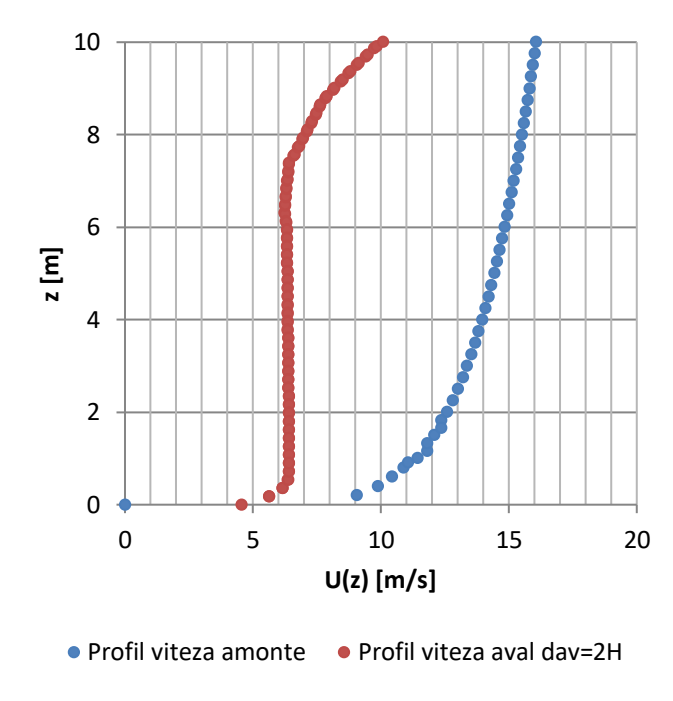


Fig. 3-94 - Speed profile U(z) downstream of the screens, for reference speed U(10)=16m/s and number of protection screens n=3, at distance dav= 2H (CT3,GT3,3, TN3,3,1,CB:40-10-4-2H, CT:16-3-2H). Comparison with the incident wind speed profile

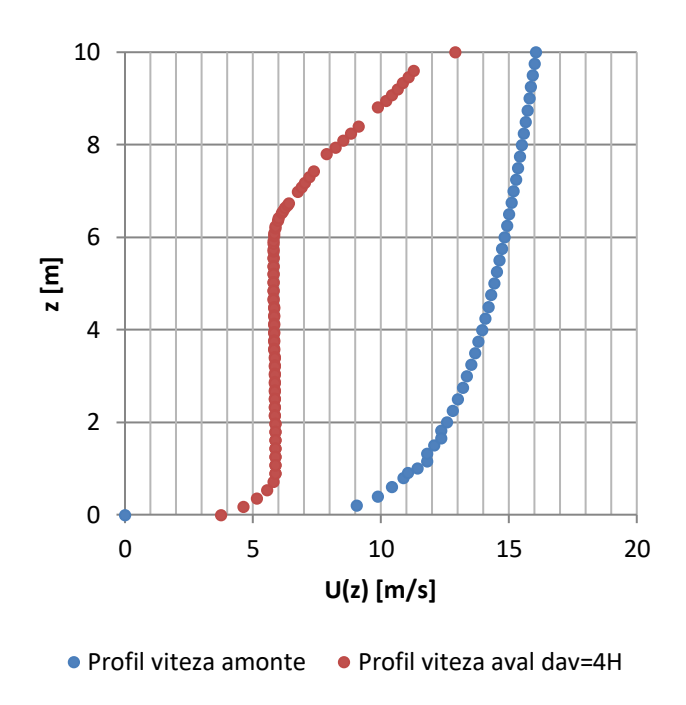


Fig. 3-95 - Speed profile U(z) downstream of the screens, for reference speed U(10)=16m/s and number of protection screens n=3, at distance dav= 4H (CT3,GT3,3, TN3,3,2,CB:40-10-4-2H, CT:16-3-4H). Comparison with the incident wind speed profile

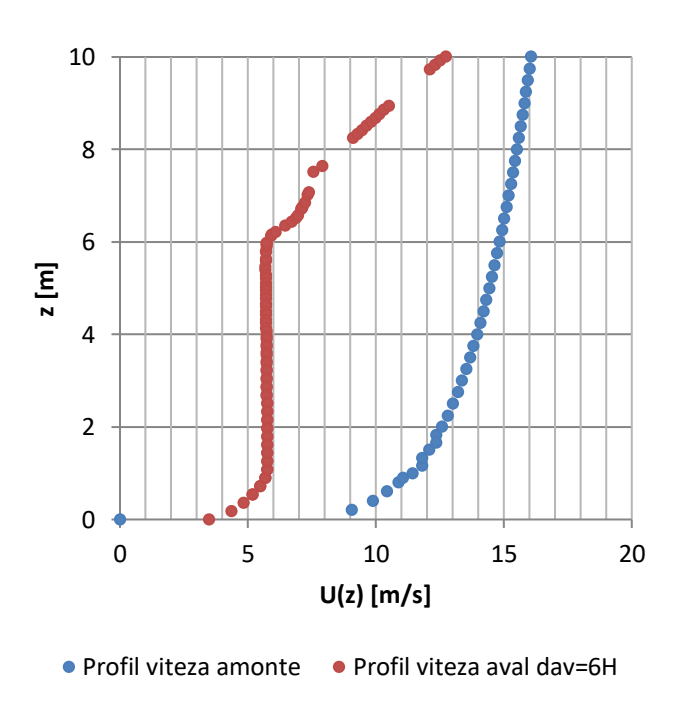


Fig. 3-96 - Speed profile U(z) downstream of the screens, for reference speed U(10)=16m/s and number of protection screens n=3, at distance dav= 6H (CT3,GT3,3, TN3,3,3, CB:40-10-4-2H, CT:16-3-6H). Comparison with the incident wind speed profile

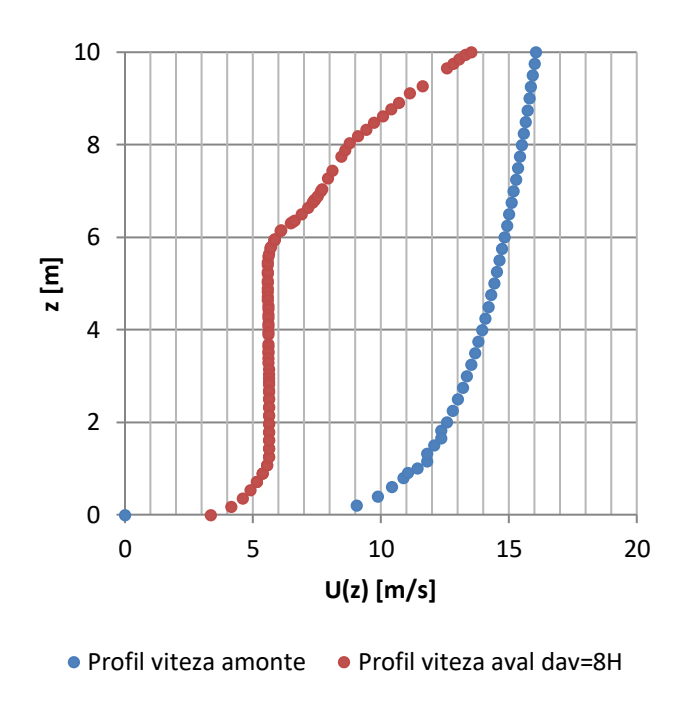


Fig. 3-97 - Speed profile U(z) downstream of the screens, for reference speed U(10)=16m/s and number of protection screens n=3, at distance day= 8H (CT3,GT3,3, TN3,3,4,CB:40-10-4-2H, CT:16-3-8H). Comparison with the incident wind speed profile

Next, wind speeds were determined at heights z_1 =0,20 m, z_2 =1,00 m si z_3 =2,00 m from the speed profiles corresponding to the downstream sections of the protection screens located at distances d_{av} =2H, d_{av} =4H, d_{av} =6H, d_{av} =8H.

Figure 3-98 shows the variation of U speeds at heights z_1 =0,20m, z_2 =1m şi z_3 =2m, depending on the downstream distance d_{av} for the reference speed U(10)=16 m/s and number of protection screens n=3 (CT3,GT3,3, CB:40-10-4-2H).

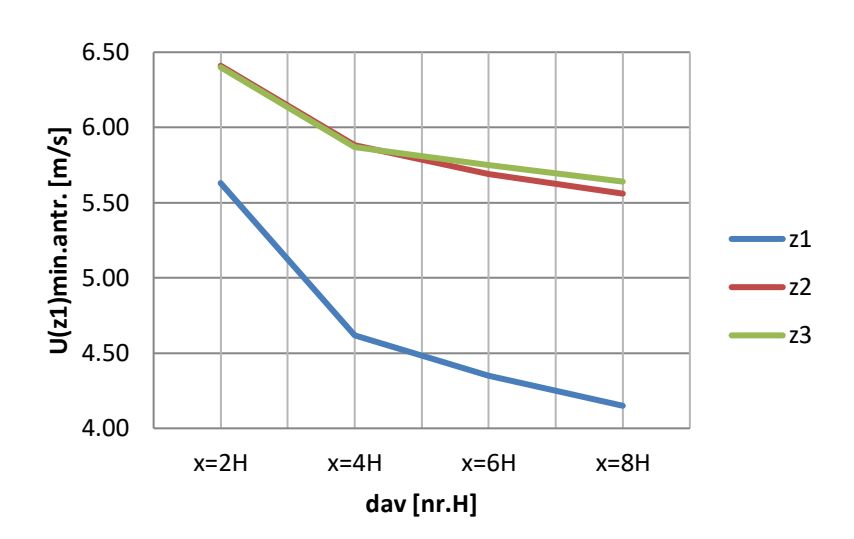


Fig. 3-98 - Variation of U speeds at heights z1=0,20m, z2=1m \pm i z3=2m, depending on the downstream distance day for the reference speed U(10)=16 m/s and number of protection screens n=3 (CT3,GT3,3, CB:40-10-4-2H)

Then, for heights z_1 =0,20 m, z_2 =1,00 m și z_3 =2,00 m, for the sections downstream of the protection screens located at distances d_{av} =2H, d_{av} =4H, d_{av} =6H, d_{av} =8H, the differences were made between the speeds on the upstream speed profile located at d_{am} =2H and the speeds from the homologous points on the downstream speed profiles, ie ΔU =U(z)am-U(z)av.

Figure 3-99 shows the variation of the speed decrease $\Delta U = U(\mathbf{z})\mathbf{am} - U(\mathbf{z})\mathbf{av}$ at the heights $z_1 = 0.20$ m, $z_2 = 1$ m şi $z_3 = 2$ m, depending on the downstream distance d_{av} for the reference speed U(10) = 16 m/s and number of protective screens n = 3 (CT3,GT3,3, CB:40-10-4-2H).

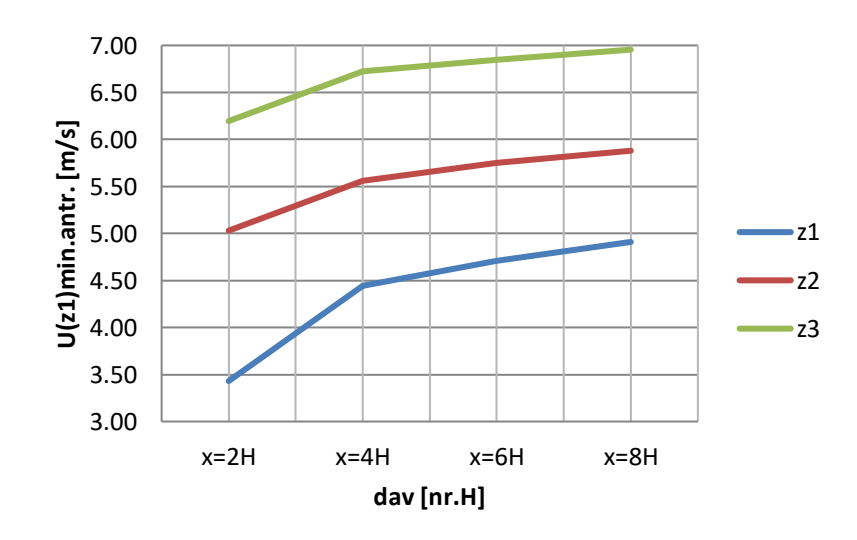


Fig. 3-99 - Variation of $\Delta U=U(z)$ am-U(z)aw speeds at heights z1=0,20m, z2=1m și z3=2m, depending on the downstream distance day for the reference speed U(10)=16 m/s and number of protection screens n=3 (CT3,GT3,3, CB:40-10-4-2H)



3.3.4 Numerical testing for the test group GT3,4 (n=4 screens) from the tests category CT3 (U(10)=16 m/s)

These numerical tests were performed for the situations included in the group of numerical tests GT3,4 which refer to the movement of air over a sandy soil provided with 4 rows of permeable protective screens. (n=4), group belonging to the category of numerical tests CT3 relating to a reference speed upstream of the protection screen (U(10)=16 m/s).

The calculation range corresponding to the GT3,4 numerical test group has a length of 100 m (10H) and a height of 20 m. At a distance of 2H = 20 m from the section entering the calculation range there is a protection screen with permeability of 40% and with height H = 10 m.

Figure 3-100 shows the diagram of the calculation range in the range of motion for the case of the location of n = 4 protection screens (CT3, GT3,4, CB:40-10-4-2H).

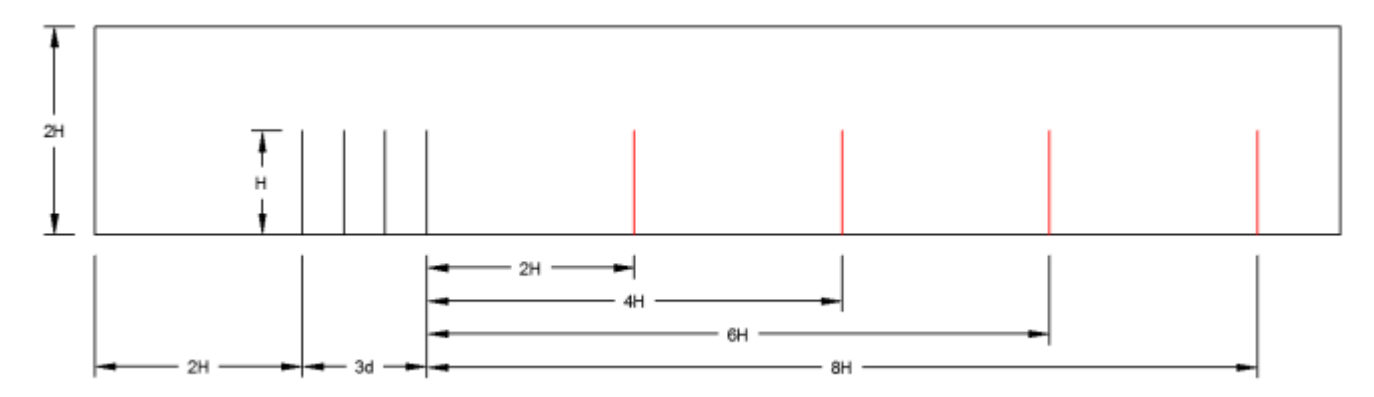


Fig. 3-100 - Schematic of the computational domain for the case of placing n=4 protection screens (CT3, GT3,4, CB:40-10-4-2H)

The calculation domain from the computational domain thus established, was then meshed, generating the computing network for calculations, with the COMSOL Multiphysics program at a level of discretization that ensures the obtaining of a speed field, on the range of motion, with a convenient approximation.

Figure 3-101 shows the discretization of the computational domain in the area of the protection screens, for a number of protection screens n=4 (CT3, GT3,4, CB:40-10-4-2H).

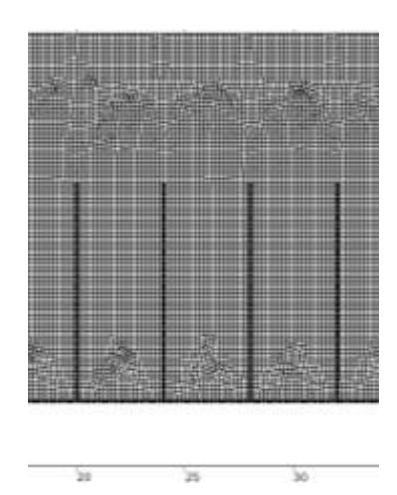


Fig. 3-101 - Discretization of the computational domain in the area of the protection screens, for a number of protection screens n=4 (CT3, GT3,4, CB:40-10-4-2H)

Applying, on the computational domain, the finite element model COMSOL Multiphysics, the velocity range in this calculation field is obtained.

Figure 3-102 shows the speed field in the computational domain for the reference speed U(10)=16 m/s and number of protection screens n=4 (CT3,GT3,4, CB:40-10-4-2H).

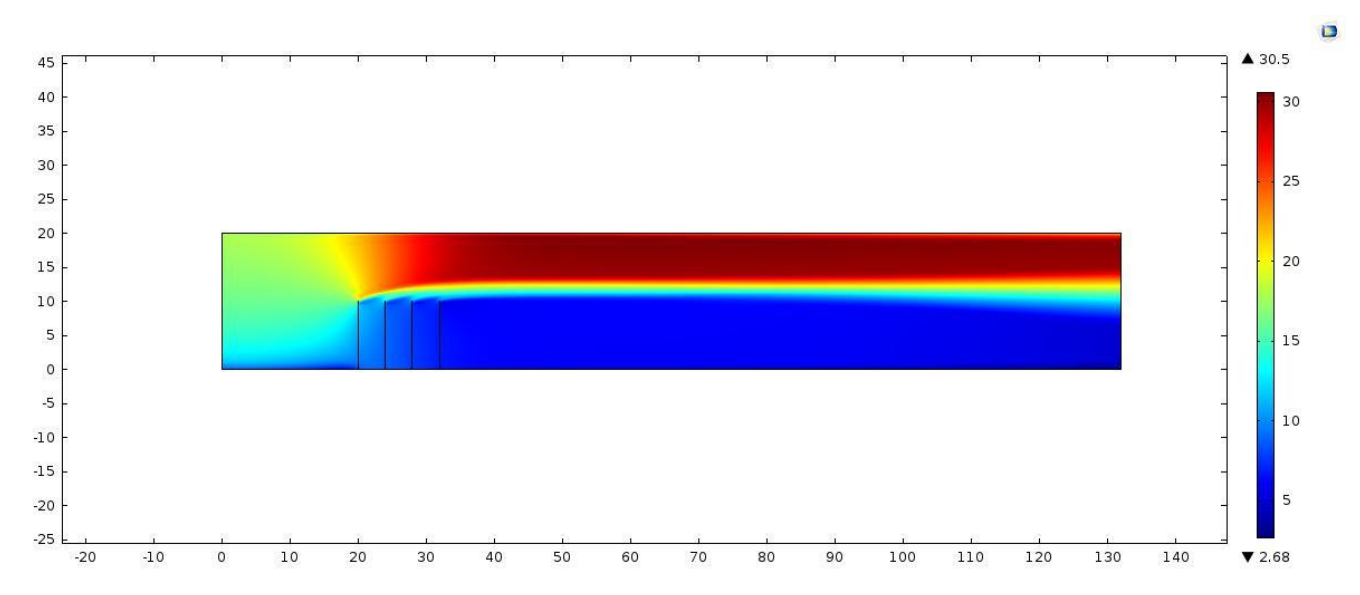


Fig. 3-102 - Speed field in the computational domain for the reference speed U(10)=16 m/s and number of protection screens n=4 (CT3,GT3,4, CB:40-10-4-2H)

From the speed field corresponding to the test group GT3,4, from the category of tests CT3, the speed profiles from 4 sections located at the downstream distances from the protection screens were extracted, $d_{av} = 2H$, $d_{av} = 4H$, $d_{av} = 6H$, $d_{av} = 8H$. These speed profiles were represented up to the height z = 10 m, because, for the present research, only the speeds at heights $z_1 = 0.20$ m, $z_2 = 1.00$ m and $z_3 = 2.00$ m are concerned, heights at which the phenomenon of sand entrainment produces.

The speed profiles in the 4 sections downstream of the protection screens ($d_{av} = 2H$, $d_{av} = 4H$, $d_{av} = 6H$, $d_{av} = 8H$), resulting from the reduction of the incident wind speed, were compared with the power law type speed profile in upstream of the protection screens, i.e. at heights $z_1 = 0.20$ m, $z_2 = 1.00$ m and $z_3 = 2.00$ m.

Figures 3-103, 3-104, 3-105, 3-106 show the speed profiles U(z) downstream of the screens, for the reference speed U(10)=16 m/s and number of protection screens n=4, at distances $d_{av}=2H$ (CT3,GT3,4, TN3,4,1,CB:40-10-4-2H, CT:16-4-2H), $d_{av}=4H$ (CT3,GT3,4, TN3,4,2,CB:40-10-4-2H, CT:16-4-4H), $d_{av}=6H$ (CT3,GT3,4, TN3,4,3, CB:40-10-4-2H, CT:16-4-6H), $d_{av}=8H$ (CT3,GT3,4, TN3,3,4,CB:40-10-4-2H, CT:16-4-8H), compared to the speed profile of the incident wind.

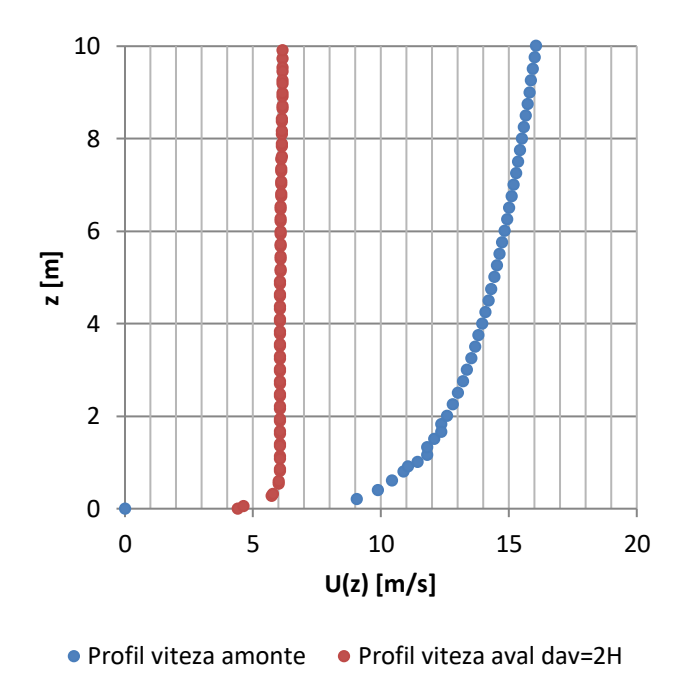


Fig. 3-103 - Speed profile U(z) downstream of the screens, for reference speed U(10)=16m/s and number of protection screens n=4, at distance dav= 2H (CT3,GT3,4, TN3,4,1,CB:40-10-4-2H, CT:16-4-2H). Comparison with the incident wind speed profile

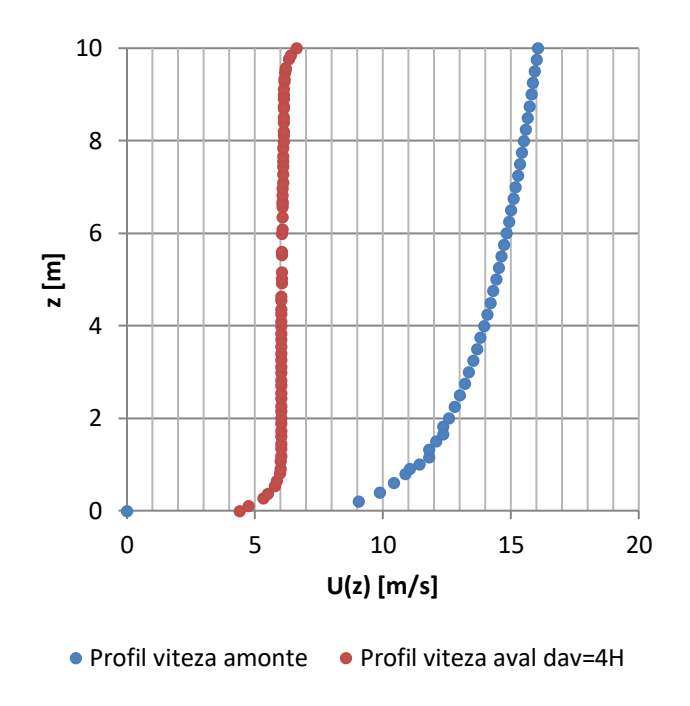


Fig. 3-104 - Speed profile U(z) downstream of the screens, for reference speed U(10)=16m/s and number of protection screens n=4, at distance dav= 4H (CT3,GT3,4, TN3,4,2,CB:40-10-4-2H, CT:16-4-4H). Comparison with the incident wind speed profile

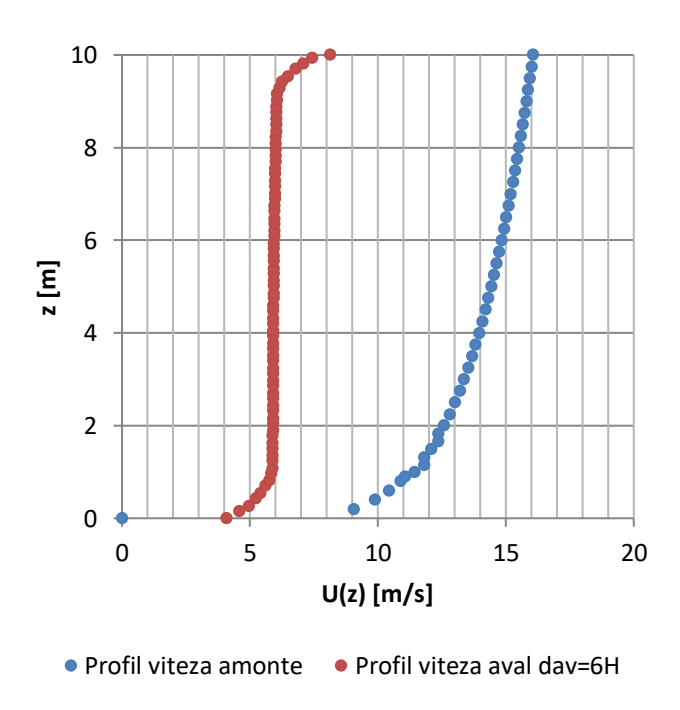


Fig. 3-105 - Speed profile U(z) downstream of the screens, for reference speed U(10)=16m/s and number of protection screens n=4, at distance dav= 6H (CT3,GT3,4, TN3,4,3, CB:40-10-4-2H, CT:16-4-6H). Comparison with the incident wind speed profile

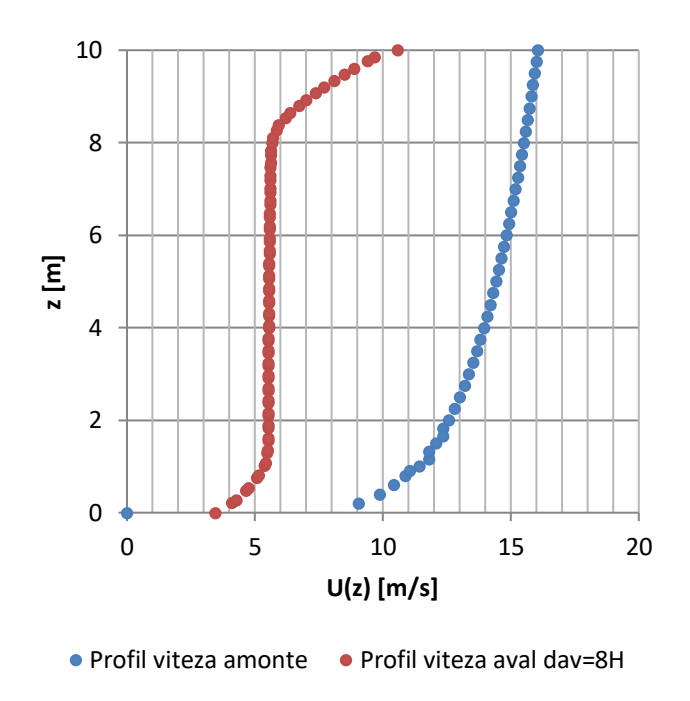


Fig. 3-106 - Speed profile U(z) downstream of the screens, for reference speed U(10)=16m/s and number of protection screens n=4, at distance dav= 8H (CT3,GT3,4, TN3,4,4,CB:40-10-4-2H, CT:16-4-8H). Comparison with the incident wind speed profile

Next, wind speeds were determined at heights z_1 =0,20 m, z_2 =1,00 m si z_3 =2,00 m from the speed profiles corresponding to the downstream sections of the protection screens located at distances d_{av} =2H, d_{av} =4H, d_{av} =6H, d_{av} =8H.

Figure 3-107 shows the variation of U speeds at heights z_1 =0,20m, z_2 =1m şi z_3 =2m, depending on the downstream distance d_{av} for the reference speed U(10)=16 m/s and number of protection screens n=4 (CT3,GT3,4, CB:40-10-4-2H).

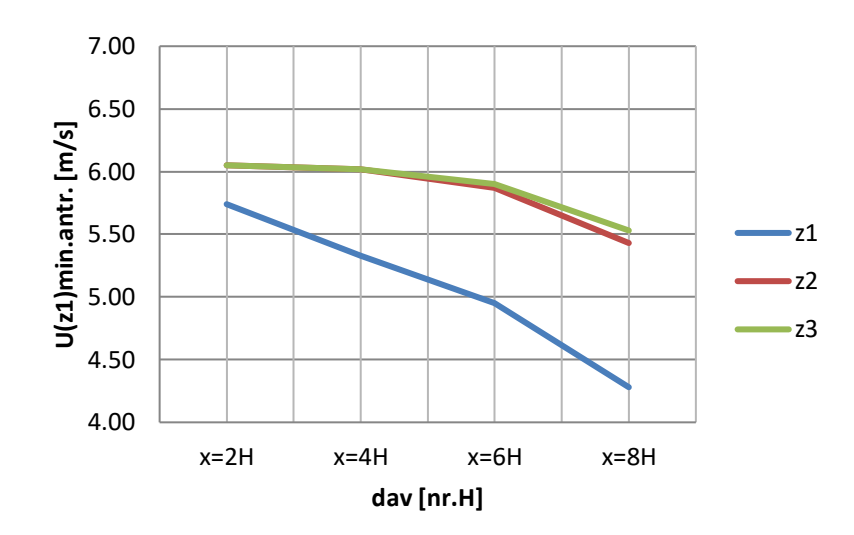


Fig. 3-107 - Variation of U speeds at heights z1=0,20m, z2=1m \ddagger z3=2m, depending on the downstream distance day for the reference speed U(10)=16 m/s and number of protection screens n=4 (CT3,GT3,4, CB:40-10-4-2H)

Then, for heights z_1 =0,20 m, z_2 =1,00 m și z_3 =2,00 m, for the sections downstream of the protection screens located at distances d_{av} =2H, d_{av} =4H, d_{av} =6H, d_{av} =8H, the differences were made between the speeds on the upstream speed profile located at d_{am} =2H and the speeds from the homologous points on the downstream speed profiles, ie ΔU =U(z)am-U(z)av.

Figure 3-108 shows the variation of the speed decrease $\Delta U = U(\mathbf{z})\mathbf{am} - U(\mathbf{z})\mathbf{av}$ at the heights $z_1 = 0.20$ m, $z_2 = 1$ m şi $z_3 = 2$ m, depending on the downstream distance d_{av} for the reference speed U(10) = 16 m/s and number of protective screens n = 4 (CT3,GT3,4, CB:40-10-4-2H).

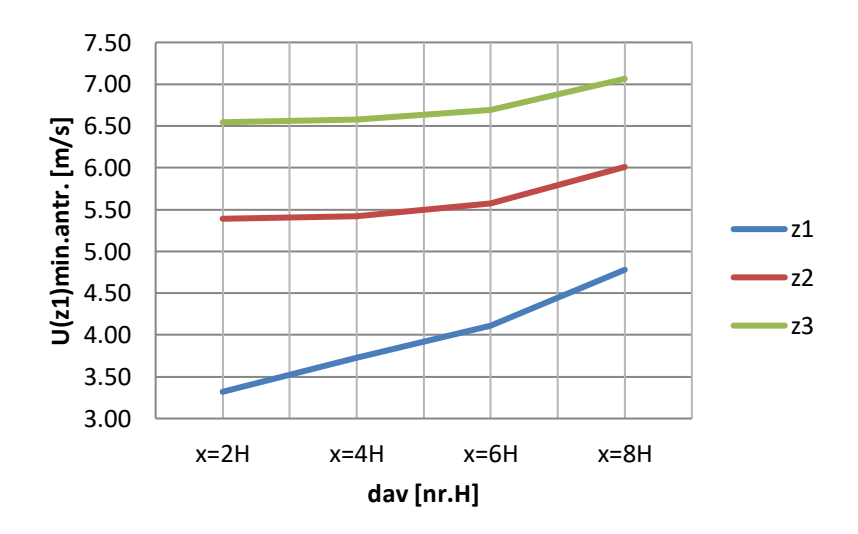


Fig. 3-108 - Variation of ΔU=U(z)am-U(z)av speeds at heights z1=0,20m, z2=1m şi z3=2m, depending on the downstream distance day for the reference speed U(10)=16 m/s and number of protection screens n=4 (CT3,GT3,4, CB:40-10-4-2H)



4. CONCLUSIONS REGARDING NUMERICAL TESTS

In view of the results of the numerical simulations represented graphically in the paragraphs of Chapter 3, a number of conclusions can be drawn as follows.

From the graphs presented in Chapter 3, it is noted that, in terms of ground speed, denoted by $U(z_1)$, it decreases with increasing distance downstream of the protective screens, denoted by d_{av} .

Considering the minimum sand entrainment speed at ground level, $U(z_1)_{minantr}$, as 4 m/s, depending on this speed two tables were made, namely table 4.1 showing the effect of wind at ground level depending on the number of screens, of the reference speed and the downstream distance for $U(z_1) < 4$ m/s and table 4.2 showing the effect of wind at ground level according to the number of screens, the reference speed and the downstream distance for $U(z_1) > 4$ m/s

This minimum sand entrainment speed at ground level, $U(z_1)_{minantr}$, was established based on Molinkov's study, presented in the work of Moţoc M. from 1963. In this study it is shown that at speeds between 0.5 m/s and 4 m/s the wind at ground level does not lift the sand granules, at speeds between 4 m/s and 7 m/s it drives sand granules with a diameter below 0.5 mm, at speeds between 7 m/s and 11 m/s entrain sand granules with a diameter between 0,5 mm and 1 mm, at speeds between 11 m/s and 17 m/s entrain sand granules with a diameter between 1 mm and 2 mm, and at speeds between 17 m/s and 28 m/s drive sand granules with a diameter between 2 mm and 5 mm.

Tab. 4.1. Effect of wind at ground level depending on the number of screens, the reference speed and the downstream distance for $U(z_1) < 4$ m/s

Number of screens - n	Reference speed $ U(10)$ [m/s]	Downstream distance - d_{av} [nr. H]	The effect of wind at the ground level – at
n = 1 screen	U(10) = 8 m/s	$d_{\rm av} = 4H - 8H$	Does not entrain sand- $U(z_1) < 4 \text{ m/s}$
n = 2 screens	U(10) = 8 m/s	$d_{\rm av} = 0H - 8H$	Does not entrain sand - $U(z_1) < 4 \text{ m/s}$
n = 3 screens	U(10) = 8 m/s	$d_{\rm av}=0H-8H$	Does not entrain sand - $U(z_1) < 4 \text{ m/s}$
	U(10) = 12 m/s	$d_{\mathrm{av}} = 0H$ - $8H$	Nu antreneazănisip- $U(z_1) < 4 \text{ m/s}$
n = 4 screens	U(10) = 8 m/s	$d_{\rm av} = 0H - 8H$	Does not entrain sand - $U(z_1) < 4 \text{ m/s}$
	U(10) = 12 m/s	$d_{\rm av}=0H-8H$	Does not entrain sand - $U(z_1) < 4 \text{ m/s}$

Tab. 4.2. Effect of wind at ground level depending on the number of screens, the reference speed and the downstream distance for $U(z_1) > 4$ m/s

Number of screens - n	Reference speed – U(10) [m/s]	Downstream distance d_{av} [nr. H]	The effect of wind at the ground level – at		
			z_1		
n = 1 screen	U(10) = 8 m/s	$d_{\rm av}=0H-4H$	Entrains sand under 0,5		
			mm -		
			$U(z_1) > 4 \text{ m/s}$		
	U(10) = 12 m/s	$d_{\rm av}=0H-8H$	Entrains sand under 0,5		
			mm -		
			$U(z_1) > 4 \text{ m/s}$		
	U(10) = 16 m/s	$d_{\rm av}=0H-8H$	Entrains sand under 0,5		
			mm -		
			$U(z_1) > 4 \text{ m/s}$		
n = 2 screens	U(10) = 12 m/s	$d_{\rm av}=0H-8H$	Entrains sand under 0,5		
			mm -		
			$U(z_1) > 4 \text{ m/s}$		
	U(10) = 16 m/s	$d_{\rm av}=0H-8H$	Entrains sand under 0,5		
			mm -		
			$U(z_1) > 4 \text{ m/s}$		
n = 3 screens	U(10) = 16 m/s	$d_{\rm av}=0H-8H$	Entrains sand under 0,5		
			mm -		
			$U(z_1) > 4 \text{ m/s}$		
n = 4 screens	U(10) = 16 m/s	$d_{\rm av}=0H-8H$	Entrains sand under 0,5		
			mm -		
			$U(z_1) > 4 \text{ m/s}$		

Numerical tests have shown that protection against sand entrainment, through screens, at different speeds of the incident wind, takes place in the following situations:

- 1. For U(10) = 8 m/s:
- n = 1 screen, protection is provided at downstream distances day = 4H 8H,
- n = 2 screens, protection is provided at downstream distances day = 0H 8H,
- n = 3 screens, protection is provided at downstream distances day = 0H 8H,
- n = 4 screens, protection is provided at downstream distances day = 0H 8H.
- 2. For U(10) = 12 m/s:
- n = 3 screens, protection is provided at downstream distances day = 0H 8H,
- n = 4 screens, protection is provided at downstream distances day = 0H 8H.

3. For U(10) = 16 m/s no group of screens n = 1, 2, 3, 4 provides protection against sand entrainment.

Therefore, for n = 1 screen and n = 2 screens, at wind speeds U(10) = 12 m/s and U(10) = 16 m/s, the wind at ground level ($U(z_1) > 4$ m/s) entrain sand below 0.5 mm, and for n = 3 screens and n = 4 screens, at wind speeds, U(10) = 16 m/s, wind at ground level ($U(z_1) > 4$ m/s) entrain sand below 0.5 mm. To reduce the speed at ground level in the cases of sand entrainment presented above, action can be taken by increasing the number of permeable protective screens or by decreasing the permeability of the protective screens, whether natural or artificial.

Also from the graphs presented in Chapter 3, it is noted that, in terms of velocities at the levels z_1 =1 m and z_2 =2 m above the ground, denoted by $U(z_2)$ and $U(z_4)$, respectively, they decrease with increasing downstream distance from the protection screens, denoted by $d_{\rm av}$. These two speeds, which are approximately equal, vary depending on the $d_{\rm av}$, with values between 0.1 m/s and 0.8 m/s, as shown in Table 4.3.

Tab. 4.3. Speed variation for $U(z_2)$ and $U(z_3)$ between $d_{av}=2H$ and $d_{av}=8H$

Test categories	CT1			CT2			СТЗ					
Test groups	GT											
	1,1	1,2	1,3	1,4	2,1	2,2	2,3	2,4	3,1	3,2	3,3	3,4
$[U(z_2)=U(z_3)]$ la $d_{av}=2H$ - $[U(z_2)=U(z_3)]$ la $d_{av}=8H$	0,10	0,15	0,20	0,40	0,25	0,30	0,60	0,60	0,30	0,40	0,80	0,60
	m/s											



5. BIBLIOGRAPHY

- 1. Almeida, G. P., Durao, D. F., & Heitor, M. V. (1993). —Wake flows behind twodimensional model hills. *Experimental Thermal and Fluid Science*(7), 87 101.
- 2. Almeida, G., Durao, D., Simoes, J., & Heitor, M. (1990). Laser-Doppler measurements of fully developed turbulent channel flow. *5th Symp. Appl Laser Techniques to Fluid Meet*, (pg. 5-12).
- 3. COMSOL CFD Module, *User's Guide*. (fara an)
- 4. Bechmann, A. (fără an). *The Bolund experiment Blind Comparison*. Preluat pe 2012, de pe DTU Wind Energy: http://www.bolund.vindenergi.dtu.dk/Blind_Comparison
- 5. Bechmann, A., Berg, J., Courtney, M. S., Jørgensen, H. E., Mann, J., & Sørensen, N. N. (2009). *The Bolund Experiment: Overview and Background*. Technical University of Denmark, Roskilde.
- 6. Benoit, C. (1994). Introduction to Geophysical Fluid Dynamics. Prentice Hall.
- 7. Bitsuamlak, G., Stathopoulos, T., & Bédard, C. (2004). Numerical Evaluation of Wind Flow over Complex Terrain: Review. *Journal of aerospace engineering*, 135-145.
- 8. Cabezon, D., Sumner, J., Garcia, B., Sanz Rodrigo, J., & Masson, C. (2011). RANS simulation of wind flow at the Bolund experiment. *Europeam Wind Energy Conference & Exhibition*, (pg. 141-143). Brussels.
- 9. Castro, J., & Haque, A. (1987). The structure of a turbulent shear layer bounding a separation region. *Journal Fluid Mechanics*, 179, 439-468.
- 10. CFD-Online. (1994). CFD Online. Preluat pe 2014, de pe http://www.cfd-online.com
- 11. Cochran, L. (2004). "Wind effects on lowrise buildings".
- 12. Coșoiu, C. (2008). *Contribuții la optimizarea proiectării și funcționării agregatelor eoliene*. Teză de doctorat, Universitatea Tehnică de Construcții București, București.
- 13. Davenport, A. (1960). *Wind Loads on Structures*. Ottawa: Technical Paper No. 88 of the Division of Building Research.
- 14. Davidson, L. (2011). Fluid mechanics, turbulent flow and turbulence modeling. Course Material.
- 15. Deaves, D., & Harris, R. (1981). A note on the use of asymptotic similarity theory in neutral atmospheric boundary layers. *Atmospheric Environment*, *16*(8), 1889–1893.
- 16. Degeratu, M. (2002). Stratul limită atmosferic. Timișoara: Orizonturi Universitare.

- 17. Drăghici, I. (1988). Dinamica Atmosferei. București: Editura Tehnică.
- 18. Dyrbye, C., & Hansen, S. O. (1997). "Wind Loads on Structures". John Wiley and sons LTD.
- 19. Fallo, D. (2007). *Wind energy resource evaluation in a site of central Italy by CFD simulations*. PhD Thesis, UNIVERSITÀ DEGLI STUDI DI CAGLIARI, Cagliari.
- 20. Garratt, J. R. (1992). The atmospheric boundary layer. Cambridge University Press.
- 21. Ghiocel, D., & Lungu, D. (1975). Wind, snow and temperature effects on structures based on probability. Tunbridge Wells: Abascus press.
- 22. Haşegan, L., Degeratu, M., Sandu, L., Georgescu, A., & Coşoiu, C. (2008). *Modelare experimentală și numerică în ingineria vântului*. (Printech, Ed.) București.
- 23. Hlevca, D. (2012). Cercetari numerice și experimentale privind controlul curgerii la tunelele aerodinamice utilizate în ingineria vântului. Teză de doctorat, Universitatea Tehnică de Construcții București, București.
- 24. Iamandi, C., & Petrescu, V. (fără an). *Mecanica fluidelor*. București: Editura Didactică și Pedagogică.
- 25. Iamandi, C., Petrescu, V., Damian, R., Sandu, L., & Anton, A. (1994). *Hidraulica Instalațiilor*. București: Editura tehnică.
- 26. Izawa, S., Kareem, W. A., Shigeta, M., & Fukunishi, Y. (2007). Hierarchical vortical structures in a homogeneous isotropic turbulent flow. *International Journal of Pure and Applied Mathematics*, 41(4), 463-469.
- 27. Jafari, S., Chokani, N., & Abhari, R. S. (2011, Martie 14-17). An immersed boundary method or efficient simulation of wind flow over complex terrain. *European Wind Energy Conference & Exhibition*, (pg. 145-150). Brussels.
- 28. Kaimal, J., & Finnigan, J. (1994). *Atmospheric boundary layer flows: Their structure and measurement*. New York: Oxford University Press.
- 29. Kornev, N. (2013). Mathematical modeling of turbulent flows. Rostock: Universitat Rostock.
- 30. Murakami, S. (1997). "Current Status and Future Trends in Computational Wind Engineeringl. *Wind.Eng. and Ind.Aero.* (67&68), 3-34.
- 31. Norris, S., & Richards, P. (2010). Appropriate boundary conditions for computational wind engineering models revisited. *The Fifth International Symposium on Computational Wind Engineering*. Chapel Hill, North Carolina.

- 32. Palmen, E., & Newton, C. W. (1969). "Atmospheric Circulation System: Their Structure and Physical Interpretatin". Academic press.
- 33. Pope, S. (2000). Turbulent flows. Cambridge: Cambridge University Press.
- 34. Prandtl, L. (1925). "Uber die ausgebildete Turbulenz". ZAMM.
- 35. Raffel, M., Willert, C., Wereley, S., & Kompenhans, J. (2007). *Particle Image Velocimetry* (ed. Second Edition). Springer.
- 36. Røkenes, K. (2009). *Investigation of terrain effects with respect to wind farm siting*. Norwegian University of Science and Technology. Tapir Uttrykk.
- 37. Schlichting, H. (1979). Boundary-Layer Theory. McGraw Hill Book Company.
- 38. Sladek, I., Bodnar, T., & Kozel, K. (2007). On a numerical study of atmospheric 2D and 3D—flows over a complex topography with forest including pollution dispersion. *Journal of Wind Engineering and Industrial Aerodynamics* 95, 1424–1444.
- 39. Sladek, I., Kozel, K., & Janour, Z. (2009). On the 2D validation study of the atmospheric boundary layer flow model including pollution dispersion. *Engineering Mechanics*, *16*(5), 323-333.
- 40. Snyder, W., & Hunt, J. (1980). Experiments on stably and neutrally stratified flow over a model three-dimensional hill. *Journal Fluids Mechanics*, *96*, 671-704.
- 41. Stangroom, P. (2004). *CFD Modelling of wind flow over terrain*. PhD Thesis, University of Nottingham, Nottingham.
- 42. Straw, M. P. (2000). "Computation and Measurement of Wind Induced Ventilation", Doctoral Thesis. University of Nottingham.
- 43. Stull, R. (1988). An Introduction to Boundary Layer Meteorology. Springer Science & Business Media.
- 44. Sutton, O. G. (1953). Micrometeorology. *Quarterly Journal of the Royal Meteorological Society*, 79(341), 457.
- 45. Taylor, P., & Teunissen, H. (1987). The Askervein Hill project: Overview and background data. *Boundary-Layer Meteorology*, *39*(1-2), 15-39.
- 46. Undheim, O. (2005). *The non-linear microscale flow solver 3DWind*. Norwegian University of Science and Technology. Trondheim: Tapir Uttrykk.
- 47. Versteeg, H. K., & Malalasekera, W. (1995). "An introduction to computational fluid dynamics *The finite volume method"*. Longman Scientific&Technical.



- 48. Wilcox, D. C. (1993). "Turbulence Modeling for CFD". DCW Industries.
- 49. http://imechanica.org/files/fluent_13.0_lecture06-turbulence.pdf
- 50. McComb W.D. *Turbulenta fluidelor (The Physics of Fluid Turbulence* in Oxford University Press) tradus de Savulescu N. St. 1997, in ed. Tehnica, Bucuresti.
- 51. Fröhlich J., Rodi W. 2002. *Introduction to Large Eddy Simulation of Turbulent Flows*, în: Closure Strategies for Turbulent and Transitional Flows, Cambridge University Press, capitolul 8, pp. 267-298.
- 52. Zhiyin Y. 2015. *Large-eddy simulation:Past, present and the future*, în: Chinese Journal of Aeronautics, vol. 28(1), pp. 11-24.
- 53. Berselli L.C., Iliescu T., Layton W.J., 2005. *Mathematics of Large Eddy Simulation of Turbulent Flows, First Edition*, în: Springer, Berlin, Heidelberg, New York, Barcelona, Hong Kong, London, Milan, Paris, Tokyo.
- 54. Vladut C. V. *Modelarea numerica si experimentala a miscarilor atmosferice la scara medie peste insula Bolund*, Teza de doctorat, 2015, Bucuresti.
- 55. https://www.researchgate.net/profile/Chitrarth_Lav
- 56. Kurien S., Taylor M.A., 2005. *Direct Numerical Simulations of Turbulence-Data Generation and Statistical Analysis*, în: Los Alamos Science, vol. 29, pp. 142-151
- 57. Laurence, D. (2002). "Applications of Reynolds Averaged Navier Stokes Equations to Industrial Flows". In van Beeck, J. P. A. J.; Benocci, C. Introduction to Turbulence Modelling, Held March 18–22, 2002 at Von Karman Institute for Fluid Dynamics. Sint-Genesius-Rode: Von Karman Institute for Fluid Dynamics.
- 58. Pope, S. B. (2000). Turbulent Flows. Cambridge: Cambridge University Press
- 59. Flórez Orrego; et al. (2012). "Experimental and CFD study of a single phase cone-shaped helical coiled heat exchanger: an empirical correlation". Proceedings of ECOS 2012 The 25th International Conference on Efficiency, Cost, Optimization, Simulation and Environmental Impact of Energy Systems, June 26–29, 2012, Perugia, Italy. ISBN 978-88-6655-322-9.
- 60. Boussinesq, J. V. (1877). "Théorie de l'Écoulement Tourbillant". Mem. Présentés par Divers Savants Acad. Sci. Inst. Fr. 23: 46–50.
- 61. Baldocchi, D. (2005), Lecture 16, Wind and Turbulence, Part 1, Surface Boundary Layer: Theory and Principles, Ecosystem Science Division, Department of Environmental Science, Policy and Management, University of California, Berkeley, CA: USA.
- 62. https://en.wikipedia.org/wiki/Turbulence_kinetic_energy



- 63. Bandoc, G. (2005) *Potențialul eolian al litoralului românesc al Mării Negre*. (Ed. MatrixRom, București.
- 64. Moțoc, M. (1963) Eroziunea solului pe terenurile agricole și combaterea ei. Editura Agro-Silvică, București.
- 65. Doroftei, B.I., Degeratu, M., Bandoc, G., Iordache, O.G., Moga, C.I. *Researches on the use of textile materials for protection against soil erosion*, Industria Textila, nr. 2/2020, pg. 163-167, București